National Library of Canada
Bibliothèque nationale du Canada

Canadian Theses Service
Service des thèses canadiennes

Ottawa, Canada
K1A 0N4

NOTICE

The quality of this microform is heavily dependent upon the quality of the original thesis submitted for microfilming. Every effort has been made to ensure the highest quality of reproduction possible.

If pages are missing, contact the university which granted the degree.

Some pages may have indistinct print especially if the original pages were typed with a poor typewriter ribbon or if the university sent us an inferior photocopy.

Previously copyrighted materials (journal articles, published tests, etc.) are not filmed.

Reproduction in full or in part of this microform is governed by the Canadian Copyright Act, R.S.C. 1970, c. C-30.

AVIS

La qualité de cette microforme dépend grandement de la qualité de la thèse soumise au microfilmage. Nous avons tout fait pour assurer une qualité supérieure de reproduction.

S'il manque des pages, veuillez communiquer avec l'université qui a conféré le grade.

La qualité d'impression de certaines pages peut laisser à désirer, surtout si les pages originales ont été dactylographiées à l'aide d'un ruban usé ou si l'université nous a fait parvenir une photocopie de qualité inférieure.

Les documents qui font déjà l'objet d'un droit d'auteur (articles de revue, tests publiés, etc.) ne sont pas microfilmés.

La reproduction, même partielle, de cette microforme est soumise à la Loi canadienne sur le droit d'auteur, SRC 1970, c. C-30.

NL-339 (r. 88/04)

Canada

THE UNIVERSITY OF ALBERTA

LINEWIDTH AND FM NOISE REDUCTION OF A 1.3 MICRON GRECC SEMICONDUCTOR LASER USING ELECTRICAL FEEDBACK

by

YING-SHU FREDERICK CHAN

A THESIS

SUBMITTED TO THE FACULTY OF GRADUATE STUDIES AND RESEARCH

IN PARTIAL FULFILMENT OF THE REQUIREMENTS FOR THE DEGREE

OF MASTER OF SCIENCE

DEPARTMENT OF ELECTRICAL ENGINEERING

EDMONTON, ALBERTA

SPRING 1988

Permission has been granted to the National Library of Canada to microfilm this thesis and to lend or sell copies of the film.

The author (copyright owner) has reserved other publication rights, and neither the thesis nor extensive extracts from it may be printed or otherwise reproduced without his/her written permission.

L'autorisation a été accordée à la Bibliothèque nationale du Canada de microfilmer cette thèse et de prêter ou de vendre des exemplaires du film.

L'auteur (titulaire du droit d'auteur) se réserve les autres droits de publication; ni la thèse ni de longs extraits de celle-ci ne doivent être imprimés ou autrement reproduits sans son autorisation écrite.

ISBN 0-315-42751-5

THE UNIVERSITY OF ALBERTA

RELEASE FORM

NAME OF AUTHOR YING-SHU FREDERICK CHAN

TITLE OF THESIS LINEWIDTH AND FM NOISE REDUCTION OF A 1.3 MICRON GRECC SEMICONDUCTOR LASER USING ELECTRICAL FEEDBACK

DEGREE FOR WHICH THESIS WAS PRESENTED MASTER OF SCIENCE

YEAR THIS DEGREE GRANTED SPRING 1988

Permission is hereby granted to THE UNIVERSITY OF ALBERTA LIBRARY to reproduce single copies of this thesis and to lend or sell such copies for private, scholarly or scientific research purposes only.

The author reserves other publication rights, and neither the thesis nor extensive extracts from it may be printed or otherwise reproduced without the author's written permission.

(SIGNED) Y.S.Chan

PERMANENT ADDRESS:

56A, HING FAT STREET,

3/FLOOR, CAUSEWAY BAY

HONG KONG

DATED DECEMBER 10 19 87

THE UNIVERSITY OF ALBERTA

FACULTY OF GRADUATE STUDIES AND RESEARCH

The undersigned certify that they have read, and recommend to the Faculty of Graduate Studies and Research, for acceptance, a thesis entitled LINEWIDTH AND FM NOISE REDUCTION OF A 1.3 MICRON GRECC SEMICONDUCTOR LASER USING ELECTRICAL FEEDBACK submitted by YING-SHU FREDERICK CHAN in partial fulfilment of the requirements for the degree of MASTER of SCIENCE.

E. W. Cormack

Supervisor

Robert Tobazyns

J. P. Aberman

Date DECEMBER 10, 1987

DEDICATION

To my family, who have been supporting and encouraging me.

To Florence, who lights up my life.

To my church, who have been praying and caring for me.

ABSTRACT

Experimental results using optical and electrical feedback simultaneously to reduce the linewidth and the FM noise of a 1.3 μm GRECC (GRIN-ROD external coupled cavity) semiconductor laser are presented. The GRECC configuration, which consists of a multimode semiconductor laser with optical feedback from a 10% reflectivity far-end coated GRIN-ROD lens, provided essentially single longitudinal mode operation with side mode suppression of at least 22 dB. The linewidth of the GRECC laser is about 8.5 MHz when the bias current is 1.7 times the threshold current. A miniature fiber Fabry-Perot interferometer was used as an optical frequency discriminator in the electrical feedback system. A simultaneous reduction of the FM noise and linewidth were obtained for the GRECC laser when electrical feedback was applied. A linewidth of 7 MHz was achieved which agrees with the results obtained from the FM noise measurements.

ACKNOWLEDGEMENT

I would like to thank my supervisor, Dr. G. D. Cormack, for his support and guidance throughout the course of this work. My special thanks also go to Jann Binder and Azmina Somani for many stimulating discussions and the use of some of their equipment. I would also like to acknowledge Dr. W. Krzymien, Yan Loke, Roop Jain, Mark Spooner, Graham Mckinnon and the personnel of the Alberta Telecommunications Research Center for much invaluable assistance and encouragement. Fruitful discussions with Dr. R. Fedosejevs have been very helpful. I should extend my gratitute to Drs. J. McMullin, P. Goud and C. Englefield for the loan of equipment.

Special thanks are extended to Herward Gans and Roman Lipiecki for fabricating the mechanical parts and Barry Arnold for coating the GRIN-ROD lenses and fiber Fabry-Perot interferometer.

I am indebted to Keith Wilcox for his technical contributions and his assistance with preparing the figures for this thesis. Kent Campbell is recognized for his technical assistance.

Finally, I would also like to express my thanks to the Alberta Telecommunications Research Center for providing an ATRC scholarship, facilities and industrial experience, to NSERC for financial assistance and to the University of Alberta for providing the graduate assistantship.

TABLE OF CONTENTS

CHAPTER PAGE

1. INTRODUCTION 1

1.1 BACKGROUND 1

1.2 OBJECTIVE OF THE THESIS 2

1.3 ORGANIZATION OF THE THESIS 3

2. SPECTRAL CHARACTERISTICS OF SEMICONDUCTOR LASERS 5

2.1 INTRODUCTION 5

2.2 LONGITUDINAL MODE SPECTRA 6

2.3 SPECTRAL FLUCTUATIONS 7
2.3.1 Spontaneous Emission 7
2.3.2 Phase Noise 9
2.3.3 Linewidth of semiconductor laser 15

2.4 SUMMARY 18

3. LONGITUDINAL MODE SELECTION AND OPTICAL FEEDBACK 20

3.1 INTRODUCTION 20

3.2 SELECTING A SINGLE LONGITUDINAL MODE 21

3.3 GRIN-ROD EXTERNAL COUPLED CAVITY (GRECC) 25
3.3.1 Experimental Set-up 25
3.3.2 Measurements and Results 27

3.4 LINEWIDTH REDUCTION USING GRECC CONFIGURATION 32
3.4.1 Theory 34
3.4.2 Linewidth Measurements 36
3.4.3 Results 38

3.5 DYNAMIC SINGLE LONGITUDINAL MODE UNDER MODULATION 41

3.6 SUMMARY 46

4. FREQUENCY MODULATION CHARACTERISTICS OF GRECC LASER .48

4.1 INTRODUCTION 48

4.2 THEORETICAL ANALYSIS 48

4.3 EXPERIMENTAL SET-UP 50

4.4 DISCUSSION 62
4.4.1 Modulation Efficiency 62
4.4.2 Other Modulation Formats 67

4.5 SUMMARY 71

5. ELECTRICAL FEEDBACK ON GRECC LASER 72

5.1 INTRODUCTION 72

5.2 PRINCIPLES OF OPERATION 74

5.3 THEORY 75
5.3.1 Bandwidth Estimation 77
5.3.2 Minimum Detectable Linewidth 80

5.4 EXPERIMENTAL SET-UP 83
5.4.1 Fiber Fabry-Perot Interferometer (FFPI) 83
5.4.1.1 Theory of a Temperature-Scanned FFPI 85
5.4.1.2 FFPI Experiment 87
5.4.2 Photodetector and Preamplifier 94
5.4.3 Wideband Amplifier 97

5.5 MEASUREMENT SYSTEMS 97
5.5.1 Longitudinal Mode Monitoring 99
5.5.2 FFPI Position Monitoring 99
5.5.3 FM Noise Measurements 99
5.5.4 Linewidth Measurements 100
5.5.5 Feedback Delay Measurements 100

5.6 RESULTS AND DISCUSSION 103

6. CONCLUSION 108

REFERENCES 110

APPENDIX I: Parameters for Hitachi HLP 5400 Laser 118

APPENDIX II: Laser Current and Temperature Controller Circuit 119

LIST OF FIGURES

FIGURE PAGE

2.1 Two downward transition mechanisms in laser operation. (a) Stimulated emission. (b) Spontaneous emission 8

2.2 Changes in the phase ϕ and intensity I of the optical field during spontaneous emission 10

2.3 Block diagram showing the direct and indirect components of the FM noise in semiconductor lasers 10

2.4 Typical FM noise spectra for a semiconductor laser 14

2.5 Block diagram for a typical FM noise spectrum measurement using a Fabry-Perot interferometer as a frequency reference 14

3.1 Schematic diagram for an external cavity laser 22

3.2 (a) Spectrum of a solitary laser. (b) Resonator loss for a laser with an external cavity. (c) Spectrum for a laser with external cavity 24

3.3 Schematic diagram for a GRECC laser 26

3.4 Experimental arrangement for obtaining the *L-I* characteristics of the GRECC laser 26

3.5 *L-I* characteristics of the solitary laser with an AR coated GRIN-ROD lens, with a 10% far-end coated GRIN-ROD lens and with a 40% far-end coated GRIN-ROD lens 28

3.6 Solitary HLP5400 multimode laser spectrum measured with a monochromator at I_{bias} = 32 mA 30

3.7 Power spectrum of the solitary HLP5400 multimode laser as measured with a scanning Fabry-Perot interferometer 30

3.8 Fabry-Perot interferometer output for the 10% far-end coated GRECC laser with I_{bias} = 34 mA 31

3.9 Power spectra for the 40% far-end coated GRECC laser 31

3.10 Power spectra for the 10% front end coated GRECC laser 33

3.11 Delayed self-heterodyne set-up for linewidth measurement 37

3.12 Trace (a) : Beat spectrum of the 40% far-end coated GRECC laser measured with the delayed self-heterodyne set-up with I_{bias} = 34 mA. Trace (b) : Computed Lorentzian beat spectrum assuming a FWHM laser linewidth of 4 MHz 39

3.13 Beat spectrum of the 10% far-end coated GRECC laser showing a linewidth of 8.5 MHz with I_{bias} = 34 mA 40

3.14 Fabry-Perot interferometer output, showing the dominant mode of the laser spectrum at I_{bias} = 32 mA 43

3.15 Modulated laser spectra with 450 MHz sine wave modulation and I_{bias} = 32 mA. 43

3.16 Modulated laser spectra with 10 Mbit/s square wave modulation 44

3.17 Beat spectrum of a 10% coated GRECC laser under CW operation 45

3.18 Beat spectrum showing spectral broadening of the laser under 200 MHz sine wave modulation 45

4.1 Phase delay between intensity modulation and frequency modulation for a Hitachi HLP 5400 semiconductor laser 51

4.2 Experimental set-up for the frequency deviation measurement 52

4.3 Power spectra for the directly modulated 10% far-end coated GRECC laser with f_m = 100 kHz, I_{bias} = 28 mA and ΔI_m = 1.8 $mA_{0\text{-peak}}$ 54

4.4 Power spectra for the directly modulated 10% far-end coated GRECC laser with f_m = 10 MHz, I_{bias} = 28 mA and ΔI_m = 2.91 $mA_{0\text{-peak}}$ 54

4.5 Power spectra for a 10% far-end coated GRECC laser with f_m = 6.5 MHz, I_{bias} = 28 mA and ΔI_m = 3.54 $mA_{0\text{-p}}$ 55

4.6 Fabry-Perot interferometer output of the power spectra for the 10% far-end coated GRECC laser with f_m = 400 MHz, I_{bias} = 28 mA and (a) ΔI_m = 0 mA, (b) ΔI_m = 1 $mA_{0\text{-p}}$, (c) ΔI_m = 1.5 $mA_{0\text{-p}}$, (d) ΔI_m = 2 $mA_{0\text{-p}}$, (e) ΔI_m = 2.5 $mA_{0\text{-p}}$ and (f) ΔI_m = 3 $mA_{0\text{-p}}$ 56

4.7 Normalized amplitude for optical carrier and various sidebands as a function of modulation current ΔI_m and frequency modulation index β. 60

4.8 Static frequency deviation for the 10% far-end coated GRECC laser when I_{bias} was changed from 28 mA to 29 mA. Trace (a) : I_{bias} = 28 mA. Trace (b) : I_{bias} = 29 mA 61

4.9 Normalized frequency deviation for the 10% coated GRECC laser versus modulation frequency 63

4.10 Effect on 1 Mbit/s FSK modulation due to both thermal and carrier density effects. (a) laser current signal and (b) demodulated waveform using an optical frequency discriminator 65

4.11 Effect on 22.5 Mbit/s FSK modulation primarily due to carrier density effect. (a) laser current signal and (b) demodulated waveform 66

4.12 Sinusoidal modulated laser spectrum for the 10% far-end coated GRECC laser with I_{bias} = 26 mA, f_m = 200 kHz and ΔI_m = 1.8 mA 68

4.13 Triangular-wave modulated laser spectrum for the 10% far-end coated GRECC laser with I_{bias} = 26 mA, f_m = 200 kHz and ΔI_m = 1.8 mA 69

4.14 Square-wave modulated laser spectrum for the 10% far-end coated GRECC laser with I_{bias} = 26 mA, f_m = 200 kHz and ΔI_m = 1.8 mA 70

5.1 Block diagram of electrical feedback configuration using optical direct frequency discrimination detection 73

5.2 Block diagram of electrical feedback configuration using optical heterodyne frequency discrimination detection 73

5.3 Analytical model for the transmittance curve of the Fabry-Perot interferometer used as an optical frequency discriminator 76

5.4 Relationship between the linewidth obtained by electrical feedback and the bandwidth of the feedback system 79

5.5 Experimental set-up for the electrical feedback with the GRECC laser 84

5.6 Computer simulations showing the normalized transmittance curve of the fiber Fabry-Perot interferometer as a function of temperature with mirror reflectivity R as a parameter 88

5.7 Experimental arrangement for characterizing the fiber Fabry-Perot interferometer 89

5.8 Characterization of the temperature controller. (a) Temperature changes in the fiber Fabry-Perot interferometer as a function of time when the scan is on. (b) Corresponding change in the thermistor voltage as a function of time 91

5.9 Linear relationship between the thermistor voltage and the temperature drop during the scan 92

5.10 Transmittance curve of the fiber Fabry-Perot interferometer as a function of thermistor voltage and temperature 93

5.11 (a) : Single mode power spectra for a 10% far-end coated GRECC laser obtained from a scanning parallel plate Fabry-Perot interferometer. (b) : Single mode frequency noise as detected from the fiber Fabry-Perot interferometer 95

5.12 (a) : Multimode power spectra for a 10% far-end coated GRECC laser obtained from a scanning parallel plate Fabry-Perot interferometer. (b) : Frequency jumps due to mode hopping as obtained from the fiber Fabry-Perot interferometer in the non-scanning operation 96

5.13 Magnitude response of the wideband amplifier 98

5.14 Schematic diagram to measure the delay time in the feedback loop. (a) without electrical feedback. (b) with electrical feedback 101

5.15 Loop time delay measurement (a) : Sampling head output without electrical feedback. (b) : Sampling head output with electrical feedback 102

5.16 FM noise spectrum for the 10% far-end coated GRECC laser with I_{bias} = 34 mA. Trace (a) : without electrical feedback. Trace (b) : with electrical feedback 104

5.17 Beat spectrum for the 10% far-end coated GRECC laser with I_{bias} = 34 mA with electrical feedback 105

A1 Schematic diagram for the laser driver circuit 120

A2 Frequency response of the current probe 121

A3 Temperature controller for the laser and fiber Fabry-Perot interferometer 123

CHAPTER 1

INTRODUCTION

1.1 BACKGROUND

The potential of coherent optical fiber transmission systems has steadily attracted a growing number of researchers over the last decade. Coherent detection shows preferable features as compared to the conventional intensity modulation direct detection (IMDD) method, because there is a 10 to 20 dB improvement in signal-to-noise ratio (SNR) when the message signal is imprinted on the frequency or phase of an optical carrier. Coherent receivers, using either homodyne or heterodyne detection, have high sensitivity which approach the shot noise limit [1]-[3]. A local oscillator is required in the front end of the receiver to produce a reference signal which is then combined with the incoming signal at the photodetector. The resulting beat signal, which carries the information in the message signal, can be detected with standard high frequency electronic circuits. Theoretically, a coherent optical fiber communication system can have an enormous bandwidth, at least 10 THz (10×10^{14} Hz), in a single mode fiber which is equivalent to about one hundred thousand full motion video channels [4].

In 1967, a coherent heterodyne detection scheme was demonstrated to be possible for space communications using 3.39 μm gas discharge He-Ne lasers [5]. Later, optical fiber transmission became possible due to the advent of low loss fibers and reliable semiconductor lasers. An important requirement to realize coherent transmission on an optical fiber is the development of a highly coherent[1] and single frequency semiconductor laser. Coherent optical fiber transmission systems could

[1] A term which is usually used to describe the spectral purity of the light source.

not be built until recently because of the excessive linewidth and unsatisfactory long term frequency stability of commercial lasers.

During the past few years, remarkable decreases in the linewidth of semiconductor lasers have been realized using optical feedback techniques [6]-[11]. External grating feedback, which has frequency selectivity capability, has been shown to achieve a linewidth of 10 kHz. Narrow linewidth could also be attained by other long external cavity methods. However, a long external cavity introduces other problems such as mechanical vibration or thermal drift in the cavity that induces instabilities in the laser operation. Therefore, further improvements are required in the source before practical systems are developed .

Two years ago, the application of electrical feedback to semiconductor lasers was shown to be successful in reducing both the linewidth and FM noise. This scheme is attractive as it is claimed to be less sensitive to mechanical vibrations [12]. A coherent optical FSK[2] transmitter [13], which incorporated electrical feedback, both eliminated the non-uniform modulation efficiency of the laser and decreased the laser linewidth. Furthermore, this particular configuration has the advantage of being a compact, potentially stable unit and finally it does not require an external modulator.

1.2 OBJECTIVE OF THE THESIS

The primary objective of this thesis is to investigate the spectral properties of a 1.3 μm InGaAsP multimode semiconductor laser configured simultaneously with both optical and electrical feedback (*dual feedback*). The optical feedback is provided from a far-end coated GRIN-ROD lens, which is responsible for suppressing unwanted longitudinal side modes and providing appreciable line

[2]Acronym for Frequency Shift Keying.

narrowing. The electrical feedback is provided through the use of an FM noise sensitive error signal from a fiber Fabry-Perot interferometer.

This thesis is concerned with the effects of these two feedback arrangements on the spectral width and FM noise of a multimode semiconductor laser.

1.3 ORGANIZATION OF THE THESIS

Chapter 2 covers the spectral properties of semiconductor lasers which are relevant to the chapters that follow. It concentrates on the inherent problems of solitary semiconductor lasers by studying how different parameters are inter-related and affect the coherence of the laser. Emphasis is on the study of phase noise and linewidth, based on the α-parameter. As there have been recent advances reported on this topic, the recent major modifications to conventional theory are emphasized.

In Chapter 3, the theory of longitudinal mode selection using an external cavity is introduced. We also propose a promising solution to the problem of selecting a single longitudinal mode which uses a coated graded-index rod (GRIN-ROD) external coupled cavity. The laser in such a cavity configuration is known as a GRECC laser. Analysis of linewidth reduction due to weak optical feedback will be treated in this chapter. The dynamic linewidth and side mode suppression under modulation are also discussed.

Chapter 4 is concerned with the frequency modulation capability of the GRECC laser. The power spectra of different modulation formats are discussed.

In Chapter 5, electrical feedback on the GRECC laser is emphasized. The linewidth, under electrical feedback conditions, is expected to depend strongly on the feedback bandwidth, the detector noise and the quality of the fiber Fabry-Perot interferometer. This chapter also explains the theory for and characterizes the operation of an optical frequency discriminator which in our case is a *fiber Fabry-*

Perot interferometer. Other major components in the feedback loop are also described. The performance of the electrical feedback system is discussed in regard to its effect on reducing the FM noise level and decreasing the laser linewidth.

Chapter 6 summarizes the entire research project and in particular emphasizes the overall performance of the GRECC laser with and without electrical feedback. The applications and potential of the GRECC laser are addressed in this chapter as also are possibilities for further research work.

CHAPTER 2

SPECTRAL CHARACTERISTICS OF SEMICONDUCTOR LASERS

2.1 INTRODUCTION

Intensive theoretical and laboratory research is presently being pursued in many institutions on intrinsic noise, such as quantum phase noise. The work is directed towards the understanding of the principles and design of high quality sources that can be used in commercial coherent systems and in sensor applications. A better knowledge of quantum noise will lead to better designs for the next generation of *solitary* semiconductor lasers. The invention of single frequency, distributed feedback lasers (DFB) is one example of the type of improved performance that should be the result of this research. A DFB laser has an excellent side mode suppression ratio that results from an internal grating configuration.

Phase noise has been treated theoretically by various authors [15]-[16], the more common method involving solving the quantum Langevin rate equations. Classical rate equations, which are often used to describe the average number of photons and carriers are inadequate to explain quantum processes in lasers. Additional terms, which are usually known as Langevin forces, are introduced to the classical rate equations to account for the statistical distribution of the time dependent variables. The derivation of these equations is outside the scope of this thesis.

This chapter provides a review of the spectral characteristics of semiconductor lasers that are significant to this project. An extensive introduction to the fundamental properties of semiconductor lasers has been provided by co-workers [17]-[18] in our research group and thus will not be described in this thesis.

However, the subject of phase noise in semiconductor lasers and its relation to linewidth will be considered.

2.2 LONGITUDINAL MODE SPECTRA

Fabry-Perot cavity semiconductor lasers have cleaved facets at both ends of the diode that are highly reflective. Standing wave patterns are formed along the laser cavity in the axial direction with the optical field distribution being spatially in phase after each round trip. The resulting permissible modes of oscillation in the cavity are known as longitudinal modes.

Stimulated emission begins in the laser when the gain and phase conditions, given by Eq. (2.1) and (2.2) respectively, are satisfied:

$$g = \sigma - \frac{1}{l} \ln r_1 r_2 \tag{2.1}$$

where g is the threshold gain, σ is the absorption loss in the laser cavity, l is the cavity length and r_1 and r_2 are the reflection coefficients of the laser facets. Also,

$$\frac{m\lambda}{2} = nl \tag{2.2}$$

where λ is the wavelength of light emission measured in the laser medium, m is an integer and n is the refractive index of the active region in the laser diode.

Below threshold, the spectrum is broad and closely resembles that of a light emitting diode (LED). When the current increases above threshold, optical output increases substantially and the optical gain begins to saturate and is clamped to its threshold value. The injected current, which exceeds the threshold current, produces stimulated emission. Stimulated photons are released when the injected carriers recombine. The spectral envelope also narrows tremendously.

Two classes of strip geometry semiconductor laser, *index-guided* and *gain-guided*, are commonly used. In index-guided buried-heterostructure (BH) lasers, the transverse optical mode is confined by a step refractive index stripe. The propagation of the stimulated emitted photons is optically confined by this narrow waveguide. Charge carriers are also concentrated into this optical waveguide by one or two narrow strip electrical contacts. This structure results in a low threshold current. The gain-guided laser maintains optical confinement only from the electrical confinement of the charge carriers. A gain profile forms in the active layer so that the injected carriers are limited to flow across a narrow strip region having a width of a few micrometers. Since there are no refractive index barriers along the active region, high edge loss for the lightwave is expected which implies a higher threshold current.

There is a remarkable difference between the longitudinal mode patterns for these two types of laser. The steady state longitudinal mode spectrum for a gain-guided laser is characterized by a large number of longitudinal modes present even well above the threshold condition. It has been shown that [20] the rate of spontaneous emission in gain-guided lasers is enhanced due to the curved wave fronts, thereby decreasing the longitudinal mode selectivity. The situation is very different in index-guided lasers. Because of the optical confinement, stimulated emission has a more substantial effect than spontaneous emission, the result being fewer longitudinal modes. In fact, some index-guided lasers have an almost single longitudinal mode spectrum at high current.

2.3 SPECTRAL FLUCTUATIONS

2.3.1 SPONTANEOUS EMISSION

Two transition mechanisms, shown in Fig. 2.1, are responsible for light emission from a laser. The first mechanism, which forms the basis of laser

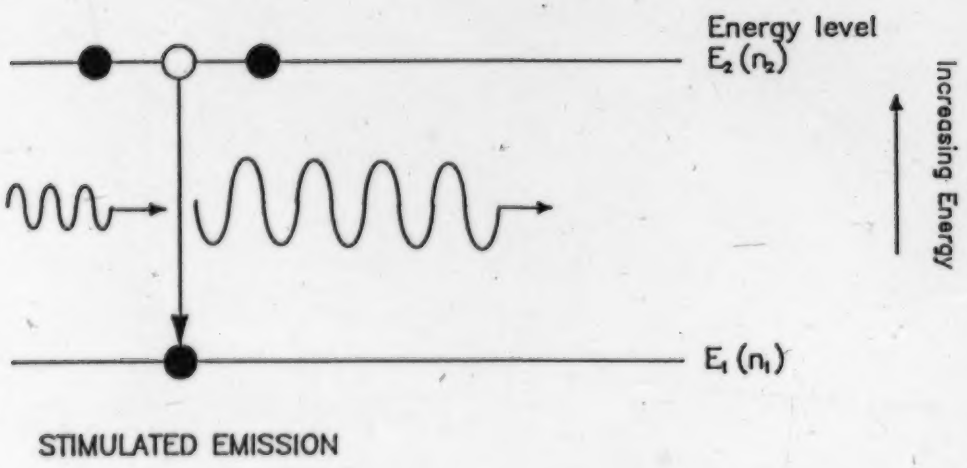

(a) Stimulated emission

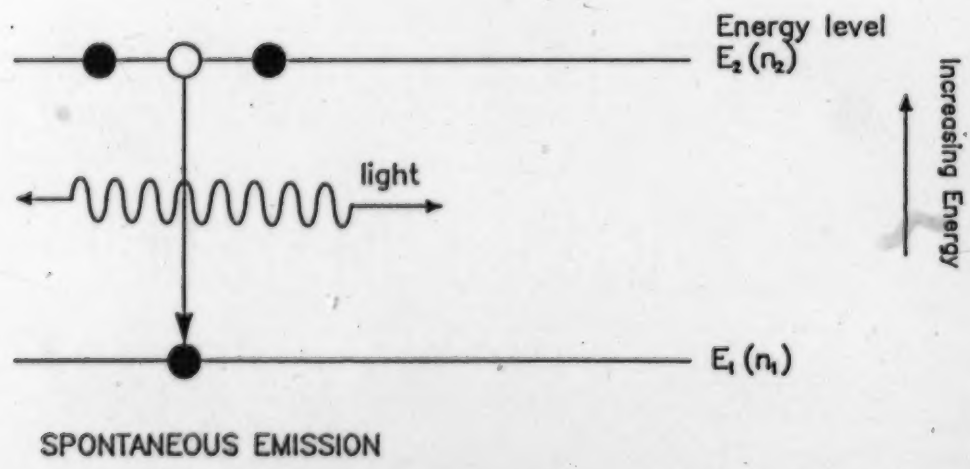

(b) Spontaneous emission

Fig. 2.1 Two downward transition mechanisms in laser operation.

operation, is known as *stimulated emission*. This occurs when an electron is induced by an external light wave to drop in energy level from one energy state to a lower energy state simultaneously emitting a photon. This photon has the same frequency, phase and direction as the input photons and the emission process is called coherent emission. The other transition mechanism, which does not depend on the presence of an optical field, is *spontaneous emission*. In this process photons of arbitrary phase and emission direction are released spontaneously. Because these spontaneously-emitted photons interfere with the coherent optical field established by the stimulated events, the phase of the total optical output varies. An alternative way to consider this result is that the coherence of the laser is reduced.

In a semiconductor laser, the phase perturbations caused by the above process result in random slight shifts of the operating frequency and optical intensity and produce phase noise. Since light is emitted in packets or quanta, such noise is also often referred to as quantum noise.

2.3.2 PHASE NOISE

An incoherent photon emitted because of spontaneous emission but having a frequency that allows coupling to a lasing mode brings about an instantaneous change in phase ϕ and intensity I of the optical field as shown in Fig. 2.2 [21]. In this figure, β represents the complex amplitude of the optical field, ΔI_i is the change in intensity, θ_i is a random angle and $\Delta\phi'_i$ is the direct phase change as a result of the i^{th} spontaneous emission event. However, a large linewidth enhancement factor α, which usually exists in semiconductor lasers, results in a delayed phase change on the optical field. The relations between quantum noise and their coupling mechanisms in semiconductor lasers can be represented in a block diagram, given as Fig. 2.3 [15]. In the diagram, FM noise refers to frequency noise which is also a well accepted measure of spectral fluctuation since frequency is the time rate change of

THE MATERIAL INVOLVED HAS BEEN REMOVED BECAUSE OF THE UNAVAILABILITY OF COPYRIGHT PERMISSION

Fig. 2.2 Changes in the phase ϕ and intensity I of the optical field during spontaneous emission [21].

THE MATERIAL INVOLVED HAS BEEN REMOVED BECAUSE OF THE UNAVAILABILITY OF COPYRIGHT PERMISSION

Fig. 2.3 Block diagram showing the direct and indirect components of the FM noise in semiconductor lasers [15].

phase whereas AM noise represents the intensity noise due to spontaneous emitted photons. Fig. 2.3 also shows how a delayed phase change (delayed FM noise) results from the instantaneous change in the field intensity.

The field intensity is related to the carrier density by means of the following equation [22],

$$\frac{dn}{dt} = -\gamma n - G(n)|E(t)|^2 + P \qquad (2.3)$$

where n is the carrier density, γ is the damping constant of the carrier density, P is the injection rate of the excited carriers per unit volume, G(n) is the gain coefficient and $|E(t)|$ is the magnitude of the optical field. This equation indicates the extra photons produce a non-equilibrium due to an increase in the optical field intensity. Therefore, the laser becomes unstable and undergoes relaxation oscillation in order to restore the steady state field intensity.

The change in carrier density also introduces a gain change, which is proportional to the change in the imaginary part of the refractive index, $\Delta n''$, and is given by [23]

$$\Delta g = -2(\omega/c)\Delta n'' \qquad (2.4)$$

where ω is the average angular frequency. The change in carrier density also results in a change in the real part of the refractive index, $\Delta n'$. This α-parameter, which is also known as the linewidth enhancement or broadening factor or simply Henry's factor [24], is defined as

$$\alpha = \frac{\Delta n'}{\Delta n''} \qquad (2.5)$$

A detailed description of the significance of the α parameter has been given by Osinski *et al.* [24]. Semiconductor lasers are found to behave differently than most other lasers due to the influence of this parameter. α depends on the structure of the laser and typically $\alpha^2 > 1$.

When the carrier density changes, the junction current through the laser diode also changes. If the noise component of the current is measured in the low frequency range, it is found that temperature modulation [25] plays a major role, as shown in the lower portion of Fig. 2.3. This temperature modulation induces frequency fluctuation Δf and is given by [15]

$$\Delta f = -f_o(\alpha_l + \alpha_n)\Delta T(t) \tag{2.6}$$

where α_l is the linear coefficient of thermal expansion, α_n is the coefficient for the change as a function of temperature, $\Delta T(t)$ is the temperature modulation and f_o is the center frequency. Since the thermal effect is known to be a slow process, this effect would only dominate at low frequency.

Fig. 2.4 [15] depicts a typical FM noise spectrum, showing three important components:

(a) a white noise spectrum due to direct phase change as a result of spontaneous emission,

(b) power independent 1/f noise spectrum due to the temperature modulation effect which dominates in the low frequency region and

(c) power dependent carrier density noise spectrum which has a flat noise spectrum at low frequency and a resonant peak at the relaxation oscillation frequency.

The last two components (b) and (c) are caused by the delayed phase change mechanism.

It has been well accepted that the FM noise spectrum $S_f(\nu)$ can be expressed as [26]

$$S_f(\nu) = \frac{\Delta\nu_{ST}}{\pi}\left[1 + \frac{\alpha^2\nu_r^4}{(\nu_r^2 - \nu^2)^2 + (\nu\gamma/2\pi)^2}\right] \tag{2.7}$$

where $\Delta\nu_{ST}$ is the linewidth given by the Schawlow-Townes formula, ν_r is the frequency at resonance and γ is the damping constant. The linewidth can be obtained from $S_f(0)$ which gives

$$S_f(0) = \frac{\Delta\nu_{ST}}{\pi}(1 + \alpha^2) \tag{2.8}$$

The factor $(1+\alpha^2)$ will be explained in the following section. Eq. (2.7) does not include the thermal contribution to the FM noise spectrum as it is believed that the flat noise spectrum is only caused by the quantum process and should be the only mechanism resulting in line broadening. The assumption is that power independent broadening is insignificant, however, the 1/f noise has been reported to be responsible for power independent spectral broadening [27].

A frequency discriminator such as a Fabry-Perot interferometer or Michelson interferometer is required for detection of the FM noise spectrum. The frequency noise is converted to intensity noise to permit detection. Fig. 2.5 is a block diagram of the equipment used to make this conversion. The equipment includes a non-scanning Fabry-Perot interferometer. The FM noise spectrum was displayed on a microwave spectrum analyzer. Absolute frequency noise measurements could have been made by locking to an absorption spectral line of gaseous atoms [28]. This technique is relatively stable to temperature changes as compared to interferometric techniques, however, for ease of making measurements, the latter method was used by the author.

THE MATERIAL INVOLVED HAS BEEN REMOVED BECAUSE OF THE UNAVAILABILITY OF COPYRIGHT PERMISSION

Fig. 2.4 A typical FM noise spectra for a semiconductor laser. The solid line indicates the total FM noise [25].

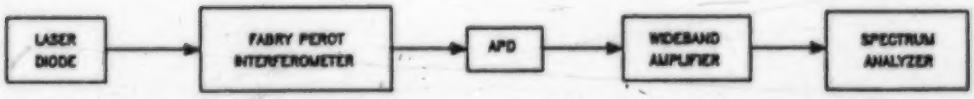

Fig. 2.5 Block diagram for a typical FM noise spectrum measurement using a Fabry-Perot interferometer as a frequency reference.

2.3.3 LINEWIDTH OF SEMICONDUCTOR LASER

Fleming and Mooradian [29] reported that the spectral linewidth of a GaAlAs CW single mode semiconductor laser is inversely proportional to the output power of the laser. The lineshape was found to be Lorentzian but yet the measured linewidth was fifty times greater than that predicted by the Schawlow-Townes relation in the conventional theory for gas lasers. Henry [21] attributed additional broadening to intensity and phase fluctuations, which change the refractive index via carrier density variations. The line was estimated to broaden by $1+\alpha^2$ where α is the linewidth enhancement factor introduced in the previous section. The modified linewidth $\Delta\nu$ is given by [21] :

$$\Delta\nu = \frac{v_g^2 h\nu g n_{sp} \alpha_m (1 + \alpha^2)}{8\pi P_o} \tag{2.9}$$

where v_g is the group velocity, $h\nu$ is the energy per photon of the laser emission, g is the gain, n_{sp} is the spontaneous emission factor, α_m is the facet loss and P_o is the output power of the laser per facet.

Subsequent investigation by various scientists [30]-[31] indicated that the linewidth of a semiconductor laser is not completely power dependent as described above. The linewidth formula was again modified to incorporate the power independent contribution which gives

$$\Delta\nu_{mod} = \Delta\nu_H + \Delta\nu_O \tag{2.10}$$

where $\Delta\nu_{mod}$ is the modified linewidth resulting from both power independent and dependent contribution, $\Delta\nu_H$ is the linewidth equation developed by Henry [21], Eq. (2.9) and $\Delta\nu_O$ is the power independent term.

The last term in Eq. (2.10) implies that even for infinite mode power, the linewidth of the laser is still finite. Recently, a 2-mode laser model [31] analyzed

using the Langevin rate equation revealed that the power independent linewidth is proportional to the *third power* of the side mode intensity. A similar analysis [32] also concluded that the linewidth is very large for multimode lasers. They expected that the linewidth would depend only on Eq. (2.9) when the laser is ideally single mode. For index-guided lasers, the power independent term $\Delta\nu_o$ was reported to be ranging from 2 MHz to 500 MHz [24]. Several other explanations [24] were also postulated for the power independent contributions:

a) 1/f component in frequency modulation (FM) noise,

b) statistical fluctuations of the numbers of electrons in the active layer and

c) thermal fluctuations of state occupancy in the valence and conduction bands.

A recent experiment [27] using delayed self-heterodyne measurements[3] verified that the 1/f component (also independent of the output power of the laser) is the predominant cause for the extra spectral spread $\Delta\nu_o$.

Vahala *et al.* [33] have shown that the lineshape of a single mode semiconductor laser was *not* exactly Lorentzian! Asymmetric side peaks, which are separated from the main peak by the relaxation oscillation frequency, were observed using a high resolution Fabry-Perot interferometer. The relative intensities of such wing patterns were approximately 4×10^{-3} as compared to the center lobe. This has led to a more vigorous analysis by Henry [34] to account for the non-ideal Lorentzian lineshape characteristics. In a recent paper [189], he considered the resonance of the phase noise at the relaxation oscillation frequency instead of assuming a white phase noise power spectrum. The mean square phase change, $<\Delta\phi^2(t)>$, was predicted to be [34]

$$<\Delta\phi^2(t)> = \frac{R_{sp}}{2I}\left[t + \alpha^2\frac{(\nu_r^2 - \gamma^2)}{2\gamma}t^2 + ...\right] \qquad (2.11)$$

[3] See Chapter 3, this thesis.

where R_{sp} is the spontaneous rate of emission into the lasing mode, I is the light intensity, α is the linewidth broadening factor, γ is the damping factor and ν_r is the relaxation oscillation frequency. In his previous treatment, only the first term was considered with the assumption that only simple phase diffusion takes place. Qualitatively, the first term can be explained by the contribution due to direct phase change inherent from spontaneous emission whereas the second term was the delayed phase change. This is due to the coupling between the intensity and gain change which causes relaxation oscillation as already shown in Fig. 2.3.

The lineshape of a semiconductor laser can be derived [34]-[36] by using the Wiener-Khintchine Theorem which yields the field spectrum from the Fourier transform of the autocorrelation of the optical field E(t),

$$E(t) = E_o \exp[j\{2\pi\nu_o t + \phi(t)\}] \tag{2.12}$$

where E_o is the peak amplitude of the optical field, ν_o is the average lasing frequency and $\phi(t)$ is the random phase fluctuation that leads to line broadening. The autocorrelation function $R(\tau)$ can be defined as

$$\begin{aligned} R(\tau) &= \langle E^*(t)E(t+\tau)\rangle \\ &= E_o^2 \langle \exp[j\Delta\phi(t,\tau)]\rangle \exp(j2\pi\nu_o\tau)) \end{aligned} \tag{2.13}$$

where $E^*(t)$ is the complex conjugate of the optical field, $\Delta\phi(t,\tau)$ represents the random phase change between t and $t+\tau$ and $\langle\ \rangle$ is the ensemble average. Using the relation [37]

$$\langle \exp[\pm j\Delta\phi(t,\tau)]\rangle = \exp[-\frac{1}{2}\langle\Delta\phi^2(\tau)\rangle] \tag{2.14}$$

and substituting Eq. (2.14) into Eq. (2.13) will lead to

$$R(\tau) = E_o^2 \exp[-\frac{1}{2}<\Delta\phi^2(\tau)>]\exp[j2\pi\nu_o\tau] \qquad (2.15)$$

where $<\Delta\phi^2(\tau)>$ is the modified mean square phase fluctuation as described in Eq. (2.11) to account for the relaxation. The field spectrum can now be obtained by taking the Fourier transform of $R(\tau)$.

For spectral linewidth calculation purposes, the Lorentzian approximation for the lineshape is quite sufficient because the wing structure usually occurs in the gigahertz region. Experimentally, the linewidth can be measured by a high resolution scanning Fabry-Perot interferometer [38]. In order to increase the resolution of this instrument for such measurements, the mirror separation in the instrument has to be very large. Thus, a Fabry-Perot interferometer is impractical for measuring the linewidths of highly coherent sources. Recently, a delayed self-heterodyne method was developed [39] for high resolution linewidth measurements and this method was used by the present author.

2.4 SUMMARY

A review of the spectral characteristics of semiconductor lasers has been presented in this chapter. Direct phase noise, which is common to all laser systems, is caused by spontaneous emission events coupling into the lasing modes. Delayed phase noise, due to the second order carrier dynamics of semiconductor lasers, is responsible for effects such as the relaxation oscillation spectral peak and the non-Lorentzian laser field spectrum.

We also pointed out that the linewidth of a semiconductor laser is broadened by a factor of $(1+\alpha^2)$ as compared to that predicted by the Schawlow-Townes formula. Moreover, the linewidth is not inversely proportional to the optical power,

but contains another power independent contribution which is due to the 1/f noise and the intensity of the side modes.

The FM noise spectrum is comprised of a *white* spontaneous emission noise spectrum, 1/f current noise spectrum and the carrier modulation noise spectrum which gives rise to a resonance peak at the relaxation oscillation frequency.

CHAPTER 3

LONGITUDINAL MODE SELECTION AND OPTICAL FEEDBACK

3.1 INTRODUCTION

Single longitudinal mode semiconductor lasers are widely used in today's optical fiber systems because of the low level of pulse distortion realizable with these lasers. A typical Fabry-Perot laser spectrum consists of several longitudinal modes approximately one nanometer apart. The presence of these multi-longitudinal modes introduces mode partition noise even though the average output power of the laser remains constant [40]-[41]. Such noise arises because different longitudinal modes undergo instantaneous fluctuations in terms of the power distribution. The received signal in an optical fiber system is distorted due to the combined effect of chromatic dispersion in the optical fiber and the spectral fluctuations of the laser. The net effect is an increase in the bit-error-rate for the system.

In very long haul transmission systems such as trans-oceanic links, a side mode suppression[4] (SMS) in the order of above 30 dB is required [42]. Distributed feedback (DFB) lasers are very suitable for this type of application as they have a SMS of 30 to 45 dB [43]. Improvement in the SMS is also possible using a short coupled cavity semiconductor laser with one of its laser facets anti-reflection coated [44] resulting in a highly single mode output with a SMS of 35 dB. The undesirable feature of this strong optical feedback is that a reduction in frequency modulation performance is expected [8]. Recently, a configuration known as a three cavity laser which consists of two external cavities was reported [45]. A short concave mirror, located at the back facet of the laser, selected a single longitudinal mode with high SMS. The second external cavity on the front facet reduced the laser linewidth

[4]Side mode suppression (SMS) is defined as the ratio of the intensity in the dominant longitudinal mode to that of the next intense mode.

using a semi-transparent GRIN-ROD lens. This configuration had the disadvantage that strong sensitivity to acoustical disturbances was observed.

In this chapter, the experimental results and the theory for the single longitudinal mode selection characteristics of an external coupled cavity laser will be presented. In particular, we will also describe a simple method which uses a far-end coated GRIN-ROD lens to perform mode selection and linewidth reduction simultaneously on an off-the-shelf multimode semiconductor laser.

3.2 SELECTING A SINGLE LONGITUDINAL MODE

Semiconductor lasers are very sensitive to optical feedback caused by reflections from nearby objects such as mirrors, fiber end surfaces and other reflecting surfaces [46]. Optical feedback may also force the laser to move into a region of unstable operation characterized by mode hopping, substantial line broadening and increased intensity noise [46]. However, under careful selected conditions, linewidth reduction and single longitudinal mode selection can be achieved.

A simple external cavity model is depicted in Fig. 3.1. It consists of a laser diode of length l and a mirror which reflects a portion of the light back into the laser cavity. The mirror is located at a distance L away from a laser facet and has a reflection coefficient[5] r_3. The reflection coefficients of the laser facets are denoted to be r_1 and r_2. Interference takes place in the laser cavity between the waves due to r_2 and r_3 with a phase that depends on the length of the external cavity, L. The passive external cavity also introduces loss which alters the gain condition for laser oscillation and is given by [44]

$$g = \sigma - \frac{1}{2l}\ln(R_1R_2) + \frac{1}{l}G \tag{3.1}$$

[5]Reflectivity, R, is equal to rr^*

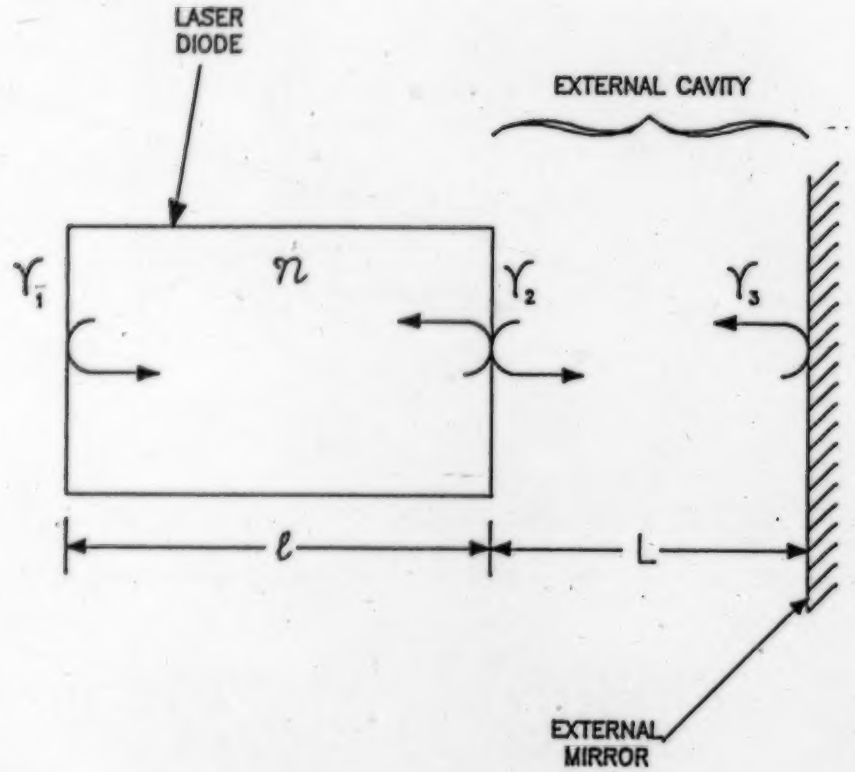

Fig. 3.1 Schematic diagram for an external cavity laser.

where g is the threshold gain, σ is the scattering loss in the active layer, R_1 and R_2 are the reflectivities for the two laser facets and G is the additional loss due to the external cavity. We can write G in terms of the phase factor ϕ_o such that

$$G = \frac{1}{2}\ln\frac{R_2(1 + 2\sqrt{R_2R_3}\cos\phi_o + R_2R_3)}{R_2 + 2\sqrt{R_2R_3}\cos\phi_o + R_3} \tag{3.2}$$

where $\phi_o = 4\pi L/\lambda$.

Fig. 3.2 (i)-(iii) shows the basic principle for longitudinal mode selection. Due to the length of the laser cavity, the laser modes are separated by

$$\Delta\nu_l = \frac{c}{2n_l l} \tag{3.3}$$

where c is the speed of light and n_l is the group index of the laser. Using $n_l = 4$ and $l = 300\ \mu m$ from Appendix I, the frequency separation of longitudinal modes $\Delta\nu_l$ is 125 GHz. In order to demonstrate how mode selection works for an external cavity with round trip time in the external cavity longer than that in the laser cavity, an arbitrary external cavity length of 1.62 mm was chosen which was a little longer than the optical length of the laser cavity. Fig. 3.2 (ii) shows the simulation for the additional loss G under the external cavity above. The frequency separation of the external cavity modes is given by

$$\Delta\nu_L = \frac{c}{2n_L L} \tag{3.4}$$

where n_L is the refractive index of the external cavity which gives the external cavity mode spacing of 92.6 GHz assuming $n_L = 1$ for air. This extra cavity thus introduces

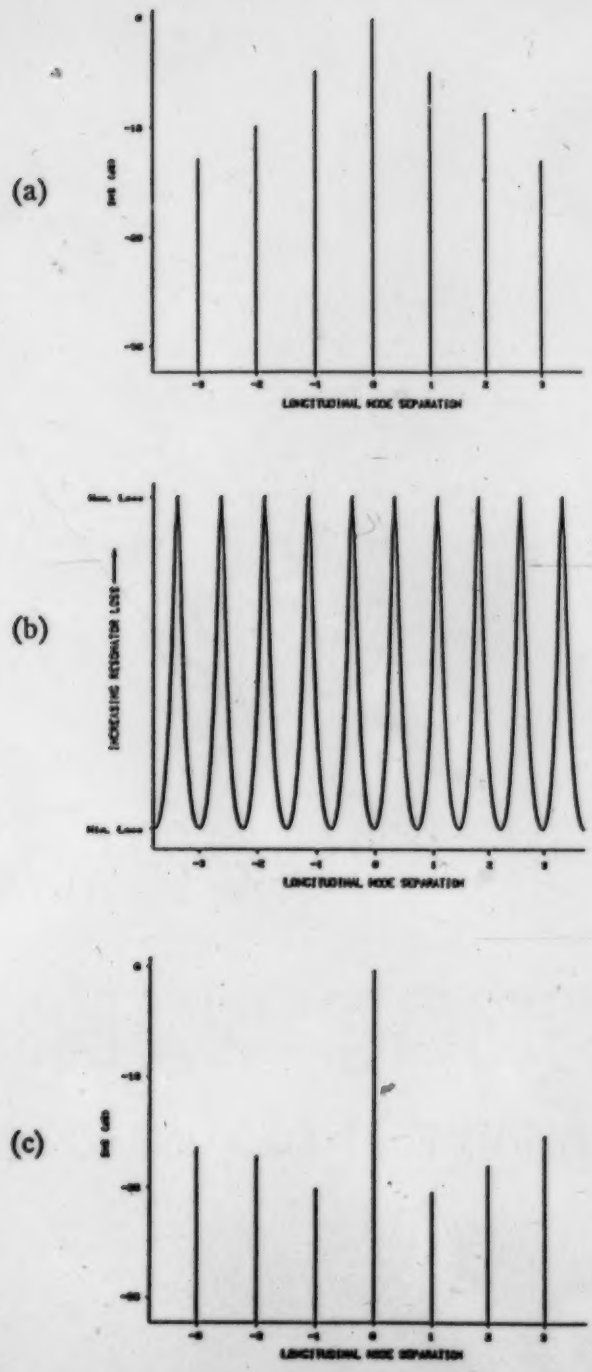

Fig. 3.2 (a) Spectrum of a solitary laser. (b) Resonator loss for a laser with an external cavity. (c) Spectrum for a laser with external cavity.

loss differences between the neighboring laser modes. The mode which suffers from the least overall loss becomes the dominant mode. The degree of side mode discrimination can be improved by changing ϕ_o in Eq. (3.2) which can be physically realized by a very fine adjustment of the position of the external mirror. A different dominant mode can also be chosen by changing the laser current or the laser temperature.

3.3 GRIN-ROD EXTERNAL COUPLED CAVITY (GRECC)

3.3.1 EXPERIMENTAL SET-UP

The operative external mirror in our experiment was a specially coated far-end of a 0.23 pitch GRIN-ROD lens. This configuration was expected to simultaneously select a single longitudinal mode and reduce the solitary laser linewidth. The GRIN-ROD lens was 4.4 mm long and had a working distance, in air to the laser, of about 230 μm yielding a total optical length of 7.3 mm for the external cavity. The particular type of GRIN-ROD lens selected is normally used to collimate a diverging beam from a fiber or a laser diode. The surface of the GRIN-ROD lens facing the laser diode was anti-reflection (AR) coated to avoid undesirable reflections directly from that facet. The far end of the lens was coated in the Optical Shop of the Department of Electrical Engineering with silicon monoxide (SiO) which resulted in a reflectivity of approximately 10 percent. The arrangement of the optical components is shown in Fig. 3.3. The GRIN-ROD lens was mounted on a piezoelectric drive which was in turn mounted on a XYZ-micrometer. The piezoelectric drive was used as a fine control for movement in the z-direction and provided a resolution of about 0.03 μm.

In order to accurately measure the output power vs. current (*L-I*) characteristic of the GRECC laser, the scheme shown in Fig. 3.4 was devised. An optical isolator was inserted between the GRIN-ROD lens and the optical detector

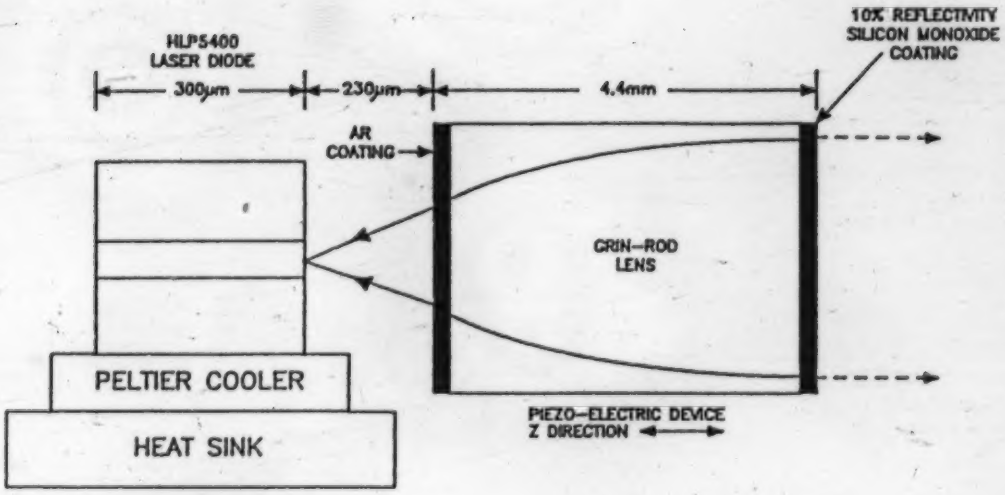

Fig. 3.3 Schematic diagram for a GRECC laser.

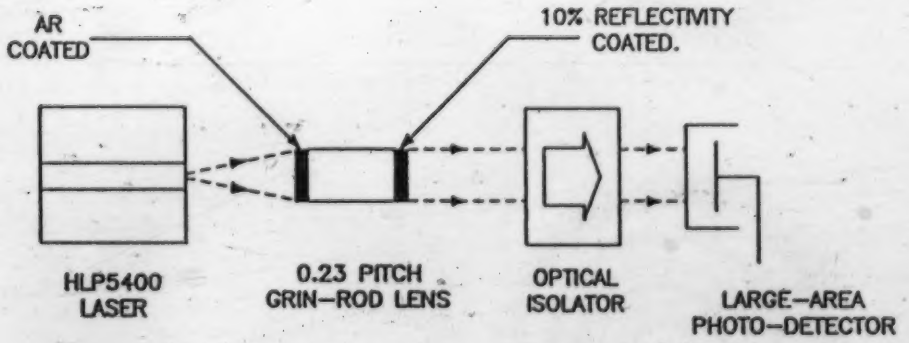

Fig. 3.4 Experimental arrangement for obtaining the *L-I* characteristics of the GRECC laser.

to eliminate any unwanted reflection from the detector surface that would affect the true readings. We also used an AR-coated and a 40 percent coated GRIN-ROD lens for comparison purposes, the surface of the lenses facing the laser facet remaining AR-coated. The *L-I* characteristics with three different GRIN-ROD lenses are shown in Fig. 3.5. The laser temperature was kept constant for all three cases. The threshold current of the laser decreased very slightly as the amount of reflectivity was increased which was due to the optical feedback [47,49]. The amount of the optical feedback can be calculated by the change of the threshold current and will be described in the following section. Undulations in the *L-I* curve were observed for the laser with the silicon monoxide coated GRIN-ROD lenses. Optical feedback is constructive when the laser frequency coincides with one of the external cavity modes. The threshold gain to sustain oscillation is reduced because the laser can be viewed as having a mirror with a higher reflectivity as in Eq. (2.1). However, constructive interference is not preserved when the bias current was altered, particularly when mode jumping and/or multimode oscillations took place. The threshold gain increases which is accompanied by a reduction in optical output. Undulation in *L-I* curves is a common phenomenon in external cavity lasers and could also be observed in the three cavity laser configuration [45]. Fig. 3.5 also indicates that the external quantum efficiency[6] decreases with increasing reflectivity which may be undesirable in practical transmission applications as a high quantum efficiency is required in order to reduce the power penalty in the system.

3.3.2 MEASUREMENTS AND RESULTS

Fig. 3.6 shows the spectrum of the solitary laser as measured with a monochromator when the bias current was equal to 32 mA. The instrument slit width was set at 50 μm which corresponds to a spectral width of 1 Angstrom. The

[6]External quantum efficiency is proportional to the slope of the *L-I* curve for $I > I_{th}$.

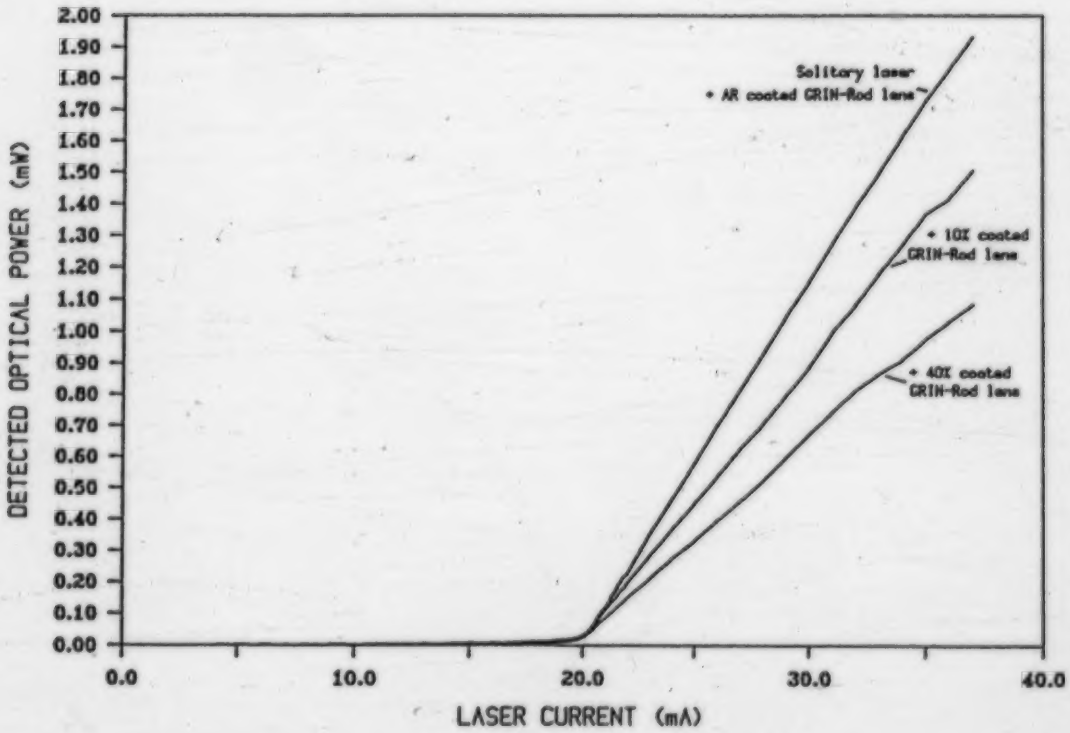

Fig. 3.5 *L-I* characteristics of the solitary laser with an AR coated GRIN-ROD lens, with a 10% far-end coated GRIN-ROD lens and with a 40% far-end coated GRIN-ROD lens.

maxima, separated by 7 Angstroms in wavelength, were due to the longitudinal mode spacing in the laser cavity . Mode competition was intense between the two modes which were favored at this laser current and temperature. The laser spectrum under similar conditiors was measured with a scanning Fabry-Perot interferometer and is displayed in Fig. 3.7. The mirrors in the interferometer were separated by a distance that was less than 275 μm. With this mirror spacing, resonant patterns were observed which were separated by approximately 550 GHz. Thus, Fig. 3.7 is a frequency aliased version of Fig. 3.6 with a repetition frequency of 550 GHz.

The effects of side mode suppression using the far-end coated GRIN-ROD lens were studied and Fig. 3.8 shows the spectrum of the 10 percent far-end coated GRECC laser when the laser current was 34 mA. Two spectral orders having a separation of 785 GHz are shown, this separation corresponding to a mirror separation of 190 μm in the Fabry-Perot interferometer. The SMS was at least 22 dB and an accurate measurement was not possible because of the high noise level (see Figs. 3.8 and 3.9). We also used a 40% far-end coated GRIN-ROD lens in this experiment under the same operating conditions as above and the result is shown in Fig. 3.9 (please note the two ordinate scales in this figure). It is expected from Eq. (3.2) that an increase in external mirror reflectivity would increase the SMS of the coupled laser due to a larger resonator loss for the neighboring modes. The observed SMS for the 40% far-end coated GRIN-ROD lens was of the same order of magnitude as that for the 10% lens. However, an accurate measurement was impossible due to the fact that the level of the side modes was very low and was comparable to the noise level. Nevertheless, the observed SMS of 20 dB was a notable desirable feature of the GRECC laser.

SMS strongly depends on the length of the external cavity. It has been reported that a concave reflector having a radius of curvature of 200 μm achieved a

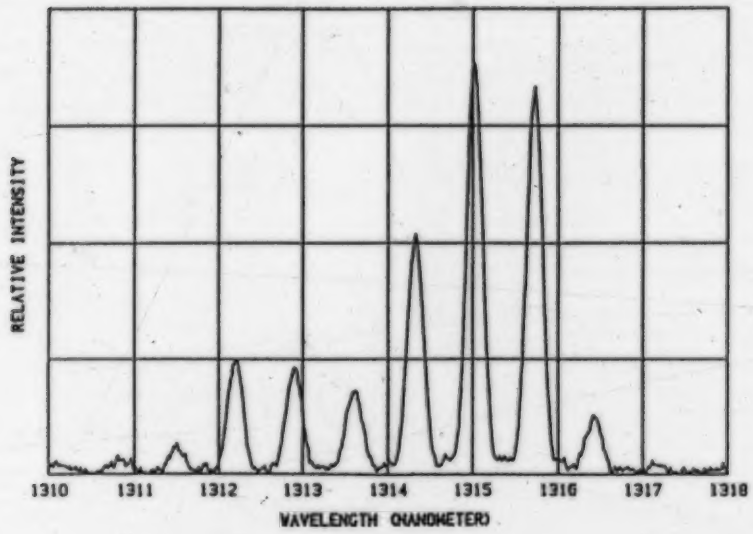

Fig. 3.6 Solitary HLP5400 multidmode laser spectrum measured with a monochromator at I_{bias} = 32 mA.

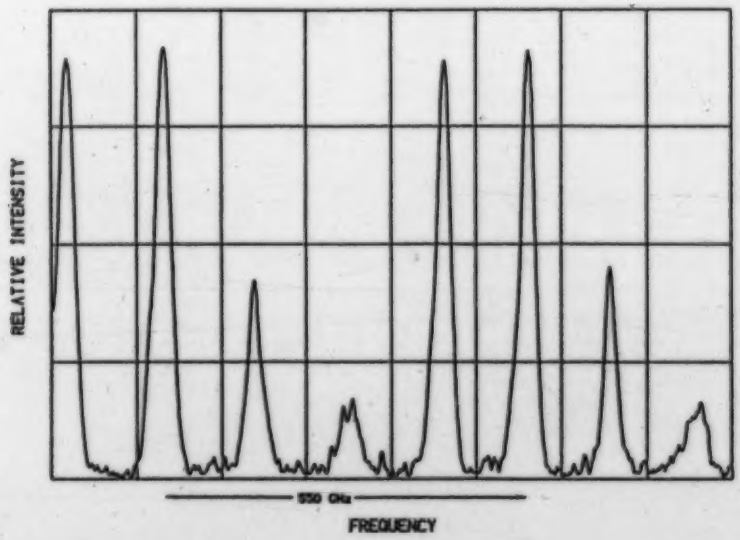

Fig. 3.7 Power spectrum of the solitary HLP5400 multimode laser at I_{bias} = 32 mA as measured with a scanning Fabry-Perot interferometer. Two spectral orders are shown.

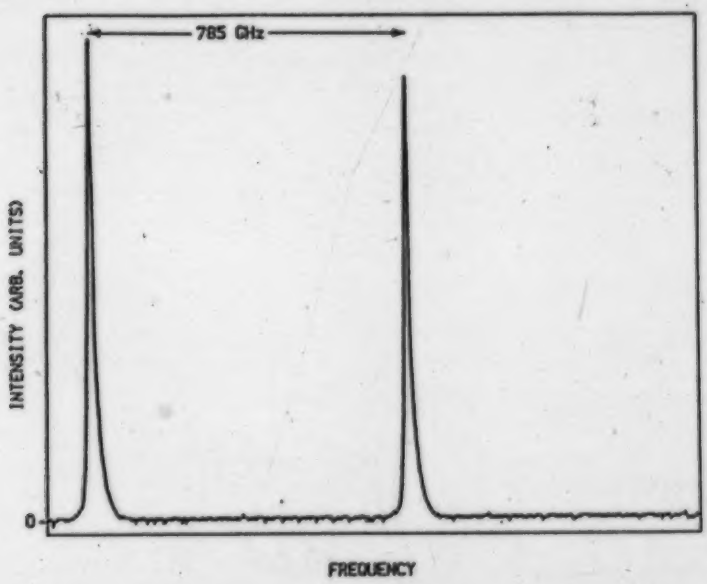

Fig. 3.8 Fabry-Perot interferometer output for the 10% far-end coated GRECC laser with I_{bias} = 34 mA. Two spectral orders are displayed.

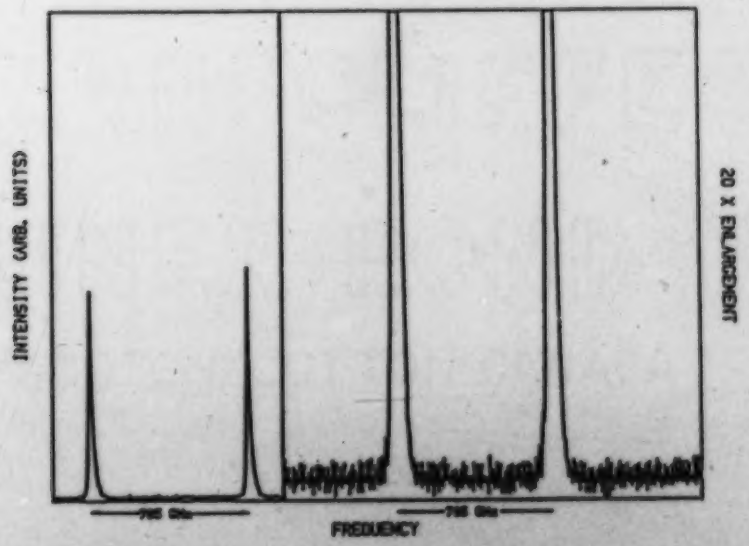

Fig. 3.9 Power spectra for the 40% far-end coated GRECC laser. Left trace:original spectra. Right trace:oscilloscope output expanded vertically by 20 times. Two spectral orders are shown in each case.

better SMS, 28 dB [45]. Since the working distance of the 0.23 pitch GRIN-ROD lens is 230 μm, we inverted the GRIN-ROD lens so that the reflective side of the lens was facing the laser. The quality of the laser spectrum, in terms the single mode oscillation, could be adjusted by translating the lens. Fig. 3.10 shows a SMS of 13 dB. A better SMS could not be attained because of insufficient effective reflection back into the very small cross-section of the laser active region. We conclude that a planar coated mirror at 230 μm does not reflect as much light as that from either a concave mirror at 200 μm or a 0.23 pitch GRIN-ROD lens with reflective coating on the far end. All subsequent work with the GRECC configuration used the far-end coated GRIN-ROD lens.

3.4 LINEWIDTH REDUCTION USING GRECC CONFIGURATION

The GRECC configuration of laser provides not only essentially single longitudinal mode operation but also a certain amount of linewidth reduction. Strong optical feedback using an external mirror or grating with an AR-coating on one of the laser facets provides a linewidth as narrow as 10 kHz [48].

In our case, we realized what is termed weak feedback from the 10 or 40 percent coated GRIN-ROD lens. The major difference between our configuration and that which is called the strong feedback case is that we did not alter the reflectivity of the laser facets. Like other external cavity configurations, the GRIN-ROD cavity serves to store the laser energy so that in the event of spontaneous emission in the active region of the laser, the photons have less effect on the phase of the light output that is generated by stimulated emission in the laser. Therefore, the GRECC configuration of laser is expected to have some narrowing effect on each individual longitudinal mode spectral component.

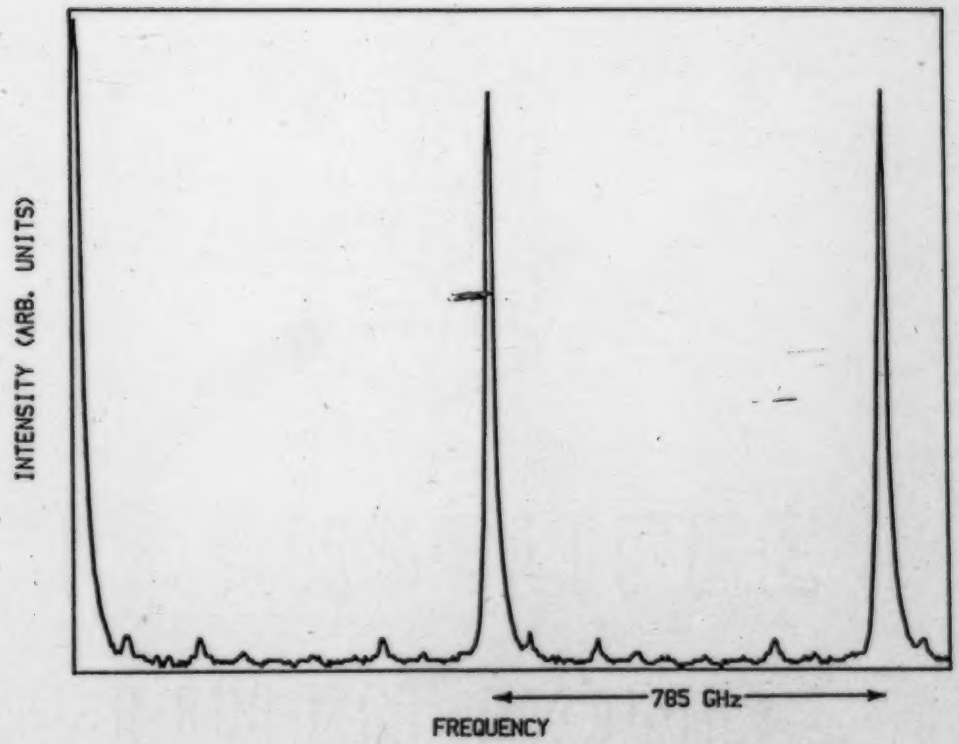

Fig. 3.10 Power spectra for the 10% front-end coated GRECC laser. Three spectral orders are shown.

3.4.1 THEORY

When external optical feedback is applied, properties of the laser such as linewidth, lasing threshold and oscillation frequency are affected. The amount of optical feedback from an external reflector can be estimated from the normalized change in the threshold current $\Delta I_{th}/I_{th}$ [49] which is given by

$$\frac{\Delta I_{th}}{I_{th}} = - \frac{\ln[\, 1 + R_m(1-R_2)/R_2 \,]}{2\sigma L - \ln (R_1 R_2)} \qquad (3.5)$$

where R_m is the unknown quantity in this equation and represents the fraction of light fed back into the active layer, σ is the scattering loss of the laser cavity, R_2 is the reflectivity of the laser facet optically coupled to the external cavity and R_1 is the reflectivity of the other facet. The amount of external optical feedback is determined by R_m and the length of the external cavity L. The feedback factor X [50] is an important parameter to describe the effect of external cavity feedback on spectral linewidth and is given by

$$X = \frac{(1-R_o)L\sqrt{R_m}}{n_1 l\sqrt{R_o}} \qquad (3.6)$$

where n_1 is the group index of the laser cavity and $R_o = R_1 = R_2$ for a symmetric laser cavity.

The GRECC configuration comprised an air medium of 230 μm and a graded index glass medium of 4.4 mm which formed a total optical length of 7.3 mm. Using the parameters from Appendix I for the HLP 5400 laser, (3.6) can be simplified to

$$X = 7.3126\sqrt{R_m} \qquad (3.7)$$

Three regions of operations have been recognized [50]-[51] with X and α as the parameters where α is the linewidth enhancement factor. When X is small, typically less than 1, the linewidth depends on the phase of the feedback from the external cavity, θ, where

$$\theta = \frac{4\pi L}{\lambda_o} \tag{3.8}$$

where λ_o is the wavelength of the laser. The laser linewidth broadens or narrows depending on the phase of the light returning from the external cavity. The linewidth is minimum when the phase is a multiple of 2π and maximum when the phase is an odd multiple of π. In the second region, where X lies typically between 1 to 13, a linewidth reduction is obtained when the phase is a multiple of 2π. However, when the phase becomes an odd multiple of π, both mode hopping and line broadening occur. The third region involves $X > 13$. A very narrow linewidth is achievable in this region which can be approximated by the equation

$$\Delta\nu_{ofb} = \frac{\Delta\nu_{sol}}{(1+X)^2} \; . \tag{3.9}$$

In this region, the linewidth becomes phase independent and strong satellite lines due to the external cavity modes start to be dominant.

External cavity modes correspond to amplified spontaneous emission noise enhancement at resonant peaks of an external cavity. Such modes were not observed in our experiments because of our weak optical feedback configuration. It will be shown shortly that $X < 1$ for our experimental configuration.

3.4.2 LINEWIDTH MEASUREMENTS

A high resolution delayed self-heterodyne [39] set-up was built by another colleague in the laboratory to measure the linewidth of a laser. Fig. 3.11 shows the block diagram of the set-up. Half the light signal was delayed by a 750 m length of single mode fiber. The rest of the signal was passed through an acousto-optic modulator where the optical frequency was frequency shifted by 80 MHz. The two signals were then combined using a second fiber-coupler and were detected by a high speed avalanche photodiode (APD). Manual polarization control was necessary because misalignment in polarization angles imposed a substantial detection sensitivity penalty. The beat spectrum, after being amplified by a wideband amplifier, was displayed on a radio-frequency spectrum analyzer with the center frequency located at 80 MHz. As long as the delay time in the fiber loop was longer than the coherence time of the laser, the mixed signals were not correlated and the entire set-up provided a very practical linewidth measurement method for linewidths over about 100 kHz. The observed beat spectrum was the frequency shifted auto-correlation of the spectrum of the electromagnetic field of the optical signal. Therefore, the actual linewidth was obtained by measuring half of the 3 dB spectral spread of the beat spectrum.

In principle, this method resembles the heterodyne detection scheme except that the local oscillator is replaced by the delayed laser output itself. The delay line is necessary to destroy spatial coherence between the beams on recombination. If the path length difference between the source and the delayed source is small, an interference pattern is observed. Interferometric measurement systems such as a Michelson interferometer utilize this principle where the path length difference between the two beams is small. However, the interference pattern is not obtained when a limiting path difference is exceeded which is commonly referred to as the coherence length. For larger path differences, the interference pattern is destroyed

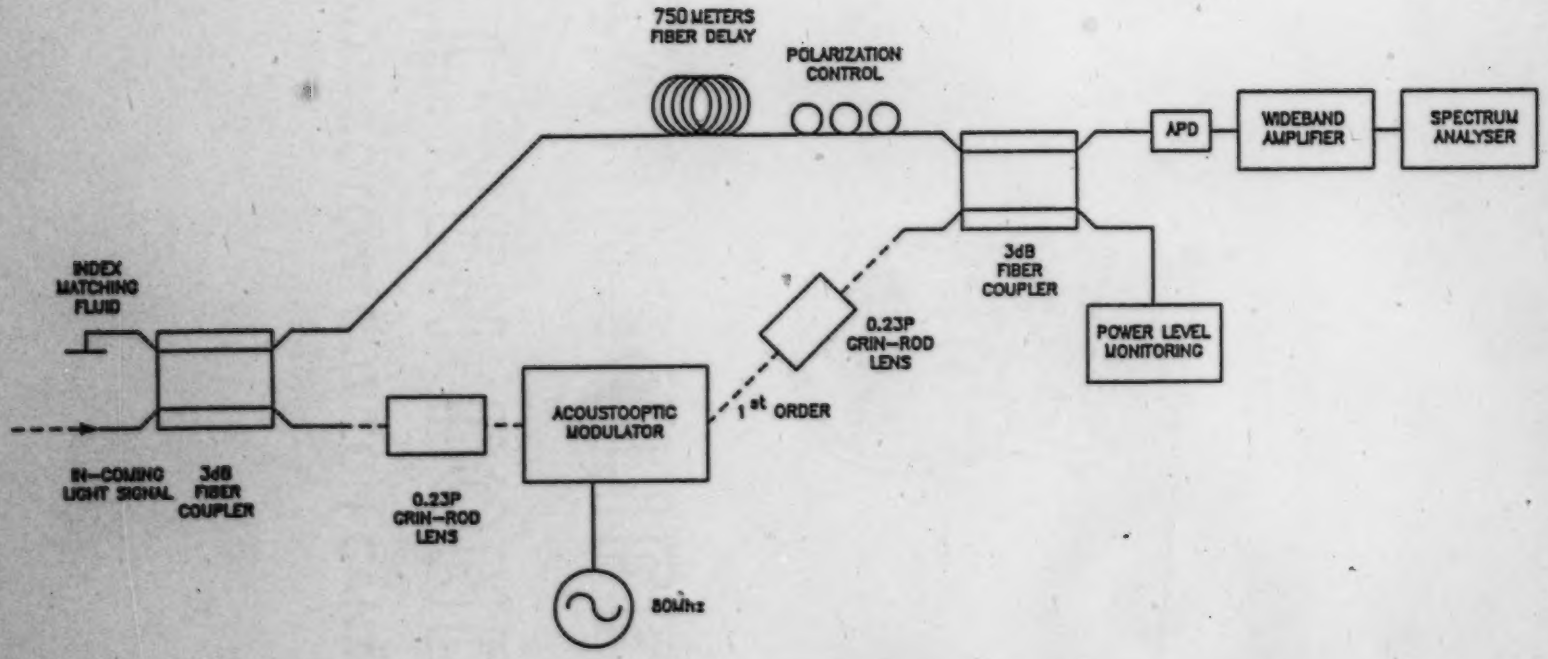

Fig. 3.11 Delayed self-heterodyne set-up for linewidth measurement.

completely because the photons emerging from the acousto-optic modulator and the delay line no longer originate from the same in-phase optical source. The length of the delay line required depends on the spectral linewidth of the source because a narrow linewidth source has a longer coherence length than that of a wide linewidth source. With our GRECC laser, a delay line of 750 meters provided a spectral resolution of 135 kHz [39] and thus our lower limit for observing linewidths was 135 kHz.

3.4.3 RESULTS

Changes in the threshold current of 0.1125 mA and 0.2 mA were observed respectively with the 10 and 40% GRECC lasers. The effective reflectivity, R_m, of the 10% GRECC laser was determined from Eq. (3.5) to be 0.85% whereas the latter laser had R_m = 1.5%. The optical feedback parameter, X[7], was evaluated from Eq. (3.7), giving X = 0.7 and X = 0.9 respectively.

The beat spectrum of the 40% coated GRECC laser is shown as curve a in Fig. 3.12. The 3 dB spectral spread of the beat spectrum equals twice the actual linewidth as explained earlier. Thus, the measured linewidth $\Delta\nu$ is 4 MHz at a bias current of 34 mA. Curve b was computed assuming the same spectral linewidth but a Lorentzian lineshape. Comparison of curves a and b show that the observed curve deviates from the theoretical Lorentzian in the wings where the background noise level in the spectrum plays a significant role. Since the feedback factor, X, was calculated to be less than one, as explained earlier the linewidth would depend strongly on the phase condition for the compound cavity. Mechanical vibrations or thermal instability in the external cavity would broaden the linewidth. Exactly this sensitivity to external stimuli was observed and, in fact, at times line broadening, together with other longitudinal modes, could be observed.

[7] X and R_m are only estimate values in our case. It has been pointed out [50] that a precise measurement of these parameters is not easy.

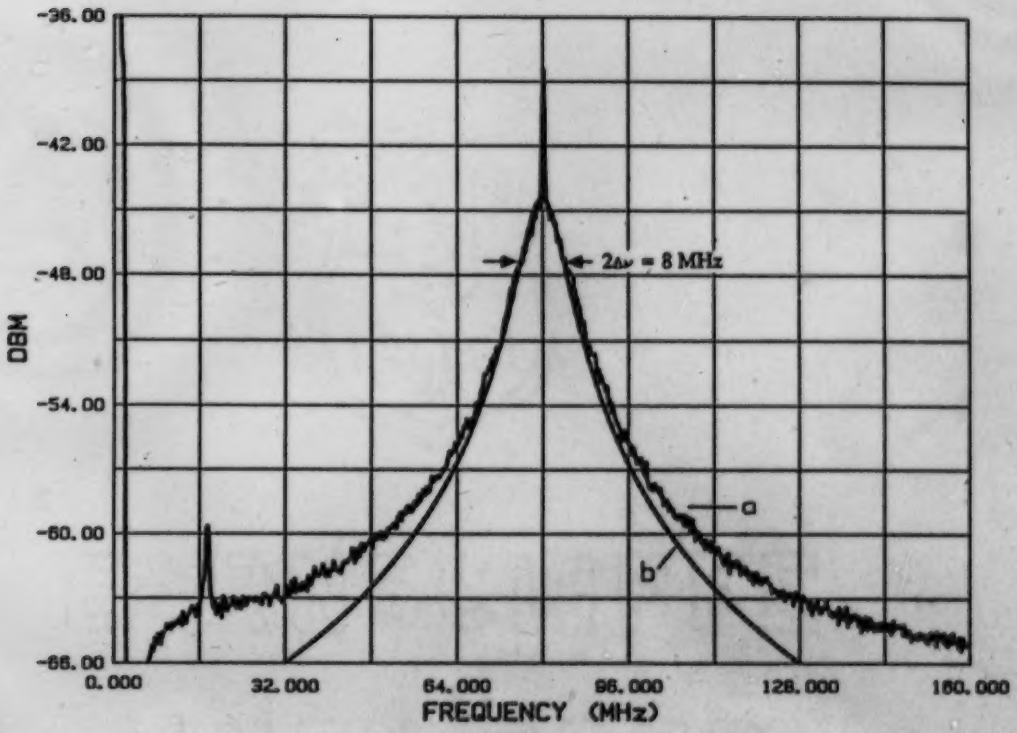

Fig. 3.12 Trace (a) : Beat spectrum of the 40% far-end coated GRECC laser measured with the delayed self-heterodyne set-up with I_{bias} = 34 mA. Trace (b) : Computed Lorentzian beat spectrum assuming a FWHM laser linewidth of 4 MHz.

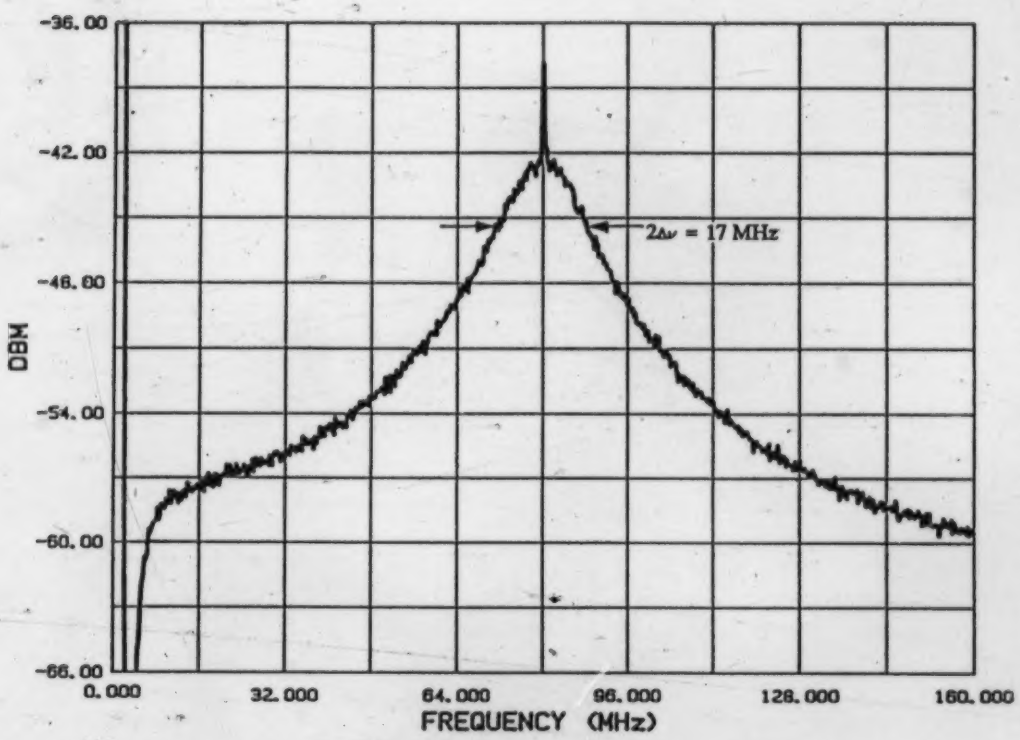

Fig. 3.13 Beat spectrum of the 10% far-end coated GRECC laser showing a linewidth of 8.5 MHz with I_{bias} = 34 mA.

The linewidth of the 10% GRECC laser under the same operating condition is obtainable from the beat spectrum which is shown in Fig. 3.13. The narrowest linewidth observed for this case was 8.5 MHz. Again, the minimum linewidth was sensitive to vibrations and temperature change which no doubt resulted in feedback phase fluctuations. When this situation occurred, the lens position could be manually adjusted to restore the correct phase for minimum linewidth.

3.5 DYNAMIC SINGLE LONGITUDINAL MODE UNDER MODULATION

It is well known that when semiconductor lasers are intensity modulated at high data rates, mode hopping and multi-longitudinal modes become nearly inevitable. The resulting increased chromatic dispersion in an optical fiber system means that either the bit rate of repeater spacing must be decreased. Moreover, in order to have reduced linewidth while using electrical feedback (one of the major objectives of this thesis), operation in the dynamic single longitudinal mode state (DSM) is required even while the semiconductor laser is being counter-modulated by an electrical feedback signal.

Since optical intensity modulation accompanies optical frequency modulation and vice versa, there is an upper limit to optical modulation depth[8] that can be imposed on a laser before the laser breaks down into multimode operation again. This limit obviously depends on the purity of the original CW lasing spectrum and it has been reported that single mode oscillation will be maintained unless the optical modulation depth exceeds 75 to 90 percent [42]. Here, we will determine the DSM characteristics for the coated GRECC laser under the two separate conditions of high speed and large signal modulation.

Fig. 3.14 shows the single mode spectrum of the 10 percent far-end coated GRECC laser under CW operation when measured with a Fabry-Perot

[8]Optical modulation depth η is defined as the ratio of the amplitude to the peak of the optical waveform, i.e., if the optical waveform is $P_0 + P_1 \sin\omega t$ then $\eta = 2P_1/(P_0+P_1)$.

interferometer. A SMS of at least 21 dB was realized when the bias current was 32 mA as shown in this figure. A variable amplitude RF signal generator was then connected to the laser driver. Fig. 3.15 shows that single longitudinal mode operation with the side modes suppressed by a factor of 20 dB relative to the dominant mode was still obtained when the GRECC laser was modulated with a 0.7 mA zero to peak 450 MHz signal. The slight decrease in the SMS can be attributed to the dynamic wavelength shift under rapid modulation which reduces the cavity loss for other side modes at certain wavelengths. Single mode oscillation under high speed modulation has recently been reported to be possible as long as the instantaneous current is kept above a certain level [52].

The large signal behavior in terms of SMS of the modulated GRECC laser was also considered. A 40% far-end coated GRECC laser was used in this experiment. The external cavity was first carefully adjusted to obtain single mode oscillation. We studied the large signal behavior by superimposing a 10 MHz square current modulation, having modulation amplitude of 10 mA peak-to-peak, on the bias current. The resulting laser spectrum is shown in Fig. 3.16. A slight enhancement of side modes is observed, nevertheless a SMS of 17 dB was obtained. In Fig. 3.16, each division in the horizontal scale is separated by 125 GHz which corresponds to the longitudinal mode spacing of the laser. The highest side mode, denoted by 'B5', belongs to the fifth mode from the dominant center mode 'B0'. As comparing to CW operation, the SMS degrades by half. This degradation should be considered as quite minor, bearing in mind the very large amplitude of pulse used in this particular experiment.

Spectral broadening was observed when the 10% far-end coated GRECC laser was modulated. Figs. 3.17 and 3.18 show the beat spectra for the laser under CW operation and 200 MHz sinusoidal modulation respectively as measured with the delayed self-heterodyne set-up. The laser was biased at 28 mA and, in the case

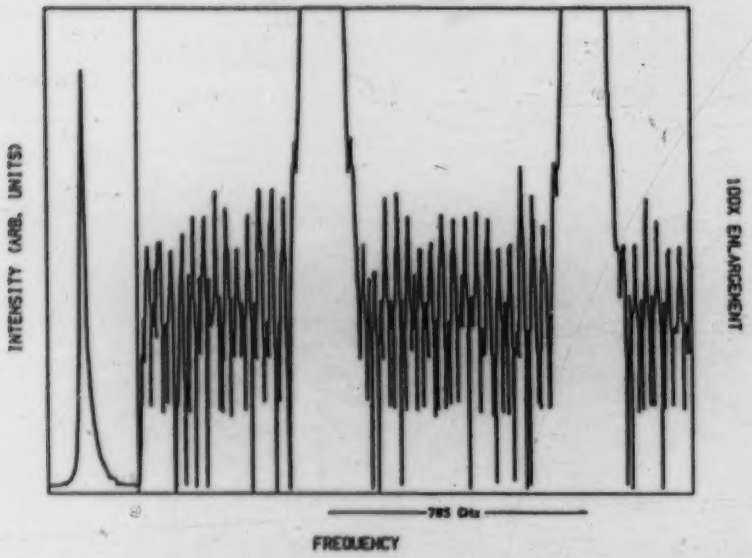

Fig. 3.14 Left trace : Fabry-Perot interferometer output, showing the dominant mode of the laser spectrum at I_{bias} = 32 mA. Right trace : expanded vertical scale by 100 times. Two spectral orders are shown.

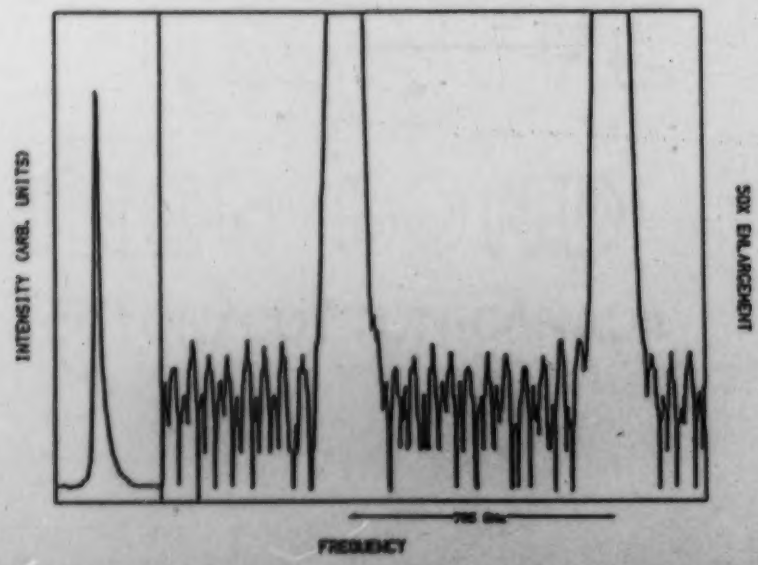

Fig. 3.15 Modulated laser spectra with 450 MHz sine wave modulation and I_{bias} = 32 mA with ΔI_m = 1.4 mA_{p-p}. Left trace : Fabry-Perot interferometer output, showing the dominant laser mode. Right trace : expanded vertical scale by 50 times with two spectral orders shown.

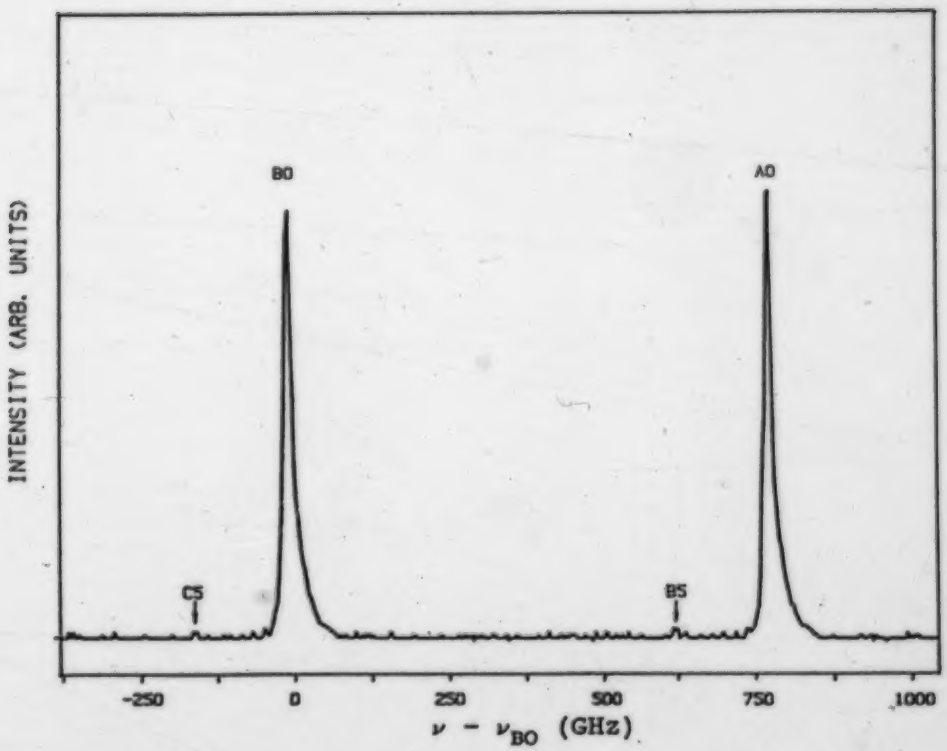

Fig. 3.16 Modulated laser spectra with 10 Mbit/s square wave modulation, I_{bias} = 32 mA and ΔI_m = 10 mA peak to peak. B0 and A0 denote the dominant mode for two different spectral orders and C5 and B5 correspond to the highest side modes of their respective spectral order.

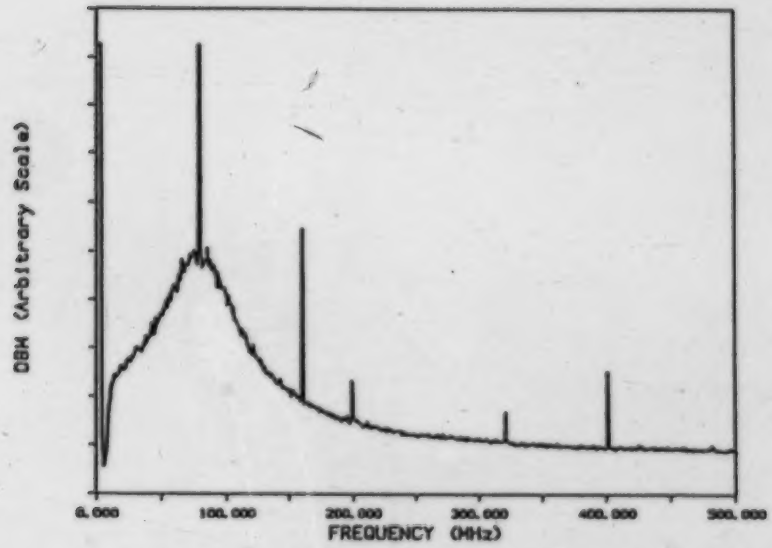

Fig. 3.17 Beat spectrum of a 10% coated GRECC laser under CW operation at 28 mA.

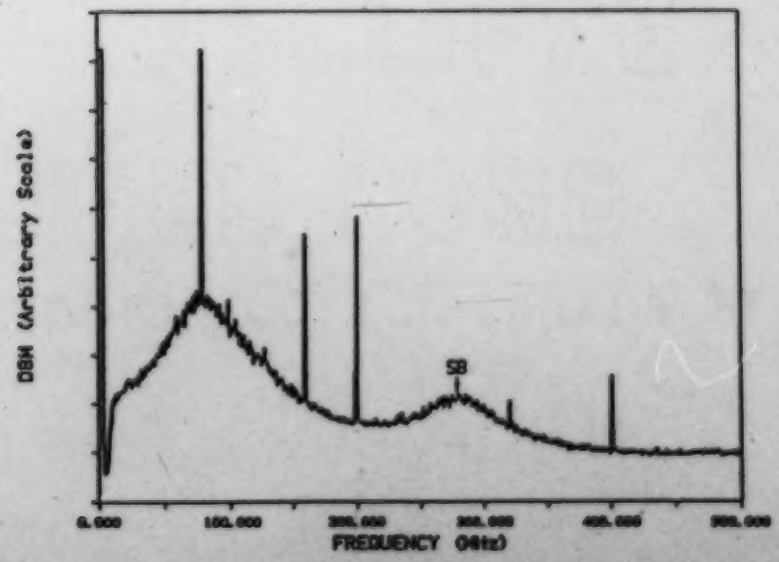

Fig. 3.18 Beat spectrum showing spectral broadening of the laser under 200 MHz sine wave modulation. "SB" indicates the appearance of a FM sideband.

of modulation, a peak modulation current of 1 mA was applied. A modulation side band, corresponding to "SB" in Fig. 3.18, appeared at 280 MHz which was 200 MHz from the 80 MHz signal. This phenomenon was due to the frequency modulation of the laser and will be treated more rigorously in Chapter 4. Strong signals, in the form of spikes, also appeared at 200 MHz and 400 MHz respectively which were directly caused by intensity modulation as detected by the APD. Weaker versions of these signals were also observed without modulation due to electromagnetic leakage into the APD when the signal generator was not connected. The remainder of the signal spikes at 80, 160 and 240 MHz were attributed to the harmonics of the acousto-optic modulator. An increase in dynamic linewidth was observed which could be explained by the decrease of SMS as the power independent linewidth is proportional to the third power of the side mode intensity [31], as discussed in Chapter 2. Therefore, the linewidth broadens with increasing side mode intensity.

3.6 SUMMARY

In this chapter we have investigated the method of selecting a single longitudinal mode using a far-end coated GRIN-ROD lens as an external reflector on one of the laser facets. It was demonstrated that a SMS of at least 22 dB could be obtained and that the actual value could have been much greater because our measurements were noise-limited. A slight degradation of SMS was observed with high speed modulation. The high SMS was preserved under large signal conditions.

The linewidth reduction obtained using the GRECC scheme was due to weak optical feedback. An increase in reflectivity from 10 to 40% reduced the linewidth even further which was as expected from Eqs. (3.7) and (3.9). It can be concluded that the GRECC scheme improves both the longitudinal mode spectrum and also results in linewidth narrowing.

The dynamic linewidth of the GRECC laser was also studied. A small amount of linewidth broadening during high speed modulation was observed which could be explained by the degradation of the SMS.

Results indicated that even though a very high SMS was not obtained, this scheme is still very attractive because of the simplicity of the configuration and the fairly high SMS and linewidth reduction realizable using a 10% coated GRIN-ROD lens which only slightly reduces the external quantum efficiency of the laser.

CHAPTER 4

FREQUENCY MODULATION CHARACTERISTICS OF GRECC LASER

4.1 INTRODUCTION

Semiconductor lasers are attractive for use in coherent optical fiber communication systems because of their small size and their high frequency current modulation capability. The carrier lifetime in the active region of an InGaAsP laser is a few nanoseconds, which means that the laser can be modulated at frequencies up to a few gigahertz.

Recent experiments have shown that semiconductor lasers can be modulated at gigabit rates [53]-[54]. Today, many different configurations of laser such as the cleaved-coupled-cavity (C^3) [55], short-coupled-cavity (SCC) [56], GRECC DFB [45] and external grating feedback laser, are being investigated in terms of narrowing the linewidth as well as improving their modulation efficiency.

The objective of this chapter is to obtain the frequency modulation response for the GRECC laser because the electrical feedback technique requires that a laser have a frequency modulation capability. We will describe some theoretical aspects of the modulated laser fields and power spectra. The effects of temperature and carrier density on high speed FSK generation will be discussed.

4.2 THEORETICAL ANALYSIS

Before we explain the experimental set-up, we will discuss some of the terms that will appear later in the experimental section. First, we are concerned with obtaining frequency modulation of the laser by altering the drive current. Thus, a modulation technique commonly referred to as direct frequency modulation. Here we present some of the fundamental concepts concerning frequency modulation characteristics of semiconductor lasers.

For simplicity, we assume that a sinusoidal current is applied to the laser which can be expressed by

$$I(t) = I_o + I_m\cos(2\pi f_m t) \tag{4.1}$$

where I_o is the bias current, I_m is the peak modulation current and f_m is the frequency of the applied modulating signal. It is well known that both the wavelength and optical power of the laser depend on the drive current, thus, this external excitation will give rise to a combined frequency modulated (FM) and intensity modulated (IM) optical field [57] which is given by

$$E(t) = E_o\{1 + m\cos(2\pi f_m t+\Phi)\}\exp\{j(2\pi f_o t + \beta\sin 2\pi f_m t)\} \tag{4.2}$$

where

$$\beta = \frac{\Delta F}{f_m} \tag{4.3}$$

and

$$m = \frac{I_m}{I_o - I_{th}} \tag{4.4}$$

Here β represents the FM index, f_o is the optical carrier frequency, E_o is the peak amplitude of the optical field, m is the IM index, Φ is the phase difference between the IM and FM, ΔF is the maximum frequency deviation from the center frequency and I_{th} is the threshold current of the laser. The inherent frequency noise component which causes spectral spread, as described in the previous chapter, is not included because its effect is small as compared to that from frequency modulation. The instantaneous optical frequency, altered by frequency modulation, becomes

$$f = f_o + \Delta F\cos(2\pi f_m t + \Phi). \tag{4.5}$$

Eq. (4.2) can be expressed in terms of the Bessel functions of the first kind [58], therefore

$$E(t) = E_o \sum_{n=-\infty}^{\infty} [\{J_n(\beta) + m/2[J_{n+1}(\beta) + J_{n-1}(\beta)]\cos\Phi\}\cos\{2\pi(f_o + nf_m)t\}$$

$$- m/2[J_{n+1}(\beta) - J_{n-1}(\beta)]\sin\Phi\sin\{2\pi(f_o + nf_m)t\}] . \quad (4.6)$$

The sideband intensity for the n^{th} spectral component is given by [58]

$$E_o^2[J_n^2 + mJ_n(J_{n+1} + J_{n-1})\cos\Phi + (m/2)^2(J_{n+1}^2 + J_{n-1}^2 + 2J_{n+1}J_{n-1}\cos 2\Phi)] \quad (4.7)$$

The phase delay Φ, which depends on the modulation frequency, Fig 4.1, causes asymmetry in the power spectrum as indicated in Eq. (4.6). The spectrum becomes symmetrical when the phase delay Φ is $\pm\pi/2$. This happens when the modulation frequency is around 5 to 10 MHz [59] as shown in Fig. 4.1.

Current modulation results in the modulation of the carrier density and the temperature in the active region. The coupling mechanism is very similar to that which generates FM noise, discussed in Chapter 2. The shift in the optical frequency caused by the current modulation depends on the modulation frequency and the phase delay as in Eq. (4.5). The modulation efficiency (MHz/mA) is determined by the carrier density and the temperature in the active region. A derivation of the relevant equations are outside the scope of our study.

4.3 EXPERIMENTAL SET-UP

Fig. 4.2 shows the experimental set-up for measuring the frequency deviation of the 10% far-end coated GRECC laser. As already mentioned in Chapter 3, this configuration selects a single longitudinal mode. The laser was biased at 1.4 times the threshold current (I_{th} = 20 mA). An optical isolator was used in the set-up to avoid any undesirable reflections back into the laser cavity. In order to measure the

THE MATERIAL INVOLVED HAS BEEN REMOVED BECAUSE OF THE UNAVAILABILITY OF COPYRIGHT PERMISSION

Fig. 4.1 Phase delay between intensity modulation and frequency modulation for a Hitachi HLP 5400 semiconductor laser [55].

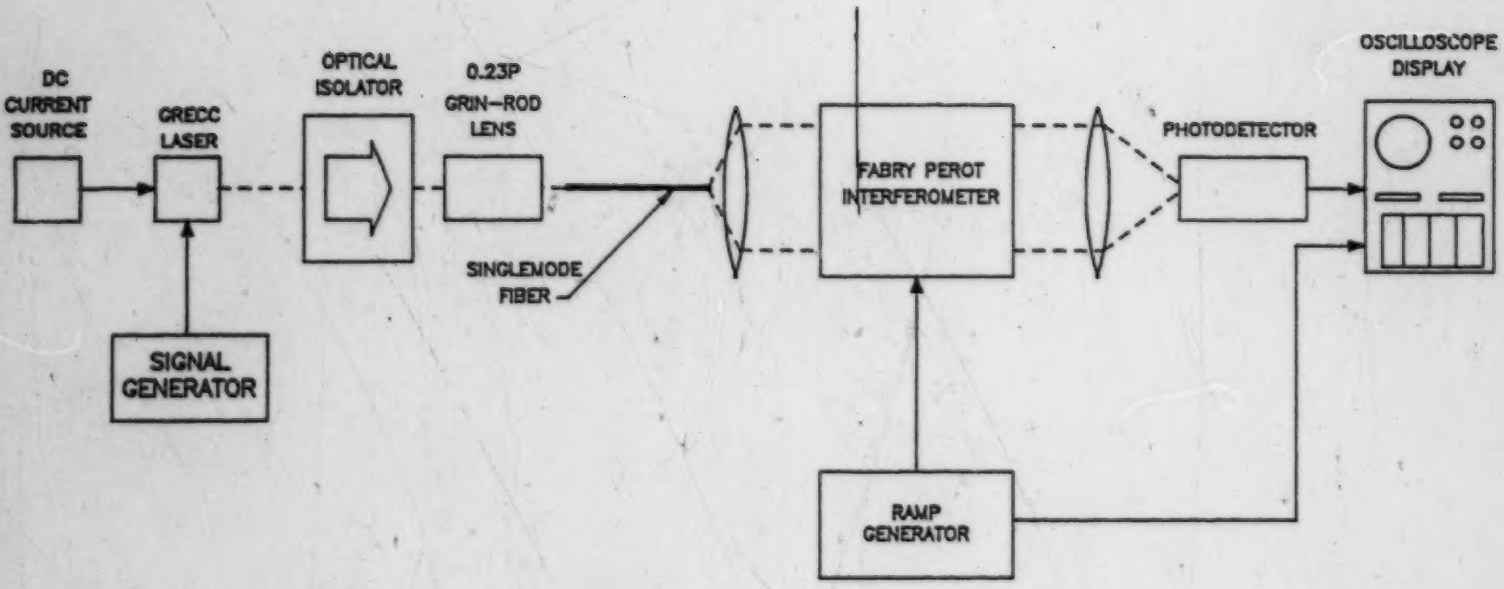

Fig. 4.2 Experimental set-up for the frequency deviation measurement.

magnitude of the modulated laser current, a high speed nanosecond current transformer was used in series with the laser diode. A detailed description of the high frequency laser driver design and the current transformer are presented in Appendix II.

A sinusoidal current was superimposed on the DC bias current in the frequency range of 1 kHz to 400 MHz. The modulated power spectra could be observed by using a scanning Fabry-Perot interferometer. A mirror separation of 7.5 cm, which corresponds to a free spectral range of 2 GHz, was used in the interferometer in order to resolve the FM sidebands. The finesse of the instrument was reduced to approximately 10 due to this larger mirror spacing.

If the modulation frequency of the applied signal was chosen in the range from 1 kHz to 40 MHz, it was observed from Figs. 4.3-4.5 that the sidebands overlapped and a spectral envelope was displayed. Fig. 4.3 shows the power spectra of the laser, modulated with a low-frequency sinusoidal signal of 100 kHz. The spectral envelope shows asymmetry with an enhancement in the lower sideband. When the modulation frequency f_m was 6.5 MHz, the modulated power spectra became symmetrical which is illustrated in Fig. 4.4. This occurs when the phase delay Φ between FM and IM is equal to $-\pi/2$ as already depicted in Fig. 4.1. If we increased the modulation frequency of the sinusoidal signal to 10 MHz, the observed power spectra became again asymmetrical as shown in Fig. 4.5. However, the upper sideband was enhanced when the modulation frequency was above 6.5 MHz. For a large modulation index, the separation between two peaks represents twice the maximum frequency deviation (2 ΔF) [57]. When a signal with a modulation frequency of 400 MHz was applied, the observed spectra were different as compared to the previous cases. Individual FM sidebands started to become evident as the modulation current was increased. Fig. 4.6 (a) to (f) depict a series of power spectra with different modulation current. The upper sideband amplitude

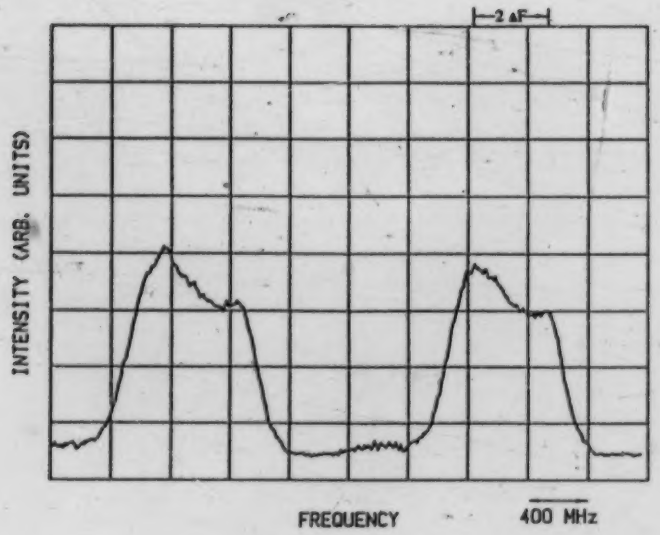

Fig. 4.3 Power spectra for the directly modulated 10% coated GRECC laser with f_m = 100 kHz, I_{bias} = 28 mA and ΔI_m = 1.8 $mA_{0\text{-peak}}$.

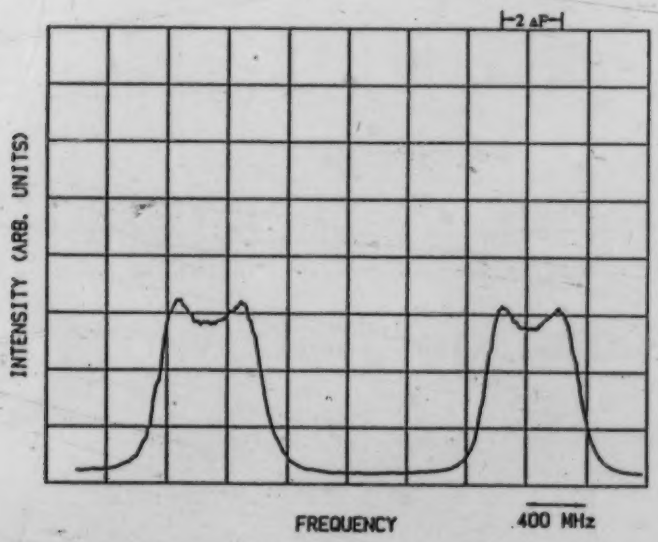

Fig. 4.4 Power spectra for a 10% coated GRECC laser with f_m = 6.5 MHz, I_{bias} = 28 mA and ΔI_m = 3.54 $mA_{0\text{-p}}$.

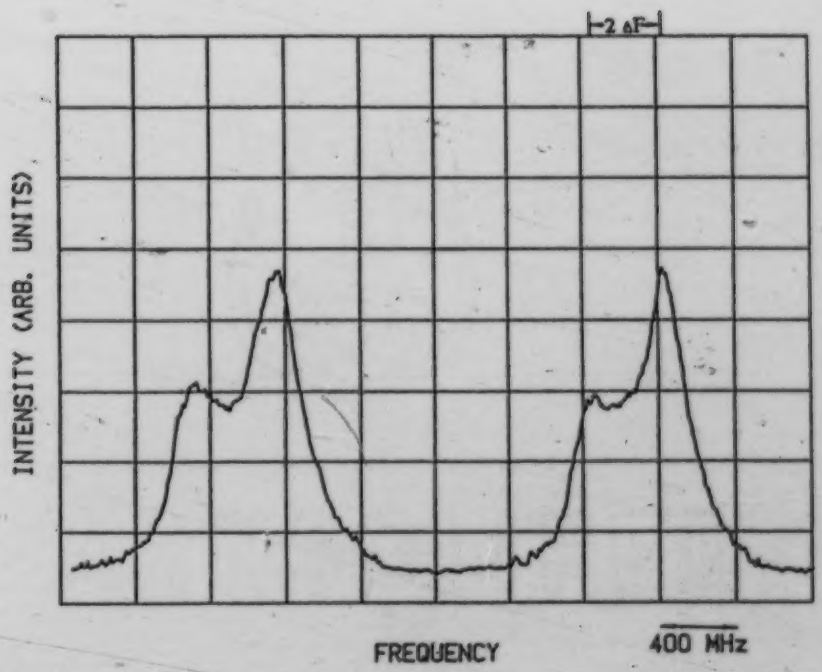

Fig. 4.5 Power spectra for the directly modulated 10% coated GRECC laser with f_m = 10 MHz, I_{bias} = 28 mA and ΔI_m = 2.91 $mA_{0\text{-}peak}$.

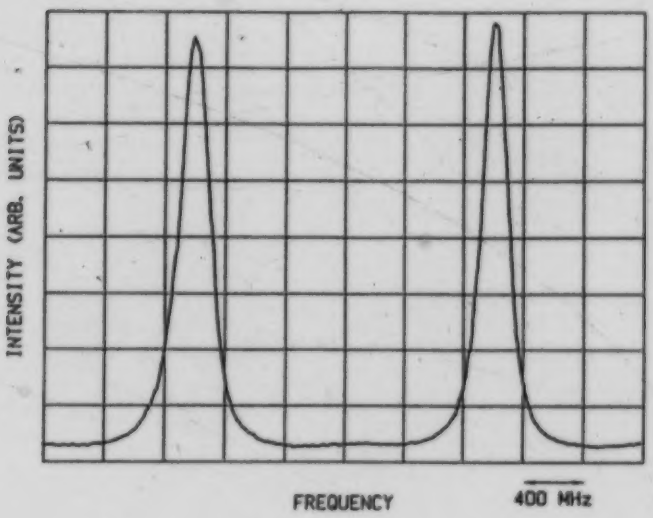

(a) ΔI_m = 0 mA

Fig. 4.6 Fabry-Perot interferometer output of the power spectra for the 10% coated GRECC laser with f_m = 400 MHz, I_{bias} = 28 mA and (a) ΔI_m = 0 mA

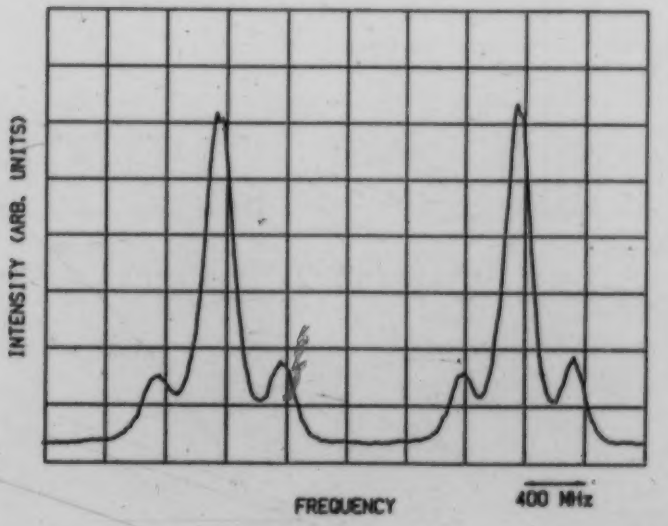

(b) ΔI_m = 1 mA_{0-p}

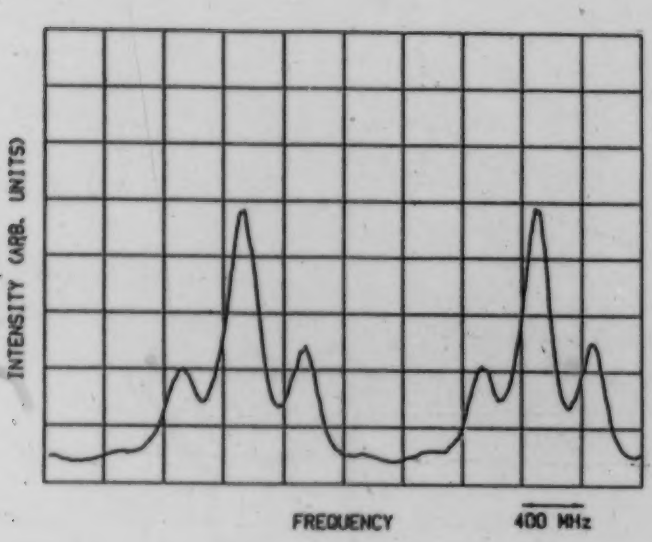

(c) $\Delta I_m = 1.5\ mA_{p-p}$

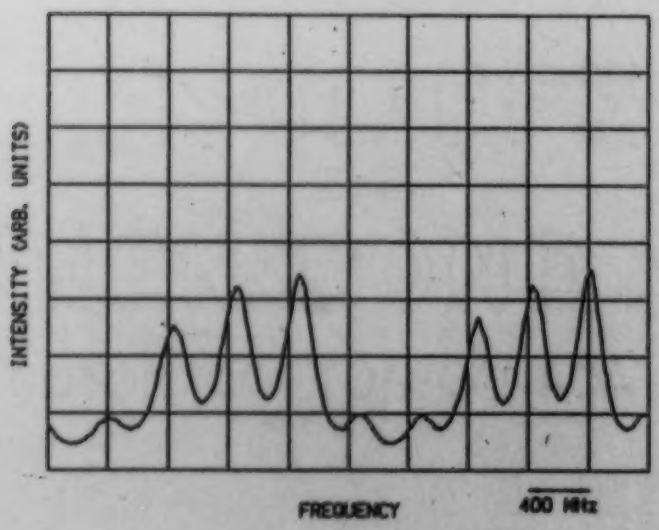

(d) $\Delta I_m = 2\ mA_{p-p}$

Fig. 4.6 Continued

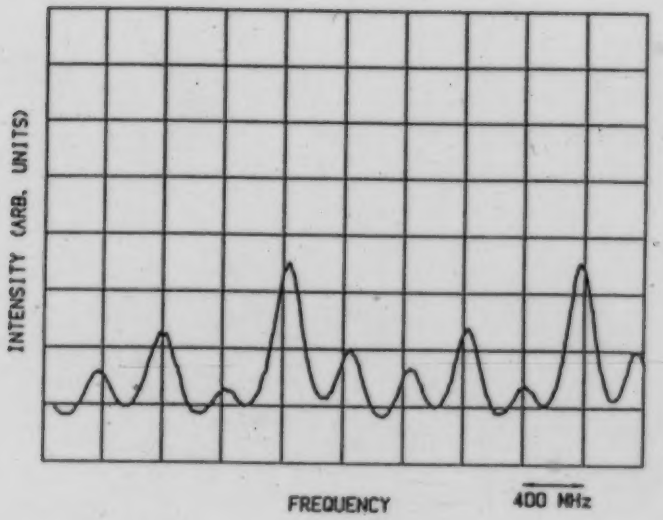

(e) $\Delta I_m = 2.5\ mA_{0\text{-}p}$

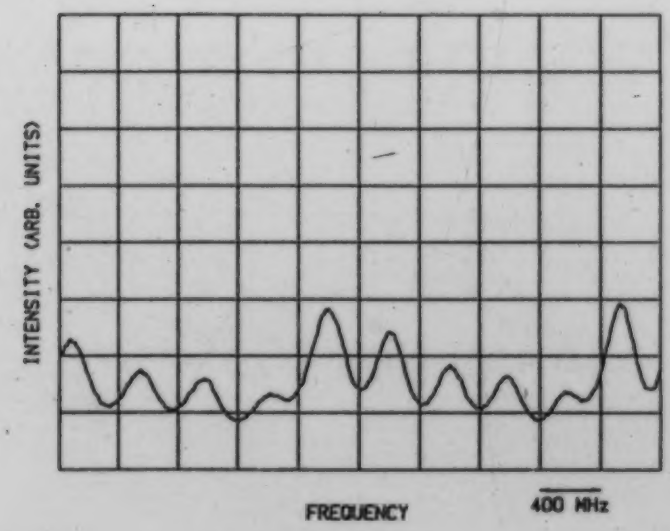

(f) $\Delta I_m = 3\ mA_{0\text{-}p}$.

Fig. 4.6 Continued

was larger than the lower sideband amplitude as expected. The amplitude of the optical carrier started to decline as the modulation current was increased. When the modulation current was equal to 2.8 mA, the optical carrier disappeared which corresponds to the frequency modulation index β approximately equal to 2.405. The maximum frequency deviation could be determined by Eq. (4.3) and was found to have the value 962 MHz for this situation. When the modulation current was increased further, the optical carrier increased again and the amplitude of the sidebands started to decrease.

To demonstrate that FM really took place in the GRECC laser, the measured normalized amplitude for the optical carrier and the first and second sidebands is plotted as Fig. 4.7 and the results are compared with the Bessel functions of the first kind. The solid and the dotted lines represent the values of the zeroth, first and second order of the Bessel functions of the first kind. Discrete points represent the experimental results obtained from the optical carrier, first and second sideband. To eliminate the effect due to IM, the intensity of matching upper and lower sidebands was averaged. The coefficient of the normalized amplitude can be obtained by taking the square root of such normalized averaged-sideband intensity [57]. In most cases, the modulated power spectra shows asymmetry. This has been explained in the previous section as the result of spurious intensity modulation. The lower sideband was enhanced in the low modulation frequency region whereas the upper sideband was enhanced in the high frequency region.

A static frequency shift was also realized when the DC bias was incremented by 1 mA. Fig. 4.8 shows the spectra obtained with two different bias currents. In the figure, trace "a" corresponds to the power spectrum obtained with 28 mA and trace "b" is the result with 29 mA. As the DC current was changed from 28 mA to 29 mA, the resonant frequency shifted to a lower frequency. This is obvious because the laser wavelength increases with a higher DC bias. The maximum frequency

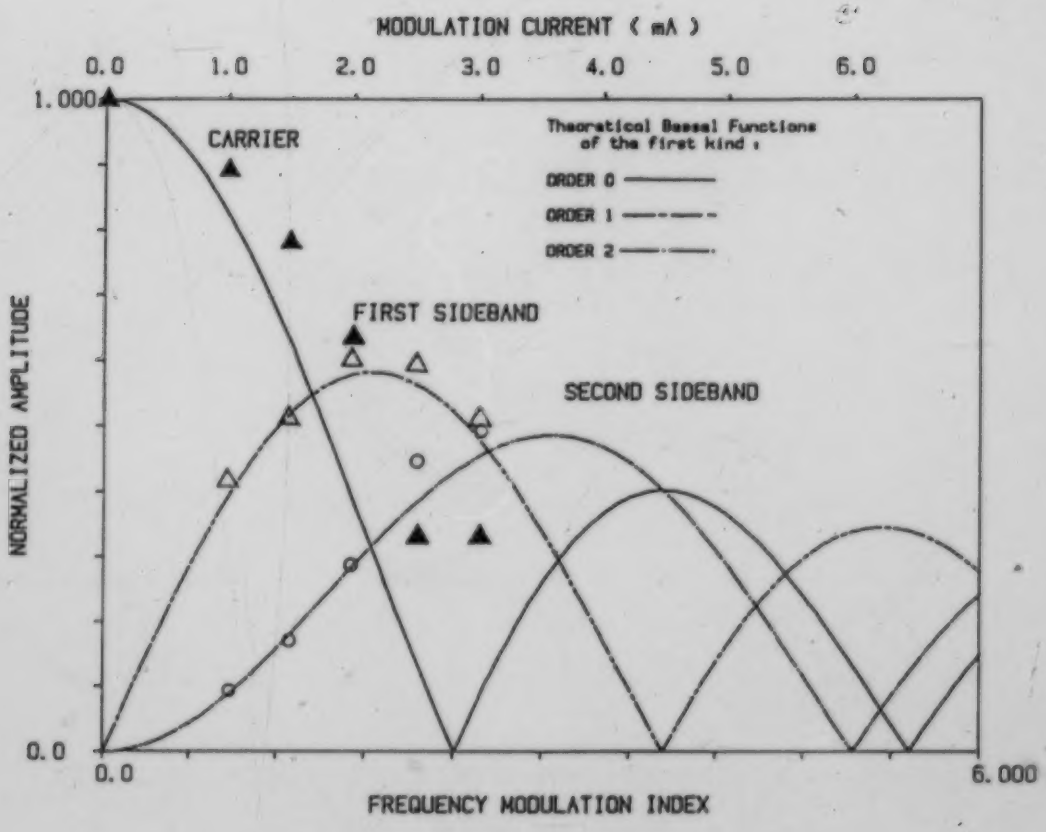

Fig. 4.7 Normalized amplitude for optical carrier and various sidebands as a function of modulation current ΔI_m and frequency modulation index β. Lines show the theoretical value of the Bessel functions of the first kind and symbols show the experimental results. Carrier :▲, first sideband :△, second sideband : ○.

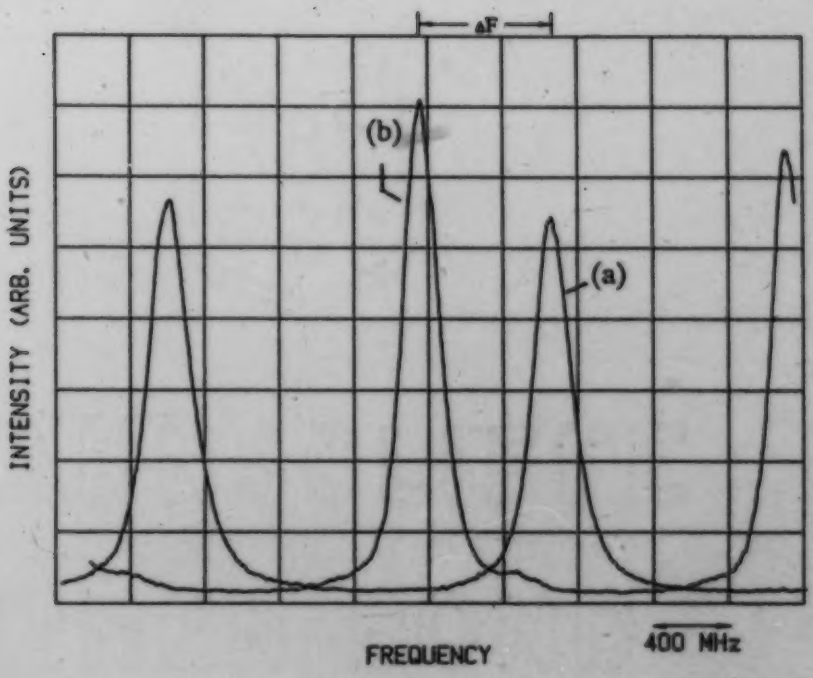

Fig. 4.8 Static frequency deviation for the 10% coated GRECC laser when I_{bias} was changed from 28 mA to 29 mA. Trace (a) : I_{bias} = 28 mA. Trace (b) : I_{bias} = 29 mA.

deviation ΔF can be obtained readily from the separation between the two resonant peaks of the spectrum.

No attempt was made to obtain data in the intermediate modulation frequency range between 40 MHz and 400 MHz because of inadequate resolution of the Fabry-Perot interferometer.

4.4 DISCUSSION

4.4.1 MODULATION EFFICIENCY

Before a laser can be used as a direct frequency modulated source, its characteristics in terms of the normalized modulation efficiency[9] have first to be determined.

The frequency modulation efficiency of the GRECC laser as measured in the present work is shown in Fig. 4.9. Each point in the figure was determined by four parameters, namely the DC bias, sinusoidal modulation frequency, magnitude of the modulation current and the maximum frequency deviation ΔF observed from the modulated power spectra.

The DC bias current affects the frequency deviation especially in the high modulation frequency region. An increase in the DC bias increases the intensity of the optical field, which clamps the quasi-Fermi level tighter and reduces the distribution of the carrier density modulation [60]. Therefore, the efficiency is less. The resonant frequency is expected to increase with a higher DC bias, a fact that can be inferred from Fig. 4.9 even though the resonant peaks were not observed at the attempted frequency range.

In an optical FSK transmission system, the optical source is usually modulated between two optical frequencies by superimposing a two-level digital signal on the bias current. The V-shaped characteristic, which is typical for most

[9] It is also sometimes referred to as FM response or the modulus of the current-to-frequency modulation transfer function (CF-MTF).[64]

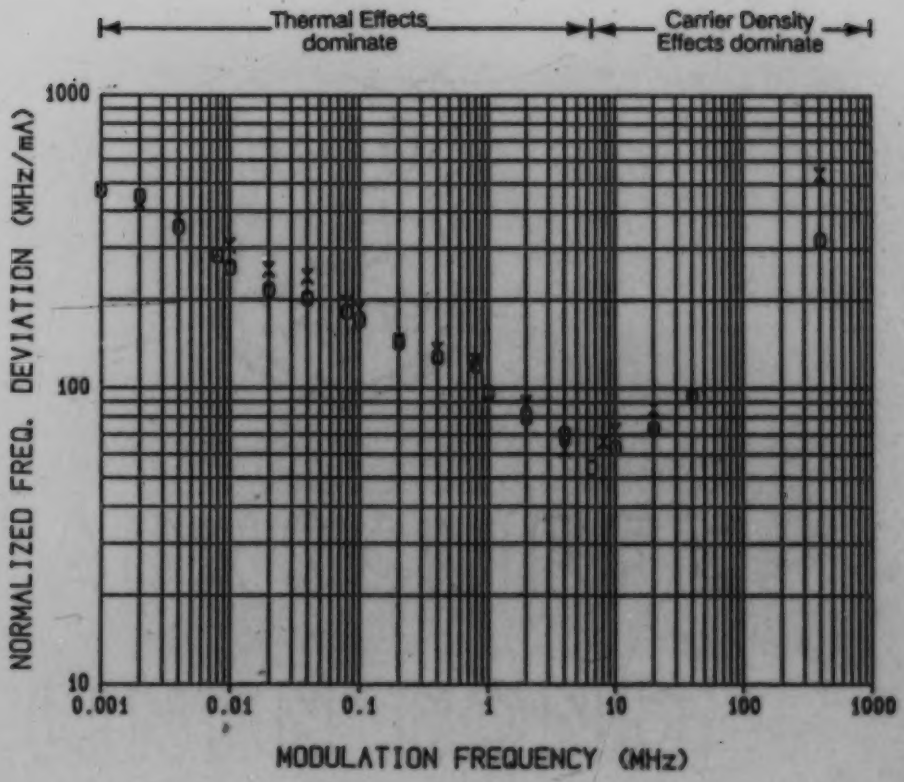

Fig. 4.9 Normalized frequency deviation for the 10% coated GRECC laser versus modulation frequency. O : I_{bias} = 28 mA, X : I_{bias} = 25 mA.

buried heterostructure semiconductor lasers, is shown in Fig. 4.9. This non-uniform response would be expected to cause impairment to high speed FSK transmission, particularly when the modulating signal contains long strings of 1's or 0's.

In order to realize the thermal and carrier density effect on optical FSK transmission, we modulated the laser with a square wave message signal with $\Delta I_m <$ 1 mA_{o-p} at (a) 1 Mbit/s and (b) 22.5 Mbit/s. A fiber Fabry-Perot interferometer[10] was used as a frequency discriminator to demodulate the original square wave signal. The output from the interferometer was detected by a high speed photodiode and could be observed with a real time oscilloscope. Fig. 4.10(a) shows the square wave modulated laser current at 1 Mbit/s. Fig. 4.10(b) depicts the demodulated waveform, showing distortion in the received signal. The observed long rise time of the demodulated waveform was due to the thermal effect, which has been dominant below 6.5 MHz in our experiment (Fig. 4.9). Since the frequency shift caused by the high frequency components of the drive current was opposite in phase with that caused by the low frequency components, the overall output did not resemble the original modulating laser current. In high bit rate FSK transmission, long 1's or 0's , which introduces finite rise time of the resultant waveform, are certainly undesirable. The laser current, shown in Fig. 4.11(a), was modulated with a square wave signal at 22.5 Mbit/s. A ringing pattern was observed in the laser current due to the frequency response of the laser driver. Fig. 4.11(b) shows the demodulated signal. Since thermal effects were negligible at these high frequencies, the output exactly follows the modulating current. At these high frequencies the carrier density effect dominates and determines the FM characteristics for the laser. The above experiments have shown the influence of FM noise on the frequency modulation characteristic of the laser. In both cases, the

[10] See Section 5.4.1, this thesis.

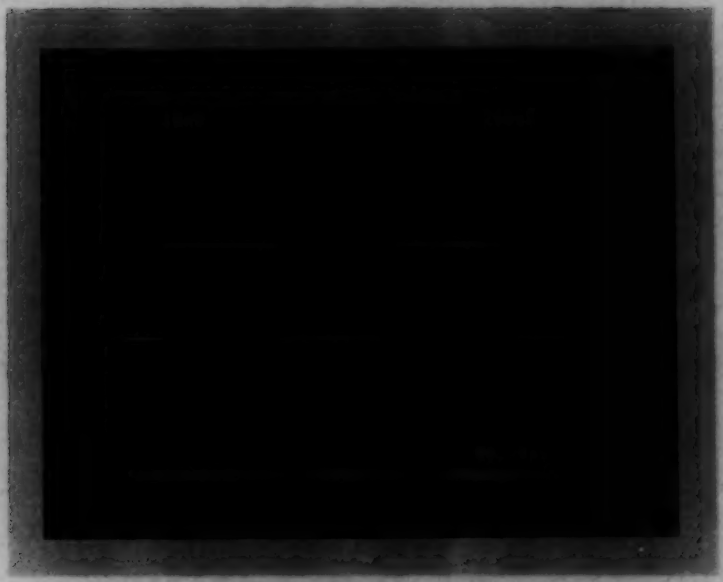

(a)

(b)

Fig. 4.10 Effect on 1 Mbit/s FSK modulation due to both thermal and carrier density effects. (a) laser current signal and (b) demodulated waveform using an optical frequency discriminator which shows a finite risetime.

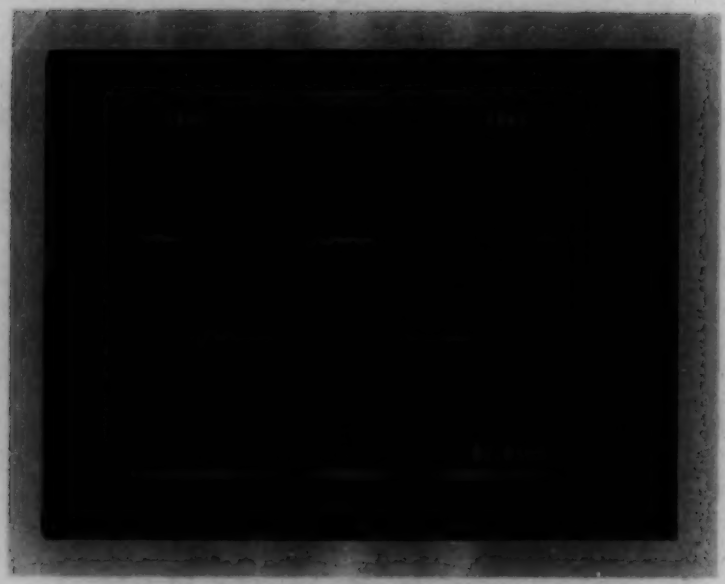

(a)

(b)

Fig. 4.11 Effect on 22.5 Mbit/s FSK modulation primarily due to carrier density - effect. (a) laser current signal and (b) demodulated waveform.

FM noise was converted to baseband noise after demodulation which would result in a high bit-error-rate in the transmission.

The non-uniform FM response can be compensated using techniques such as pre-equalization [62]-[63] of the modulation signal or by using Manchester coding (also known as bi-phase encoding) [65] to avoid long strings of 1's or 0's. Electrical feedback [13] has also been shown to both substantially linearize the non-uniform FM response at modulation frequencies below 10 MHz and to reduce the FM noise.

4.4.2 OTHER MODULATION FORMATS

Two other types of periodic modulation format, triangular and square wave[11] modulation, were also considered.

The same experimental set-up was used as shown in Fig. 4.2. In order to easily compare the spectra, the laser temperature, magnitude of the modulating current and the modulation frequency were kept the same in all three cases. The laser current was biased at 1.3 times the threshold current and the modulating current was 1.8 $mA_{o\text{-}p}$ at 200 kHz.

Spectra for the three modulation formats are shown in Figs. 4.12-4.14. All spectra were asymmetric with enhanced lower sideband envelopes. The smoothest spectrum, shown in Fig. 4.13, was observed for triangular wave modulation. This modulation should have produced a rectangular spectrum but the observed deviation from this shape was no doubt caused by the spectral components arising from the unwanted intensity modulation that always results when the laser current is changed. In the case of FSK modulation, the spectrum would be expected to be centered on two frequencies, that is $f_o + \Delta F$ and $f_o - \Delta F$. In Fig. 4.14, the observed spectrum was centered on these two frequencies with deviations which are due to

[11] Also known as optical frequency shift keying (FSK) modulation.

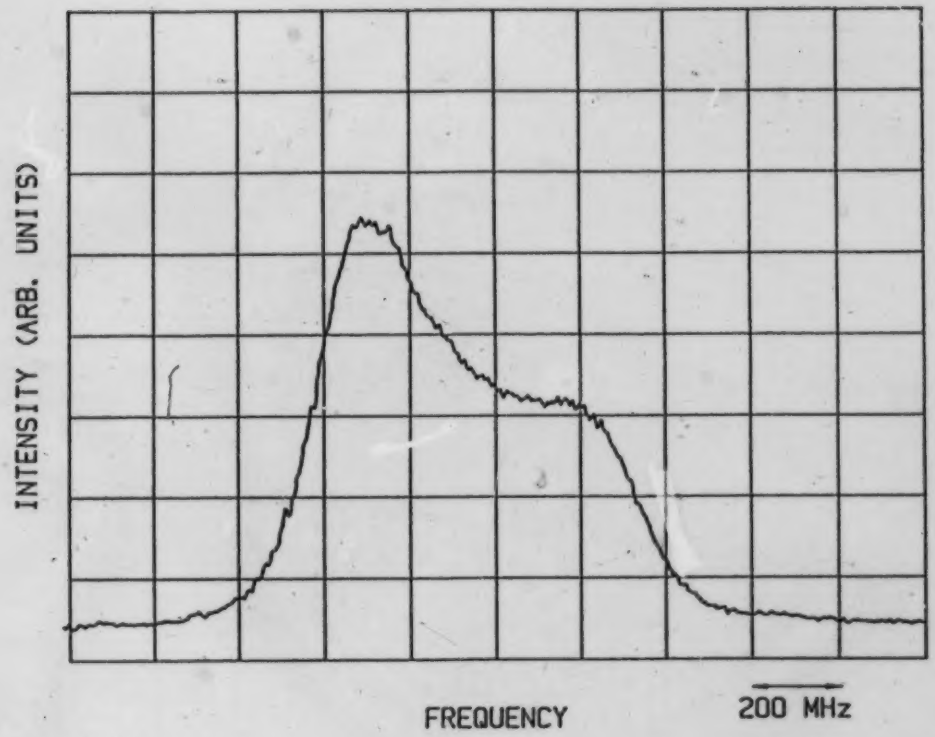

Fig. 4.12 Sinusoidal modulated laser spectrum for the 10% coated GRECC laser with I_{bias} = 26 mA, f_m = 200 kHz and ΔI_m = 1.8 mA.

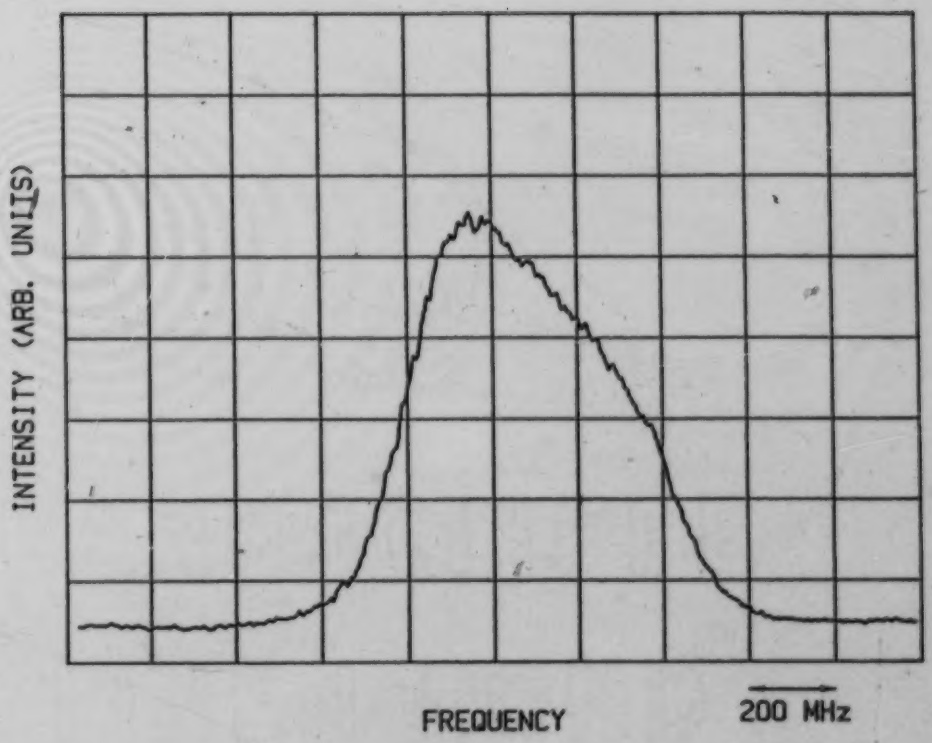

Fig. 4.13 Triangular-wave modulated laser spectrum for the 10% coated GRECC laser with I_{bias} = 26 mA, f_m = 200 kHz and ΔI_m = 1.8 mA.

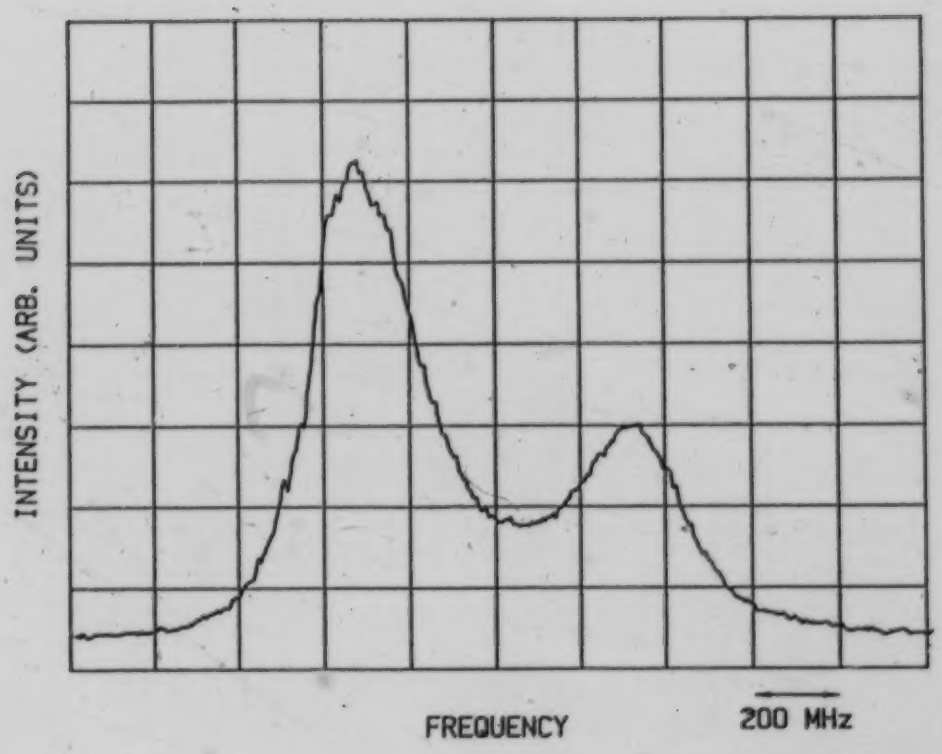

Fig. 4.14 Square-wave modulated laser spectrum for the 10% coated GRECC laser with I_{bias} = 26 mA, f_m = 200 kHz and ΔI_m = 1.8 mA.

the intensity modulation, finite linewidth of the laser and the non-uniform FM response of the BH laser.

4.5 SUMMARY

In summary, the spectral properties of single mode semiconductor lasers under injection current modulation have been described in this chapter.

In the theoretical analysis, the power spectra include the influence of a combined intensity, frequency modulation as well as the phase delay. The skewness of the power spectra also reveals the strong effect of IM on the FM spectral shape and modulation characteristics.

The modulation capability of the GRECC semiconductor laser has been determined experimentally. The thermal and carrier density effects, which are opposite in phase, determine the frequency modulation capability of semiconductor lasers. We have demonstrated how these two mechanisms determine the high speed FM response of an optical FSK system. An experimental investigation of the power spectra with sinusoidal, triangular and square wave (FSK) modulation was also presented.

An understanding of the frequency modulation capability for a GRECC laser is essential before we attempt to describe the additional effects that are caused by including electrical feedback. These additional effects will be described in the following chapter.

CHAPTER 5

ELECTRICAL FEEDBACK ON GRECC LASER

5.1 INTRODUCTION

Chapters 3 and 4 show that the GRECC laser can oscillate in a single longitudinal mode and can be modulated. Therefore, this laser is suitable as the basic source in a configuration having electrical feedback control of the linewidth.

Quantum FM noise, originating from the coupling between carrier density and photons as described in Sect. 2.3.2, does not reveal itself when direct optical detection is used. However, this FM noise can be detected with an optical frequency discriminator such as a Michelson interferometer or Fabry-Perot interferometer in which the frequency modulation fluctuations are converted into amplitude modulation fluctuations. An electrical feedback system is realized by counter-modulating the laser with the amplitude modulation fluctuations mentioned above using a classical negative feedback control method. Fig. 5.1 shows a block diagram of the experimental set-up [66]. The negative feedback alters the optical frequency of the laser to minimize the linewidth. Successful operation depends on the GRECC laser having a high frequency modulation efficiency.

The scheme is quite similar to that for frequency stabilization used by other authors [67]-[68], in which the oscillation frequency of the laser is locked to some external frequency reference such as an absorption spectral line of a gas. Again, the error signal is extracted and fed back to counter-modulate the laser injection current or temperature. The only difference between these two systems is that line narrowing demands a very large feedback bandwidth.

Fig. 5.2 depicts the second approach [69] using electrical feedback. The idea is to combine the light of the laser under test with a stable master laser so that the beat frequency can be detected by a high speed detector and amplified with a high

THE MATERIAL INVOLVED HAS BEEN REMOVED BECAUSE OF THE UNAVAILABILITY OF COPYRIGHT PERMISSION

Fig. 5.1 Block diagram of electrical feedback configuration using optical direct frequency discrimination detection [66].

THE MATERIAL INVOLVED HAS BEEN REMOVED BECAUSE OF THE UNAVAILABILITY OF COPYRIGHT PERMISSION

Fig. 5.2 Block diagram of electrical feedback configuration using optical heterodyne frequency discrimination detection [69].

frequency amplifier. The feedback signal contains the FM noise of both lasers and therefore requires a *very stable* master laser which might make the design more complicated.

A recent article using the second approach for electrical feedback stabilization is based on two 0.8 μm AlGaAs single mode lasers [70] which were simultaneously used to :

a) stabilize the center frequency of field spectrum,

b) reduce the linewidth and FM noise,

c) lock the frequency offset to another coherent source (master laser) and to

d) provide stable and wideband frequency sweeping.

The master laser, being line-narrowed by the first scheme, can pass its ultra-high coherence properties or any desired frequency offset/sweep onto the slave laser through the latter scheme. This system is particularly useful when used as the optical source in a coherent Frequency Division Multiplexing System (FDM) because a wideband, tunable, line-narrowed, optical frequency synthesizer can all be realized with a single slave laser.

The results of the author's theoretical and experimental studies on the characteristics of FM noise and linewidth reduction of the GRECC laser with electrical feedback will be reported in this chapter. The servo-control system will be described and characterized and the theoretical limits of the linewidth reduction scheme will be derived and explained. The experimental results will be compared to both theoretical formulations and results appearing in the literature.

5.2 PRINCIPLES OF OPERATION

It has been pointed out in Sect. 2.3.1 that spontaneous emission events in semiconductor lasers are the direct cause of the FM noise. However, this FM noise level can be reduced by the use of electrical feedback. The purpose of this section is

to describe qualitatively how the servo-control system performs the FM noise reduction. The description in the following sections is based on the author's experimental set-up which was identical to the first model of electrical feedback as described in Sect. 5.1 except that a GRECC laser, instead of a DFB laser, was used in our experiment.

We assume that the phase noise causes the optical frequency of the laser to increase. In order to restore this frequency to its original value, we alter the laser current using a wideband feedback system. Such a system utilizes direct injection current modulation and thus alters the carrier density to produce the desired frequency deviation. We have already described in Chapter 4 how a decrease in laser current would cause a reduction in the optical frequency due to the carrier density effect. A Fabry-Perot interferometer and an inverting pre-amplifier were used to generate a feedback control signal which was proportional to the slope of the transmittance curve of the interferometer as shown in Fig. 5.3. An increase in optical frequency increases the transmittance which results in a decrease in the pre-amplifier output due to its inverting characteristic. The instantaneous laser current is reduced and the laser frequency is pulled back to its center frequency. A similar control principle applies when the laser tries to oscillate at a lower frequency.

5.3 THEORY

In this section, we will consider the theory for an electrical feedback system to control laser frequency. The following derivation is based mainly on the paper by Ohtsu *et al.* [66]. We will discuss the bandwidth required for the feedback system and the minimum linewidth that can be achieved.

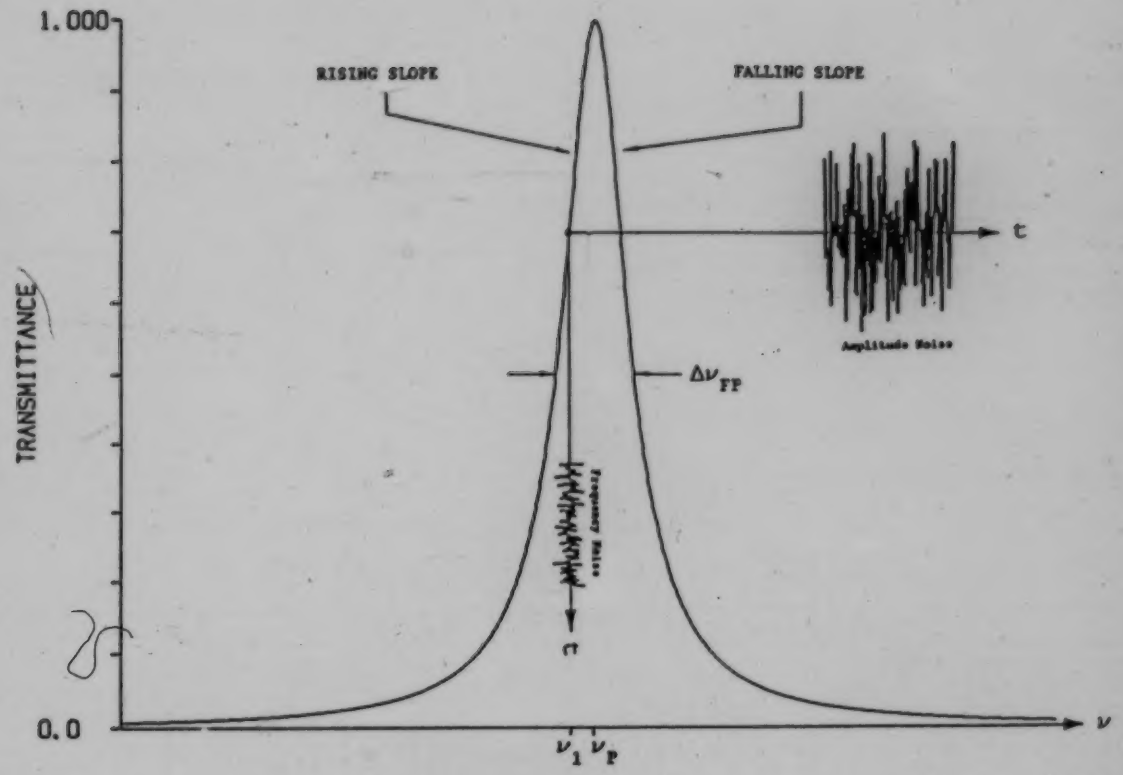

Fig. 5.3 Analytical model for the transmittance curve of the Fabry-Perot interferometer used as an optical frequency discriminator, showing how frequency noise is converted to amplitude noise by this detection.

5.3.1 BANDWIDTH ESTIMATION

The optical field of the laser can be expressed by

$$E(t) = E_o \exp[j\{2\pi\nu_o t + \psi(t)\}] \tag{5.1}$$

where ν_o is the center oscillation frequency, E_o is the peak amplitude of the optical field and $\psi(t)$ represents the phase fluctuations.

The frequency fluctuations $\delta\nu(t)$ can be derived from the phase fluctuations using

$$\delta\nu(t) = \frac{1}{2\pi}\frac{d\psi(t)}{dt}, \tag{5.2}$$

or in terms of their noise spectra

$$S_f(f) = f^2 S_\psi(f) \tag{5.3}$$

where $S_f(f)$ and $S_\psi(f)$ are the FM noise and phase noise spectrum respectively.

It has been pointed out in Eq. (2.8) that the linewidth broadening arises from the 'flat portion' of the frequency noise spectrum near DC. By using electrical feedback, it is expected that the FM noise spectrum be reduced by a factor of g where g is proportional to the loop gain [66]. Therefore,

$$S_f(f) = \begin{cases} S_f(0)/g & , (f \le f_c) \\ S_f(0) & , (f > f_c) \end{cases} \tag{5.4}$$

where $S_f(0)$ is the FM noise spectrum at DC and f_c is the cutoff frequency of the servo-control system. It is apparent that the bandwidth of the electrical feedback system should extend from DC to a frequency approximately f_c.

It is well known that the solitary laser linewidth $\Delta\nu_{SOL}$ is proportional to $S_f(0)$ and is given by

$$\Delta\nu_{SOL} = \pi S_f(0) \quad . \tag{5.5}$$

Hence, the linewidth under feedback $\Delta\nu_{FB}$ can be expressed as

$$\Delta\nu_{FB} = \Delta\nu_{SOL}/g \quad . \tag{5.6}$$

In order to estimate the spectral linewidth of the laser under feedback conditions, we obtain the autocorrelation function $R_E(\tau)$ of the optical field which can be obtained similarly to Eq. (2.15),

$$\begin{aligned} R_E(\tau) &= \langle E(t+\tau)E^*(\tau)\rangle \\ &= E_o^2 \exp[j2\pi\nu_o\tau - \langle\delta\psi^2(\tau)\rangle/2] \\ &= E_o^2 \exp[j2\pi\nu_o\tau - 2(\pi\nu_o\tau)^2\sigma_y^2(\tau)] \end{aligned} \tag{5.7}$$

where $\langle\ \rangle$ denotes ensemble average, * represents the complex conjugate and $\sigma_y^2(\tau)$ is the Allan variance of the frequency fluctuations[12].

From Eq. (5.4), the Allan variance under electrical feedback conditions can be expressed as [66]

$$\sigma_y^2(\tau) = \begin{cases} S_f(0)/2g\tau\nu_o^2 & ,(\tau \geq 1/\pi f_c) \\ S_f(0)/2\tau\nu_o^2 & ,(\tau < 1/\pi f_c) \quad . \end{cases} \tag{5.8}$$

The lineshape can be derived from Eq. (5.7), and is given by

$$I(\nu) = 4\int_0^\infty R_E(\tau)\cos(2\pi\nu\tau)d\tau \quad . \tag{5.9}$$

[12]The Allan variance $\sigma_y^2(\tau)$ is a time domain measure of the frequency stability. It is the second order moment for frequency fluctuations relative to the center frequency and is usually expressed as $\langle\delta\nu^2\rangle/\nu_o^2$ or $\langle\delta\psi^2(\tau)\rangle/(2\pi\tau\nu_o)^2$

THE MATERIAL INVOLVED HAS BEEN REMOVED BECAUSE OF THE UNAVAILABILITY OF COPYRIGHT PERMISSION

Fig. 5.4 Relationship between the linewidth obtained by electrical feedback and the bandwidth of the feedback system [66].

The spectral lineshape and FWHM linewidth under feedback conditions can be obtained by solving Eqs. (5.7) to (5.9). Fig. 5.4 [66] shows the relationship between this linewidth and the cutoff frequency for the feedback. It was reported [66] that as $f_c > \Delta\nu_{SOL}$, $\Delta\nu_{FB}$ will approach a constant value. This suggests that an alternative to a very large bandwidth amplifier in the feedback experiment is to have high gain in the feedback loop.

5.3.2 MINIMUM DETECTABLE LINEWIDTH

The noise, mainly due to the detector and feedback amplifier, decreases the performance of the FM noise reduction circuit. The ultimate linewidth is limited by the minimum detectable FM noise signal that the control circuit can respond to.

We will lock the laser frequency on the maximum rising slope of the Fabry-Perot transmittance curve as shown in Fig. 5.3. The power fluctuation δP incident into the detector can be described as

$$\delta P = P_i \delta T_{FP}(\nu) + T_{FP}(\nu)\delta P_i , \tag{5.10}$$

where P_i is the incident power into the Fabry-Perot interferometer, $T_{FP}(\nu)$ is the transmittance at frequency ν, $\delta T_{FP}(\nu)$ is the amplitude fluctuation due to FM-IM conversion and δP_i is the fluctuation of the input power.

For simplicity, we will assume that intensity fluctuations are very small compared to frequency fluctuations. Thus, Eq. (5.10) becomes [66]

$$\delta P \simeq P_i \delta T_{FP}(\nu) . \tag{5.11}$$

If a Lorentzian approximation for the transmittance curve is assumed,

$$T_{FP}(\nu) = \frac{(\Delta\nu_{FP}/2)^2}{[(\nu-\nu_r)^2+(\Delta\nu_{FP}/2)^2]} . \tag{5.12}$$

Here, $\Delta\nu_{FP}$ is the FWHM transmittance for the Fabry-Perot Interferometer and ν_r is the resonant frequency.

The maximum slope of Eq. (5.12) can be obtained by locating the point of inflection of the Lorentzian curve. We assume that the slope at ν_1 is the same in the vicinity as well so that the fluctuations in the transmittance can be written by the following differential [66]

$$\delta T_{FP} = \frac{3\sqrt{3}}{4\Delta\nu_{FP}}\delta\nu \tag{5.13}$$

where $\delta\nu$ is the frequency fluctuations. The FWHM $\Delta\nu_{FP}$ of a Fabry-Perot cavity can be expressed in terms of its optical length nL and mirror reflectivities R and is given by

$$\Delta\nu_{FP} = \frac{c}{2nL}\frac{1-R}{\pi\sqrt{R}} . \tag{5.14}$$

Using Eqs. (5.13) and (5.14), Eq. (5.11) can be written as

$$\delta P = \frac{3\sqrt{3}\pi}{2}\frac{nL}{c}\frac{\sqrt{R}}{1-R}P_i\delta\nu \tag{5.15}$$

The detector noise determines the minimum detectable change in the laser output power, δP_{min}, using [28]

$$\delta P_{min} = \sqrt{16 P_D P_N} \tag{5.16}$$

where $P_D = P_i T_{FP}(\nu)$ is the power incident on the detector and P_N is the detector noise power which can be expanded into

$$P_N = FkTB + h\nu_o B/\eta \tag{5.17}$$

where B is the measurement bandwidth, kT is the thermal noise energy, $h\nu_o$ is the photon energy, F is the detector noise figure, and η the quantum efficiency. The minimum detectable noise from the detector thus becomes

$$\delta P_{min} = \sqrt{\{16[FkBT + h\nu_o B/\eta][P_i T_{FP}(\nu)]\}} \tag{5.18}$$

Therefore, the minimum detectable FM noise signal $\delta\nu_{min}$ can be calculated when Eq. (5.15) and Eq. (5.18) are equal. This happens when the signal-to-noise ratio (S/N) is equal to one.

Re-arranging the terms, we get an expression for a minimum detectable $\delta\nu$, denoted as $\delta\nu_{min}$, with

$$(\delta\nu_{min})^2 = \frac{16\ [c(1-R)]^2\ (FkTB + h\nu_o B/\eta)}{9\pi^2\ (nL)^2\ R\ P_i} \tag{5.19}$$

The FWHM linewidth of the laser can be related to the frequency fluctuations by the following [72]

$$\Delta\nu = \{\pi\nu_o^2\sigma_y^2(\tau)\}/2B\ . \tag{5.20}$$

By substituting Eq. (5.17) into Eq. (5.18), we obtain the minimum linewidth under electrical feedback $\Delta\nu_{FBmin}$ as given by [66,72]

$$\begin{aligned}\Delta\nu_{FBmin} &= \{\pi(\delta\nu_{min})^2\}/2B \\ &= \frac{8\ [c(1-R)]^2\ (FkT + h\nu_o/\eta)}{9\pi\ (nL)^2\ R\ P_i}\end{aligned} \tag{5.21}$$

Eq. (5.21) represents the minimum linewidth that can be achieved with electrical feedback, assuming that the detector noise is the limiting factor.

In this section, we have described the design criteria for the electrical feedback system based on the minimum linewidth that can be achieved. In order to obtain narrow linewidth, a low-noise photodetector and a high reflectivity Fabry-Perot interferometer should be used. High optical output power may also result in linewidth reduction.

5.4 EXPERIMENTAL SET-UP

The experimental set-up for the electrical feedback laser frequency controller is shown in Fig. 5.5. The GRECC laser was biased at 1.7 times the threshold current and its output beam was collimated through an optical isolator with a 0.23 pitch AR-coated GRIN-ROD lens. This isolator provided an optical isolation of 25 dB for light going back into the laser cavity. A second GRIN-ROD lens focused the light into a 3 dB single mode fiber coupler. In addition to splitting the light for measurement purposes, the first 3-dB fiber coupler was found useful as a mode stripper to suppress cladding modes other than the fundamental mode supported by the fiber. Moreover, it could be butt-coupled into the Fiber-Fabry-Perot interferometer directly from its output fiber without using other optical components since they are both single mode fibers. The unused input portion of this fiber-coupler was dipped into index matching fluid to avoid any additional standing wave interference.

The same laser driver was used as in the direct frequency modulation experiment. In the following sections, we will discuss and characterize the rest of the components in more detail.

5.4.1 FIBER-FABRY-PEROT INTERFEROMETER (FFPI)

Due to the large bandwidth required of all components in the feedback system, the delay time of the feedback loop has to be as short as possible. A

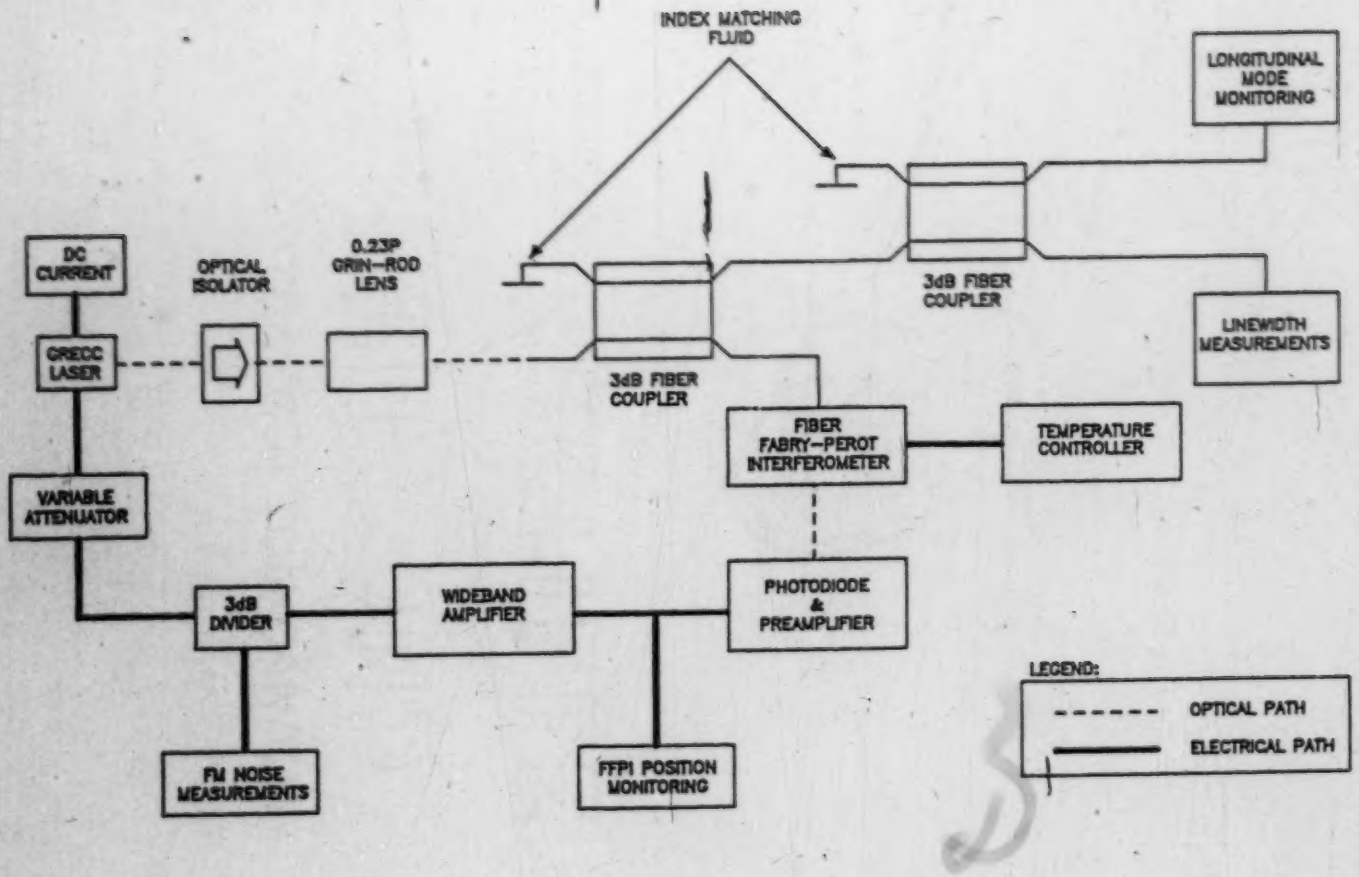

Fig. 5.5 Experimental set-up for the electrical feedback with the GRECC laser.

conventional parallel plate Fabry-Perot interferometer requires long collimating optics which result in an instrument of about 1 meter in length. The optical transit time in such an instrument is too long for the present experiment. Therefore, in order to decrease the delay time, we built a miniature temperature-scanned interferometer using a 1 cm. length of single mode fiber.

5.4.1.1 THEORY OF A TEMPERATURE-SCANNED FFPI

A fiber-Fabry-Perot interferometer has an advantage over a conventional Fabry-Perot interferometer in that it does not require bulky optics. Its compactness and reduced device volume enables environmental control. The FFPI is found very useful in applications such as optical spectrum analyzers, optical tunable filters and interferometric sensors.

Most FFPIs use either piezo-electric devices or a temperature controller to change the optical length of the fiber [73]-[77]. Here, we are concerned with a temperature controller and will now present a theoretical analysis of the transmittance behavior of the FFPI as a function of temperature.

Consider a single mode fiber of length L and reflectivity R at both ends. The round trip phase shift ϕ can be expressed by

$$\phi = \frac{4\pi nL}{\lambda} \tag{5.22}$$

where λ is the wavelength in vacuum and n is the refractive index of the fiber.

Using the same derivation as for Fabry-Perot etalons [78], we obtain the normalized transmittance, T_{FFP}, of a FFP as follows

$$T_{FFP} = \frac{(1-R)^2}{(1-R)^2+4R\sin^2(\phi/2)} \tag{5.23}$$

It is obvious from Eq. (5.23) that the transmittance T_{FFP} is strongly affected by the round-trip phase shift ϕ and has a value of unity whenever the phase shift ϕ is a multiple of 2π. The separation between two such unity transmissions is known as the free spectral range (FSR) and is expressed very often in terms of frequency, $\Delta\nu_{FP} = c/(2nL)$, where c is the speed of light.

A temperature change δT, which alters the optical length of the fiber, introduces a phase change $\delta\phi$ given by

$$\delta\phi = \frac{4\pi}{\lambda}\left(n\frac{dL}{dT} + L\frac{dn}{dT}\right) - \frac{4\pi nL}{\lambda^2}\frac{d\lambda}{dT}\delta T \qquad (5.24)$$

Since it is assumed that the laser emits a single wavelength, we can neglect the last term in the above equation. Thus

$$\delta\phi = \frac{4\pi}{\lambda}\left(n\frac{dL}{dT} + L\frac{dn}{dT}\right)\delta T \qquad (5.25)$$

Here $(1/L)(dL/dT)$ represents the relative thermal expansion coefficient of the fused silica for the FFPI which is about $4\times10^{-7}/°C$ and $(1/n)(dn/dT)$ is approximately $6.89\times10^{-6}/°C$ [79]. Since the free spectral range is achieved when the phase changes by 2π, we calculate the corresponding temperature change ΔT using Eq. (5.25). With λ = 1.314 mm, L = 10.9 mm and n = 1.45, ΔT is approximately equal to 5.6 °C and a FSR $\Delta\nu_{FSR}$ = 9.5 GHz is obtained.

The finesse *F*, a measure of the resolution of the FFPI, is defined as

$$F = \frac{\pi\sqrt{R}}{1 - R} \qquad (5.26)$$

and the limiting resolution of this instrument $\Delta\nu_{1/2}$ (the FWHM value) is

$$\Delta\nu_{1/2} = \frac{\Delta\nu_{FSR}}{F} \quad . \tag{5.27}$$

The finesse F can also be read directly from the transmittance curve by measuring the ratio of the FSR to $\Delta\nu_{1/2}$ for the resonance peak. Assuming a reflectivity of 90% in our case, an *instrument finesse* of 28 is expected.

Fig. 5.6 shows a calculated normalized transmittance curve of the FFPI as a function of temperature with the reflectivity R as a parameter using Eq. (5.23). We should point out that in our model, we do not consider the loss due to fiber attenuation because we expect that the loss is almost negligible for this short fiber length. In order to provide good frequency discrimination for the FM noise, a large finesse is required which can be realized by high reflectivity coatings.

5.4.1.2 FFPI EXPERIMENT

The FFPI set-up is shown in Fig. 5.7. The resonator was prepared from a piece of 10.9 mm long single mode fiber with its plastic protective jacket carefully removed. Both ends of the fiber had to be polished and the end faces made perpendicular to the fiber axis. High reflective mirrors could be obtained by coating those polished ends with dielectric materials. The coatings consisted of five $\lambda/4$ layers of Zinc Sulphide (ZnS) alternating with four $\lambda/4$ layers of Thorium Tetrafluoride (ThF_4). With these alternating coatings, a mirror reflectivity of at lease 90% was expected.

The coated fiber was placed on a copper block containing a V-groove holder machined to 165 μm deep. Both ends of the V-groove were made wider to ensure that the fiber ends were not tilted due to imperfections at the ends of the V-groove. We then covered the copper block with a similar one in order to provide a

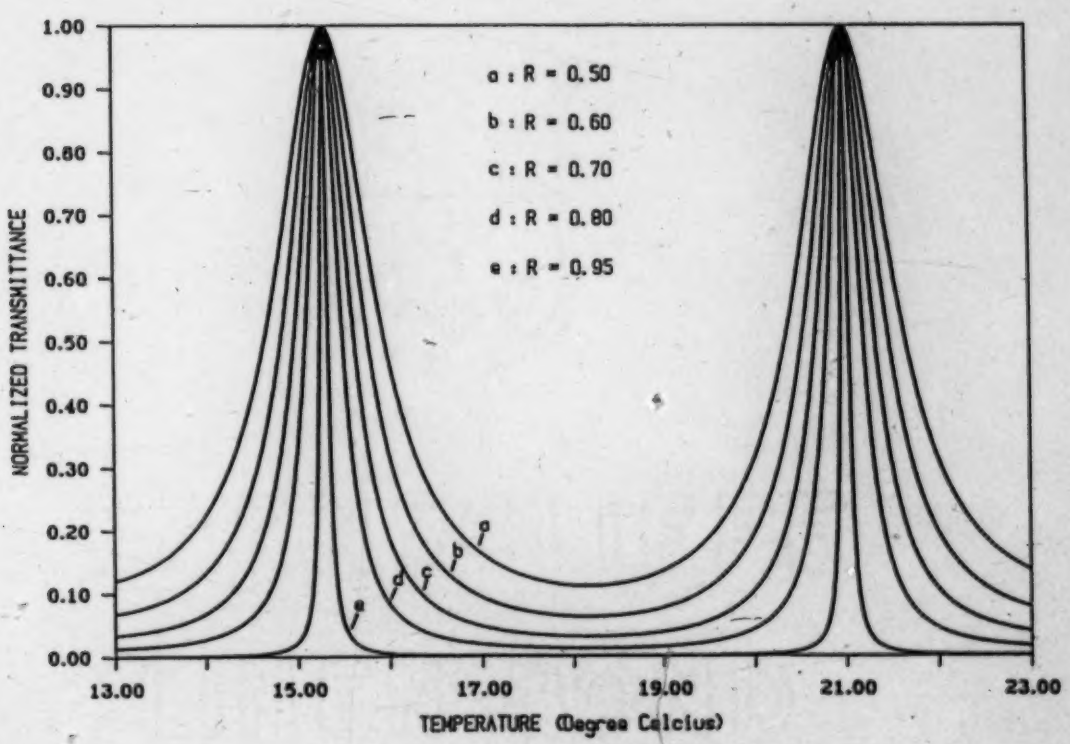

Fig. 5.6 Computer simulations showing the normalized transmittance curve of the fiber Fabry-Perot interferometer as a function of temperature with mirror reflectivity R as a parameter.

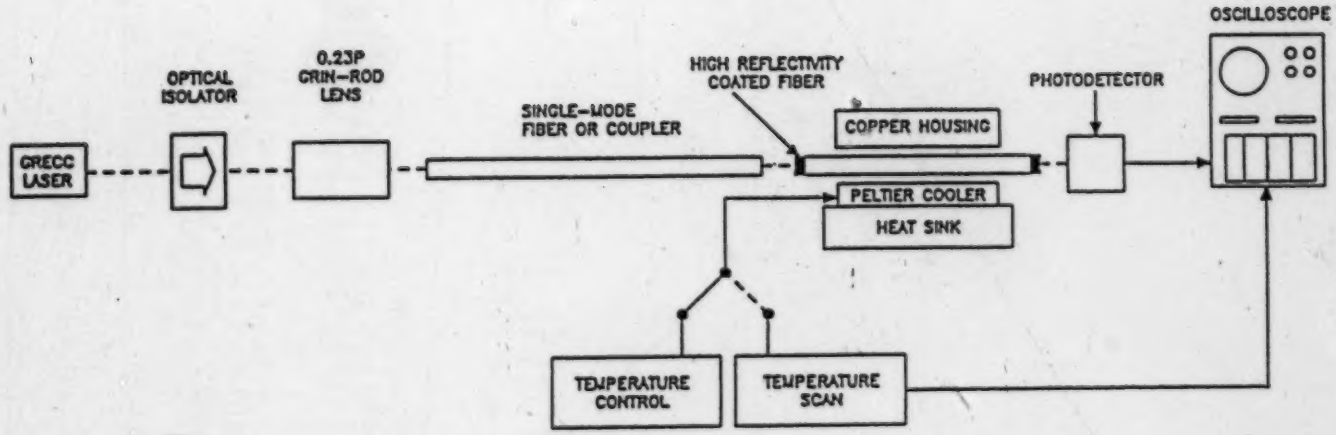

Fig. 5.7 Experimental arrangement for characterizing the fiber Fabry-Perot interferometer.

homogeneous temperature environment and some mechanical protection for the coated fiber. By purposefully controlling the temperature of the entire device (copper blocks and fiber), a FPPI is obtained that functions as a temperature-tuned optical spectrum analyzer.

The temperature control unit comprised a Peltier cooler, proportional-integral-differential (PID) feedback control circuit and a thermistor which was buried inside the copper housing. This controller could be set to stabilize and maintain the temperature of the copper housing to an accuracy of about $\pm 5 \times 10^{-3}$ degree Celcius. This thermal stability is particularly important because if the transmittance varies due to thermal fluctuations, the feedback signal will be erroneous. With the PID feedback disconnected, the steady rise in temperature of the FFPI permitted the unit to be used as a scanning optical spectrum analyzer.

Because a precise digital thermometer was not always available to measure the transmittance of the FFPI with respect to temperature, the temperature change was determined from the potential drop across the thermistor. A Fluke 2190A digital thermometer with Cu/Constantine thermocouple was used in the initial calibration. It had 0.1 °C resolution and an accuracy of ±0.3 °C. It also provided an analog output of 1 mV per degree Celcius. Fig. 5.8 (a) and (b) show the change of temperature of the FFPI and the voltage drop across the thermistor respectively versus time. A direct relationship between the thermistor potential and instantaneous temperature of the FFPI could be obtained from these two figures. It can be concluded from Fig. 5.9 that the thermistor voltage is inversely proportional to the temperature of the FFPI. Therefore the transmittance of the FFPI could readily be related to the potential difference across the thermistor.

Fig. 5.10 shows the free spectral range (FSR) of an optical spectrum as obtained with the FFPI. Experimentally a finesse of only 7 was achieved instead of 28 as calculated in Sect. 5.4.1.1. This finesse reduction may be related to the

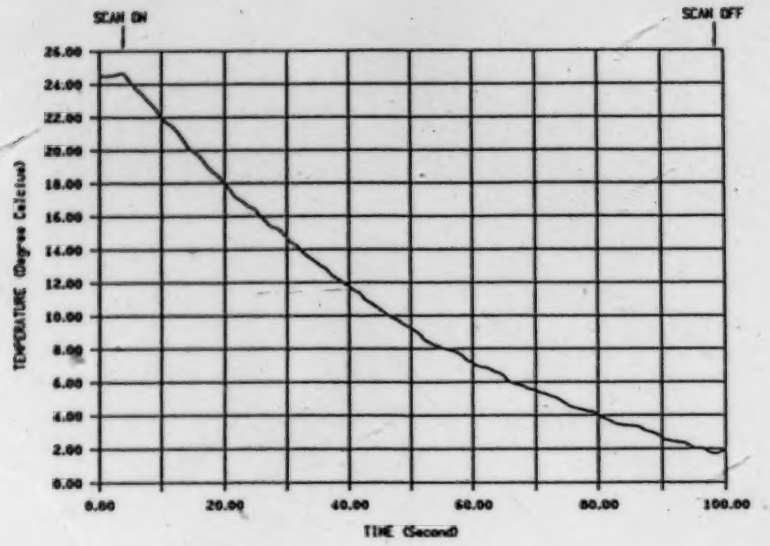

(a)

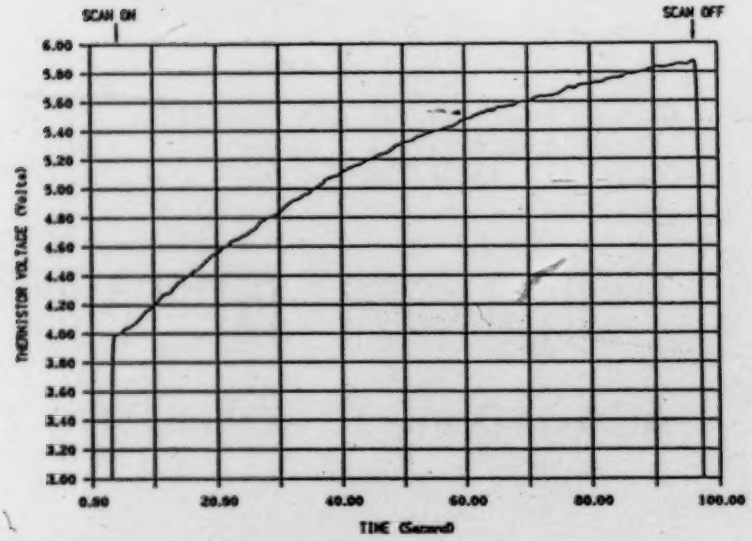

(b)

Fig. 5.8 Characterization of the temperature controller. (a) Temperature changes in the fiber Fabry-Perot interferometer as a function of time when the scan is on. (b) Corresponding change in the thermistor voltage as a function of time.

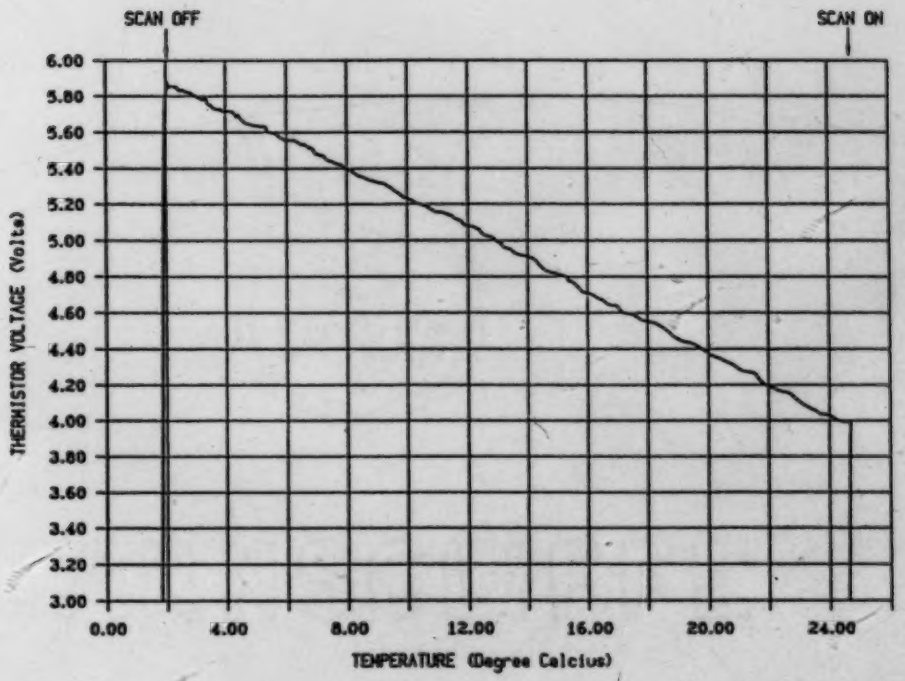

Fig. 5.9 Linear relationship between the thermistor voltage and the temperature drop during the scan.

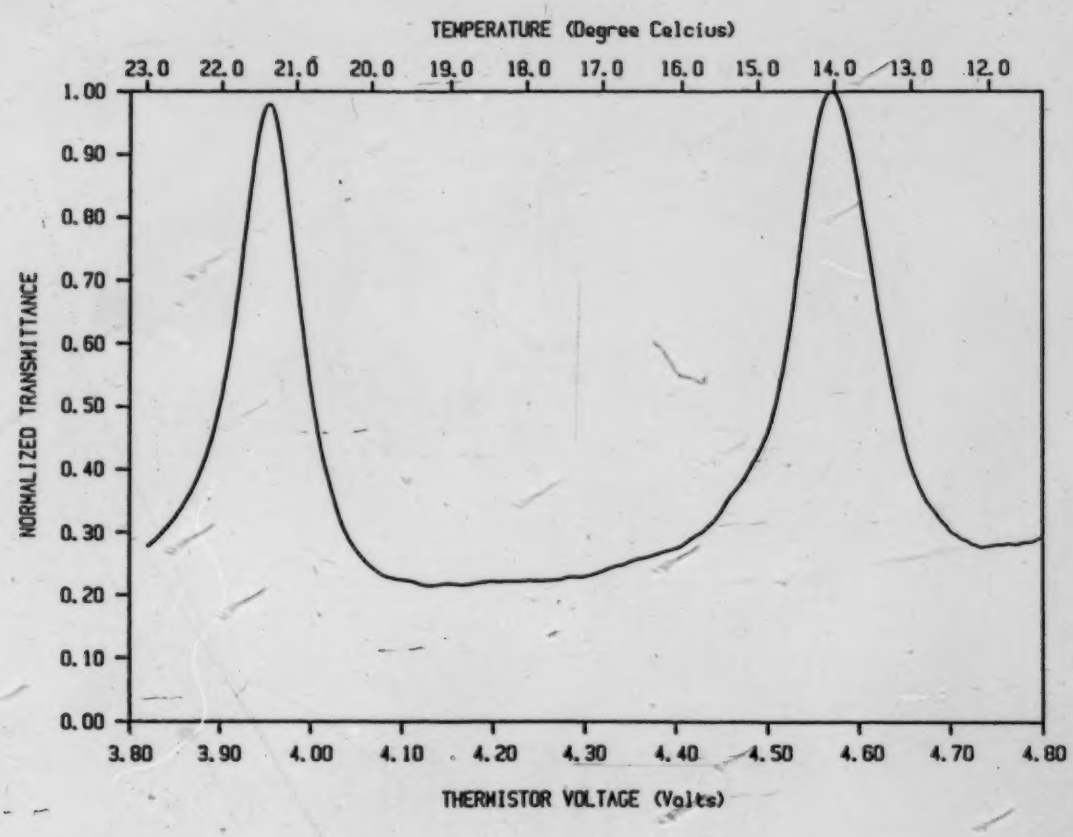

Fig. 5.10 Transmittance curve of the fiber Fabry-Perot interferometer as a function of thermistor voltage and temperature.

accuracy of the $\lambda/4$ coating process, the mismatch of the linear polarization in successive passes [76] or the imperfect alignment of the set-up. Since the length of the coated fiber was 10.9 mm, the free spectral range as determined by the separation between the two resonance peaks was calculated to be 9.5 GHz. In order to scan across two resonance peaks, a temperature difference of 7.5 °C was required which is close to the theoretical estimate, based on the thermal expansion coefficient, of approximately 5.6 °C. This deviation can be explained by the fact that a portion of each fiber end was not covered by the temperature-controlled copper housing, in order to achieve better alignment.

The frequency discrimination characteristics of the FFPI are illustrated in Figs. 5.11 to 5.12. The optical frequency of the GRECC laser was locked onto the rising-slope of the FFPI by adjusting the temperature of the control unit. Fig. 5.11(a) shows the power spectrum for a single mode laser as measured by a parallel plate scanning Fabry-Perot interferometer. The transmittance of the FFPI output in Fig 5.11(b) shows slight fluctuations because of the FM noise of the single mode laser. In Fig. 5.12(a), the GRECC laser oscillates in a multimode condition. Large frequency jumps due to mode hopping within the laser are converted into large amplitude fluctuations by the FFPI as shown in Fig. 5.12(b). This mode hopping phenomenon is very useful in the FFPI alignment process because we can adjust the position between the fiber and the FFPI without scanning the temperature of the FFPI. So, when a large amplitude fluctuation is observed, it indicates approximate alignment.

5.4.2 PHOTODETECTOR AND PREAMPLIFIER

A compact photo-detector unit was used to observe the intensity fluctuation in the output signal at the output of the FFPI. This detector was a RCA C30979E InGaAs 1.3 to 1.5 μm photodiode having a quantum efficiency of approximately

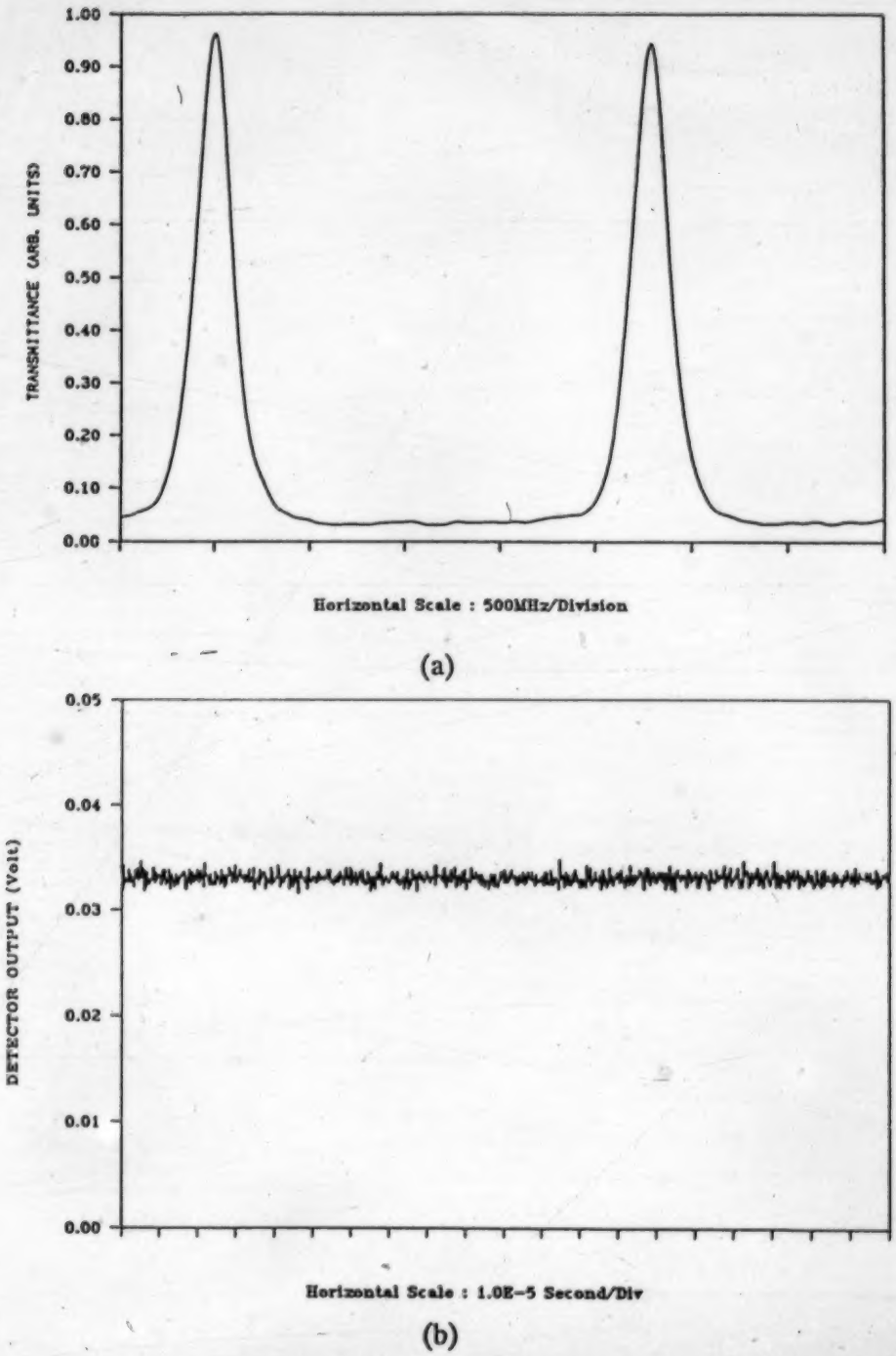

Fig. 5.11 (a) : Single mode power spectra for a 10% coated GRECC laser obtained from a scanning parallel plate Fabry-Perot interferometer with two spectral orders shown. (b) : Single mode frequency noise as detected from the fiber Fabry-Perot interferometer.

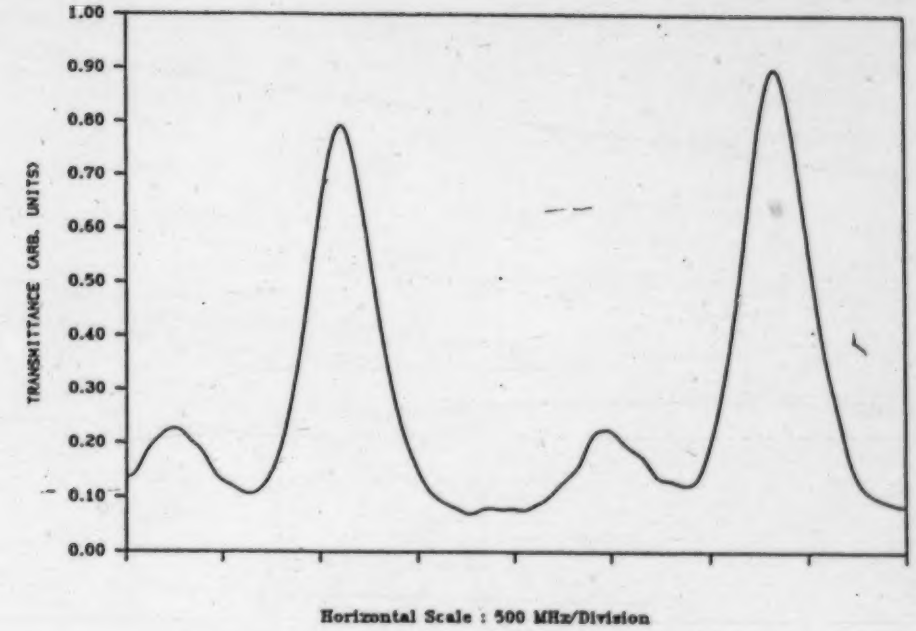

(a)

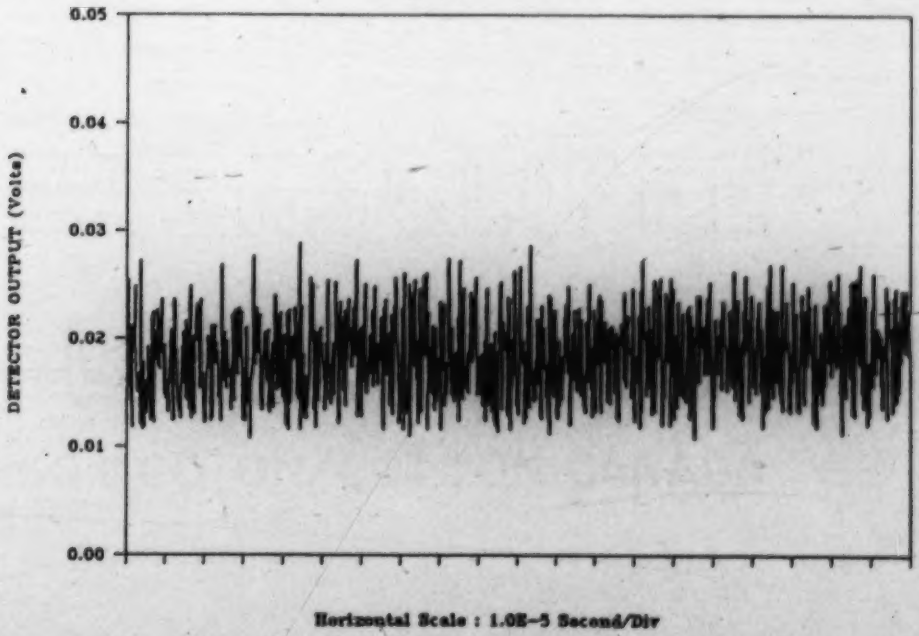

(b)

Fig. 5.12 (a) : Multimode power spectra for a 10% coated GRECC laser obtained from a scanning parallel plate Fabry-Perot interferometer, showing two spectral orders. (b) : Frequency jumps due to mode hopping as obtained from the fiber Fabry-Perot interferometer in the non-scanning operation.

60%. This photodiode was connected to an inverting wideband operational amplifier (Comlinear CLC103AI) connected as a transimpedance amplifier with a flat gain response from DC to 100 MHz. The laser frequency was locked onto the maximum slope of the FFPI transmittivity curve as indicated in Fig 5.3 so that the error signal would become phase-reversed because of the inverting characteristics of the pre-amplifier.

5.4.3 WIDEBAND AMPLIFIER

Another wideband amplifier was necessary to supply enough gain for the detected error signal so that there would be sufficient frequency correction through current injection. It has been pointed out in the theoretical section that the feedback gain has a substantial effect on the FM noise reduction factor, provided that the feedback bandwidth is adequate.

The wideband amplifier was composed of three Avantek monolithic silicon IC amplifiers (MSA-0335-2X) with each input and output matched to 50 ohms. The magnitude response of this amplifier was obtained by means of an impulse testing technique [80]. The 0.1 μF chip blocking capacitors used between the three stages resulted in a lower cutoff frequency of 35 kHz. The overall bandwidth was approximately 1 GHz and the gain was 37 dB. Fig. 5.13 shows the magnitude response of the calibrated amplifier.

5.5 MEASUREMENT SYSTEMS

This section will describe several major measurement and real-time monitoring systems that were incorporated into the experimental set-up. In full operation, the following four monitoring and measurement systems were required simultaneously.

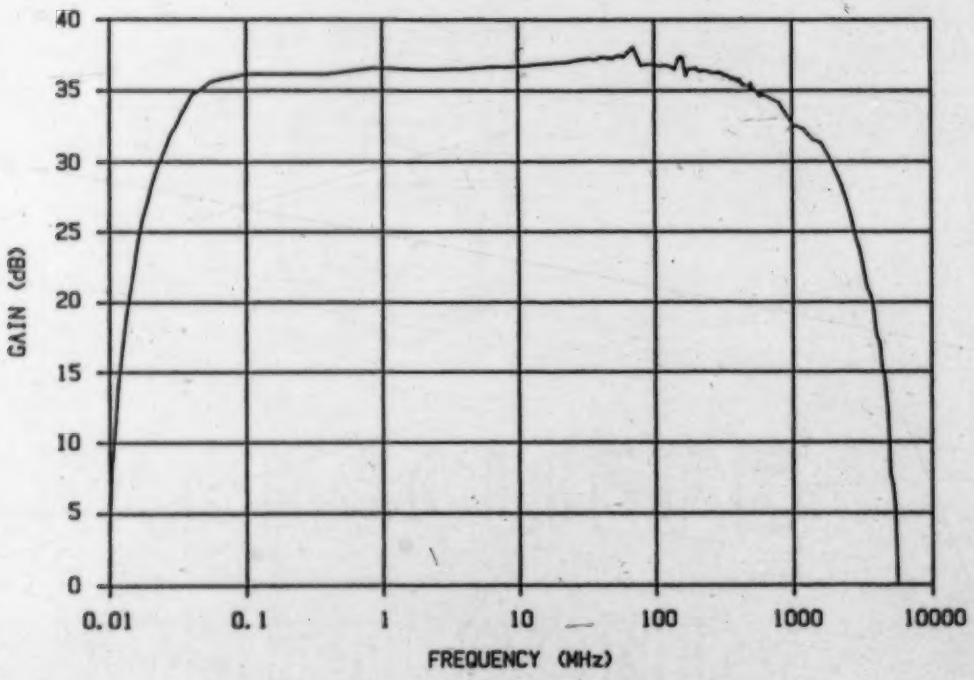

Fig. 5.13 Magnitude response of the wideband amplifier.

5.5.1 LONGITUDINAL MODE MONITORING

The purpose of this monitoring was to ensure that the GRECC laser was still oscillating in a single longitudinal mode when electrical feedback was applied. The line profile monitoring was realized using a scanning parallel-plate Fabry-Perot interferometer and the overall arrangement was identical to that in Fig. 4.2 except that the signal generator was not connected. This monitoring was important because there were occasional fluctuations in the spectrum which could be due to mechanical instability or temperature fluctuation between the 10% coated GRIN-Rod lens and the laser diode, causing a phase mismatch and excitation of other side modes. Manual adjustment of the z-position of the GRIN-ROD lens with a piezo-electric drive was then required to suppress the unwanted sidemodes and thus restore single mode operation of the laser.

5.5.2 FFPI POSITION MONITORING

The efficiency of FM noise to AM noise conversion in the non-scanning operation of the FFPI depends strongly on where the laser frequency was locked along the transmittance curve. Since the position was sensitive to the temperature of the FFPI and the optical frequency which might be changed due to re-adjustment in the dominant mode, it's position had to be monitored. The problem was solved by scanning the FFPI with temperature once to see the shape of the transmittance curve; we then fixed the temperature when the output was on the maximum rising slope of the curve.

5.5.3 FM NOISE MEASUREMENTS

In order to observe the power spectrum of the FM noise with a spectrum analyzer, a 3-dB power divider was inserted at the output of the wideband amplifier. This power divider consisted of a 3-port resistor network which matched input and

output lines to 50 ohms. One of its output ports was connected to the spectrum analyzer where the power distribution of the FM noise in the frequency range of interest was displayed. The results concerning the FM noise reduction will be discussed in the following section.

5.5.4 LINEWIDTH MEASUREMENTS

The same delayed self-heterodyne set-up as described in Sect. 3.4.2 was used to measure the linewidth of the GRECC laser with electrical feedback applied. A 3 dB fiber coupler as shown in Fig. 5.5 was used to split some of the optical signal from the output of the electrically stabilized GRECC laser . The rest of the signal was used in the fiber Fabry-Perot interferometer for extracting the instantaneous FM noise signal, if any. The FWHM linewidth, which could be readily observed with the spectrum analyzer and the delayed self-heterodyne set-up, was a measure of the spectral quality of the GRECC laser with electrical feedback.

5.5.5 FEEDBACK DELAY MEASUREMENTS

The time delay in the electrical feedback system is important because excessive delay decreases the bandwidth of the FM noise reduction. A simple calibration system using a Tektronix 7S12 TDR/Sampler unit was devised as shown in Fig. 5.14(a) and (b) to measure the delay time in the feedback loop. We first connected a Tektronix S-52 pulse generator head to a S-4 Sampling head with two separate cables to obtain an input unit step response as in Fig. 5.15(a). We then removed the connections between the laser driver and attenuators in our electrical feedback system and inserted the system between the pulse generating head and the sampling head with the same cables as shown in Fig. 5.14(b). An output step response was obtained as depicted in Fig. 5.15(b) which was due to the FM-AM conversion from the FFPI. The delay time in the control loop could be obtained by

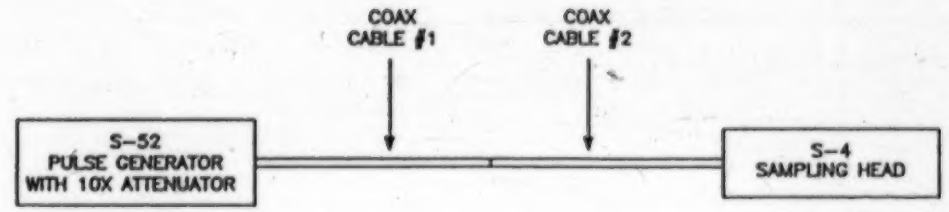

(a)

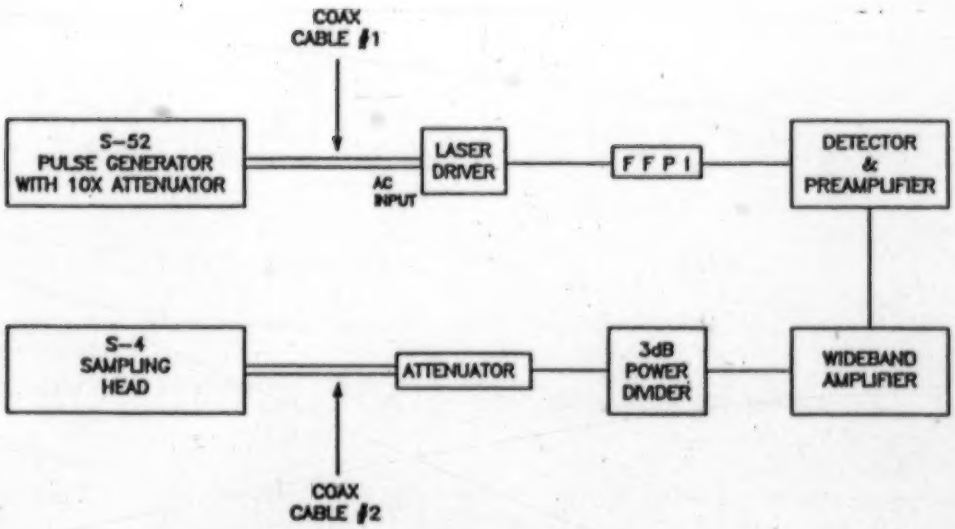

(b)

Fig. 5.14 Schematic diagram to measure the delay time in the feedback loop. (a) without electrical feedback. (b) with electrical feedback.

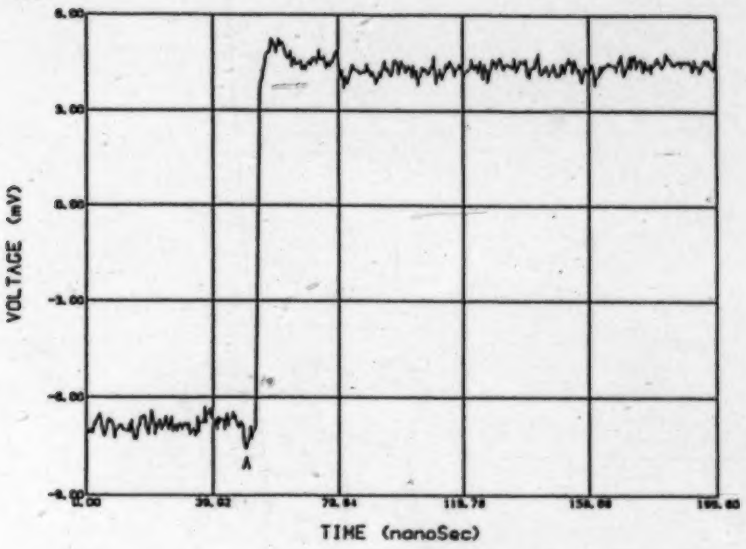

(a)

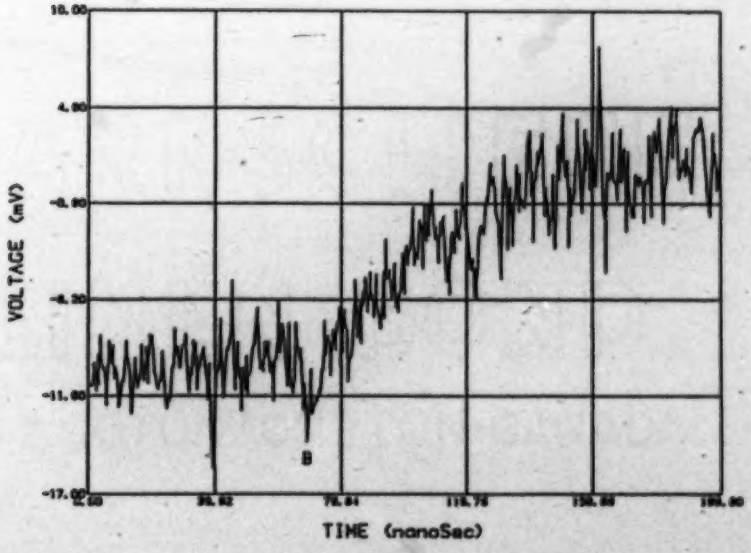

(b)

Fig. 5.15 Loop time delay measurement (a) : Sampling head output without electrical feedback. (b) : Sampling head output with electrical feedback. Loop delay time = $time_B$ - $time_A$

the time difference between B and A in Figs. 5.15(a) and (b). This output step response indicates severe roll off which was due to the influence of the thermal effect during frequency discrimination. The result was about 20 nanoseconds. Unfortunately, the loop time could not be further reduced because several bulky XYZ-micrometers were used in the experiment for precise light coupling which occupied some space.

5.6 RESULTS AND DISCUSSION

Fig. 5.16 (a) and (b) show the measured power spectra of the FM noise for a 10% far end coated GRECC laser with and without electrical feedback respectively. Measurements were carried out in the range from 0 to 60 MHz. The corresponding FM noise spectrum $S_f(f)$ was calibrated from the slope of the frequency discriminator (3.6mV/GHz) and the frequency response of the wideband amplifier (37dB gain) and is shown as the ordinate on the right hand side of Fig. 5.16. It was observed that the FM noise spectrum is almost *flat*, Fig. 5.16 (a), when electrical feedback was not connected. The flat spectrum was expected because the FM noise is considered to be white in the megahertz range as a result of spontaneous emission noise and carrier noise as shown in Fig. 2.4. When electrical feedback was applied, the average FM noise spectrum was reduced as shown in the lower trace of Fig. 5.16. However, the FM noise spectrum was enhanced at about 55 MHz due to the positive feedback of the servo-control system. The time delay in the feedback loop and the phase delay in each individual electronic component and between the intensity modulation and frequency modulation of the laser attributed to this positive feedback at 55 MHz.

A minimum linewidth of 7 MHz was obtained with electrical feedback as shown in Fig. 5.17. Without electrical feedback, the minimum linewidth of the GRECC laser was 8.5 MHz as depicted in Fig. 3.13. The same solitary HLP 5400

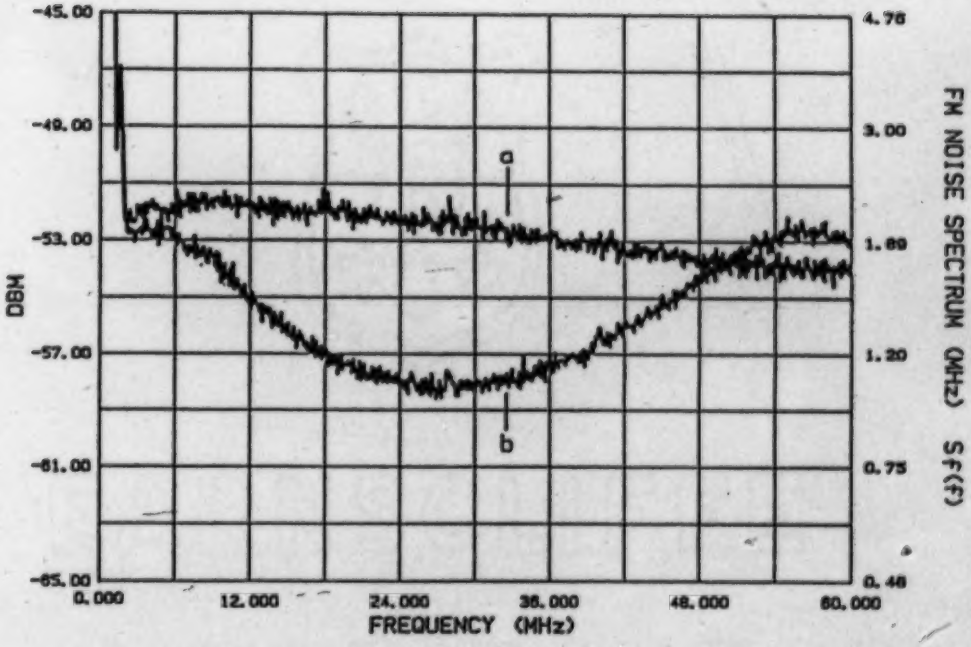

Fig. 5.16 FM noise spectrum for the 10% coated GRECC laser with I_{bias} = 34 mA. Trace (a) : without electrical feedback. Trace (b) : with electrical feedback.

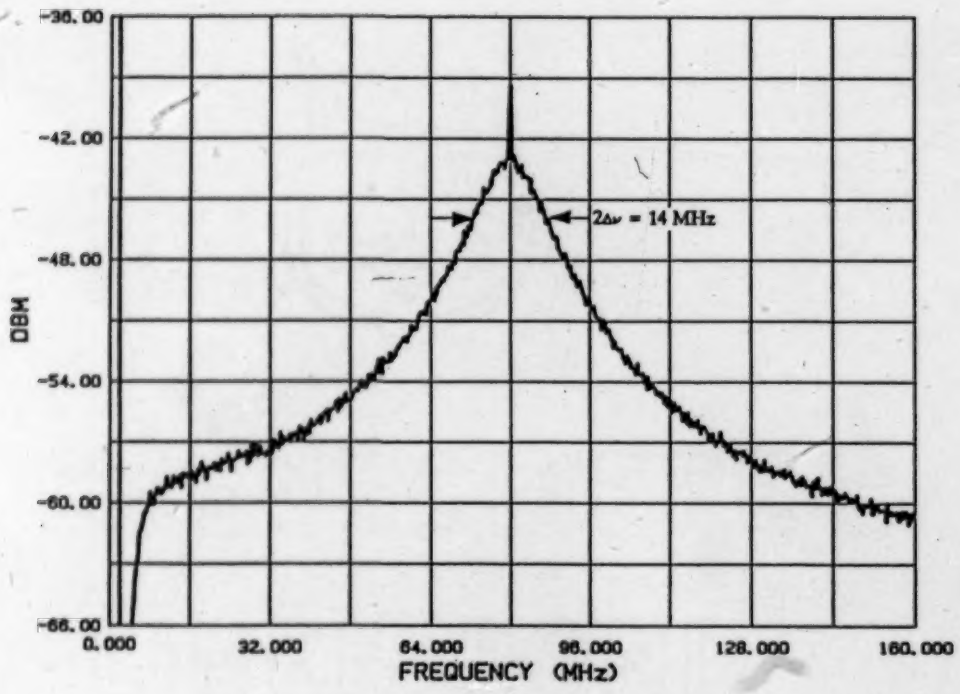

Fig. 5.17 Beat spectrum for the 10% coated GRECC laser with I_{bias} = 34 mA with electrical feedback.

laser has been reported to have a linewidth of 90 MHz [30] at the same output power of 2.6 mW for a single dominant mode. Thus, linewidth reduction has been shown to be possible with this *dual* feedback configuration!

We have shown in Chapter 2 that the white FM noise component is related to the linewidth. For trace (a), an average FM noise component of 1.9 MHz corresponds to a FWHM linewidth of 6 MHz using Eq. (2.8). Similarly, the average FM noise component under electrical feedback conditions is approximately 1.5 MHz, the linewidth was estimated to be 4.7 MHz. The linewidths that were converted from the measured FM noise spectrum were in close agreement with those measured directly from the delayed self-heterodyne set-up.

A similar observation for the FM noise spectrum for a DFB laser with electrical feedback had been reported [66]. Ohtsu *et al.* [66] observed a reduction of FM noise spectrum with enhancement behavior at certain frequencies which are also related to positive feedback. A minimum linewidth of 330 kHz at 3.5 times the threshold, with FFPI reflectivity of 90-95%, was obtained in their case.. Since electrical feedback was used simultaneously with optical feedback in our experiment, multimode oscillation occurred occasionally as a result of phase mismatch between the laser and external cavity. Therefore, we did not apply a larger bias current because frequency jumps were converted to very large amplitude fluctuation as shown in Fig. 5.12 which may may have caused irrecoverable damage to the laser.

In order to further reduce the linewidth , the finesse of the FFPI should be improved by increasing the reflectivity of the FFPI to more than 95% to ensure a better frequency discrimination. The copper housing of the FFPI should also be insulated from environmental temperature changes. Because temperature modulation is in opposite phase with carrier density modulation, it is difficult to reduce the FM noise spectrum by using just a proportional amplifier. To minimize

the detectable FM noise, it is likely that a more stringent requirement should be imposed on the frequency response and the noise floor of the pre-amplifier and wideband amplifier.

CHAPTER 6

CONCLUSION

This thesis has been concerned with reducing the linewidth and phase noise of a multimode semiconductor laser by using a *dual* electrical/optical feedback configuration. Optical feedback was realized with a GRECC (GRIN-ROD lens external coupled cavity) laser and electrical feedback used a FM noise dependent error signal.

A new approach has been presented for suppressing side modes of a multimode semiconductor laser using a far-end coated GRECC configuration. A SMS of *at least* 22 dB was achieved; the actual value being limited by the noise floor of the measurement system. A linewidth reduction from 90 MHz to 8.5 MHz was attained with a 10% far-end coated GRECC laser. With a 40% far-end coated GRECC laser, a further line narrowing to 4 MHz was observed. The GRECC laser was demonstrated to be capable of being frequency modulated by changing the injection current. The modulation was in accord with the conventional theory of frequency modulation which involves Bessel functions of the first kind. A frequency modulation efficiency of more than 65 MHz/mA was obtained for a 10% far-end coated GRECC laser. The modulation efficiency curve was observed to have a V-shape which can be attributed to temperature and carrier density effects. A SMS of at least 17 dB was preserved for the GRECC laser under the two separate conditions of high speed modulation and large signal modulation.

A miniature temperature controlled fiber Fabry-Perot interferometer (FFPI) was successfully developed. The device had a finesse of 7 and a physical length of 10.9 mm. A reflective coating was applied to both end of the polished ends of the fiber which resulted in a free spectral range of 9.5 GHz.

The electrical feedback system, when applied to a 10% far-end coated GRECC laser, has been demonstrated to reduce the linewidth from 8.5 MHz to 7 MHz. The corresponding average FM noise spectrum was reduced from 1.9 MHz to 1.5 MHz, which is in good agreement with the observed amount of linewidth reduction. However, an undesirable increase in the FM noise spectrum was observed at 55 MHz which was due to the positive feedback in the servo-control system.

Three overall conclusions resulting from this work on the dual feedback configuration of laser are as follows :

1) The far-end coated GRECC laser should be studied in more depth because it does show considerable promise for future applications[13]. In particular, the issues of mechanical stability and system performance in a coherent system are worthy of future research work.

2) The potential of the FFPI as a fiber-optic sensor should be investigated. Potential applications of this fiber interferometer include a temperature or pressure sensor, a scanning optical spectrum analyzer and a tunable optical filter.

3) The electrical feedback system has been shown to be promising to reduce both linewidth and FM noise. Further investigations should include the realization of a directly modulated transmitter with a DFB laser simultaneously with electrical feedback. Subsequent work on reducing the transit time in the feedback loop could concentrate on optoelectronic integration for the components in the feedback path.

[13]Present commercially available hermatically sealed packaged lasers have already utilized *AR-coated* on both sides of the GRIN-ROD lens to couple light into the pigtail fiber.

REFERENCES

[1] Y.Yamamoto and T.Kimura, "Coherent optical fiber transimssion systems," *IEEE J. Quantum Electron.*, Vol. QE-17, No. 6, pp 919-935, 1981.

[2] F.Favre *et al.*, "Progress towards heterodyne-type single mode fiber communication systems," *IEEE J. Quantum Electron.*, Vol. QE-17, No. 6, pp.897-906, 1981.

[3] T.Kimura, "Coherent optical fiber transmission," *J. Lightwave Technol.*, vol. LT-5, no. 4, pp.414-428, April 1987.

[4] R.A.Linke and P.S.Henry, "Coherent Communications," *Photonics Spectra*, pp.134-138, May, 1987.

[5] F.E.Goodwin, "A 3.39 μm infrared optical heterodyne communication system," *IEEE J. Quantum Electron.*, Vol. QE-3, No.11, pp.524-531, 1967.

[6] S.Saito and Y.Yamamoto, "Direct observation of Lorentzian lineshape of semiconductor laser and linewidth reduction with external grating feedback," *Electron. Lett.*, vol. 17, pp.325-327, April, 1981.

[7] O.Nilsson, S.Saito and Y.Yamamoto, "Oscillation frequency, linewidth reduction and frequency modulation characteristics for a diode laser with external grating feedback," *Electron. Lett.*, vol. 17, pp.589-591, Aug., 1981.

[8] G.Elze *et al.*, "Experiments on modulation properties and optical feedback chacteristics of laser diodes stabilized by an external cavity or injection locking," *J. of Lightwave Technol.*, vol. LT-2, pp.1063-1069, Dec., 1984.

[9] C.J.Nielson and J.H.Osmundsen, "Linewidth stabilization of semiconductor lasers in an external cavity, " *J. of Opt. Comm.*, vol. 5, pp.42-45, 1984.

[10] F.Favre and D.Le Guen, "FM noise and linewidth reduction in semiconductor laser coupled to a single-mode fiber resonator," IOOC-ECOC, pp.837-840, 1985.

[11] L.Goldberg *et al.*, "Spectral characteristics of semiconductor lasers with optical feedback," *IEEE Trans. on Microwave Theory and Techniques*, vol. MTT-30, No. 4, pp.401-409, April, 1982.

[12] M.Ohtsu and S.Kotajima, "Linewidth reduction of a 1.5 μm InGaAsP laser by electrical feedback," *Jpn. J. Appl. Phys.*, vol. 24, No. 4, pp.L256-L258, April, 1985.

[13] S.Saito, O.Nilsson and Y.Yamamoto, "Coherent FSK transmitter using a negative feedback stabilized semiconductor laser," *Electron. Lett.*, vol. 20, pp.703-704, Aug., 1984.

[14] Y.Suematsu, "Long-wavelength optical fiber communication," *Proc.IEEE*, vol. 71, No. 6, pp.692-721, June, 1983.

[15] Y.Yamamoto, "AM and FM quantum noise in semiconductor lasers-Part I: Theoretical analysis," *IEEE Quantum Electron.*, vol. QE-19, No. 1, pp.34-46, Jan., 1983.

[16] H.Haken, *Light - Laser light dynamics*, vol. 2, North-Holland Physics Publishing, 1985.

[17] R.Anderson, "An investigation of the effects of external cavity feedback on semiconductor lasers," *M.Sc. Thesis*, U. of Alberta, Spring, 1986.

[18] D.B.Mudryk, "The promise of coherent optical fiber communications," *M.Eng. Report*, U. of Alberta, Fall, 1986.

[19] M.Ettenberg, "Laser diode systems and devices," *IEEE Circuits and Devices Magazine*, vol. 3, no. 5, pp.22-25, Sept., 1987.

[20] R.F.Kazarinov, C.H.Henry and R.A.Logan, "Longitudinal mode self-stabilization in semiconductor lasers," *J. Appl. Phys.* vol. 53, No. 7, pp.4631-4644, July, 1982.

[21] C.H.Henry, "Theory of the linewidth of semiconductor lasers," *IEEE J. Quantum Electron.*, vol. QE-18, No. 2, pp.259-264, Feb., 1982.

[22] P.Spano, S.Piazzolla and M.Tamburrini, "Phase noise in semiconductor lasers: A theoretical approach," *IEEE J. Quantum Electron.*, vol. QE-19, No. 17, pp.1195-1199, July, 1983.

[23] C.H.Henry, R.A.Logan and K.A.Bertness, "Spectral dependence of the change in refractive index due to carrier injection in GaAs lasers," *J. Appl. Phys.*, vol.52, No. 7, pp.4457-4461, July, 1981.

[24] M.Osinski and J.Buus, "Linewidth broadening factor in semiconductor lasers - an overview," *IEEE J. Quantum Electron.*, vol. QE-23, No. 1, pp.9-29, Jan., 1987.

[25] Y.Yamamoto, S.Saito and T.Mukai, "AM and FM quantum noise in semiconductor lasers-Part II: Comparison of theoretical and experimental results for AlGaAs lasers," *IEEE J. Quantum Electron.*, vol. QE-19, No. 1, pp.47-58, Jan., 1983.

[26] K.Kikuchi and T.Okoshi, "Measurement of FM noise, AM noise, and field spectra of 1.3 μm InGaAsP DFB lasers and determination of the linewidth enhancement factor," *IEEE J. Quantum Electron.*, vol. QE-21, No. 11, pp.1814-1818, Nov., 1985.

[27] K.Kikuchi and T.Okoshi, "Measurement of spectra of and correlation between FM and AM noises in GaAlAs lasers," *Electron. Lett.* vol. 19, No. 20, pp.812-813, Sept., 1983.

[28] K.Shimoda, "Ultimate stability of methane-stabilized lasers," *Jpn. J. Appl. Phys.*, vol. 12, No. 8, pp. 1222-1226, Aug. 1973.

[29] D.Welford and A.Mooradian, "Output power and temperature dependence of the linewidth of single-frequency cw (GaAl)As diode lasers," *Appl. Phys. Lett.*, vol 40, No. 10, pp. 865-867, May, 1982.

[30] W.Elsasser and E.O.Gobel, "Multimode effects in the spectral linewidth of semiconductor lasers," *IEEE J. Quantum Electron.*, vol. QE-21, No. 6, pp.687-691, June, 1985.

[31] U.Kruger and K.Petermann, "The power-independent part of the semiconductor laser linewidth, explained by the rate equation," ECOC, Sept., 1987.

[32] M.J.Adams, "Linewidth of a single mode in a multimode injection laser," *Electron. Lett.* vol. 19, No. 17, pp.652-653, 1987.

[33] K.Vahala, Ch.Harder and A.Yariv, "Observation of relaxation resonance effects in the field spectrum of semiconductor lasers," *Appl. Phys. Lett.*, vol. 442, No. 3, pp.211-213, Feb., 1983.

[34] C.H.Henry, "Theory of the phase noise and power spectrum of a single mode injection laser," *IEEE J. Quantum Electron.*, vol. QE-19, No. 9, pp.1391-1397, Sept. 1983.

[35] S.Piazzolla and P.Spano, "Analytical evaluation of the line shape of single-mode semiconductor lasers," *Optical Comm.*, Vol. 51, No. 4, pp.278-280, Sept., 1984.

[36] P.B.Gallion and G.Debarge, "Quantum phase noise and field correlation in semiconductor laser systems," *IEEE J. Quantum Electron.*, vol. QE-20, No. 4, pp.343-349, April, 1984.

[37] H.E.Rowe, *Signal and Noise in Communication Systems*, D.Van Nostrand Company. Inc., 1965.

[38] T.Takakura, K.Iga and T.Tako, "Linewidth measurement of a single longitudinal mode AlGaAs laser with a Fabry-Perot interferometer," *Jpn. J. Appl. Phys.*, vol. 19, No. 12, pp.L725-L727, Dec., 1980.

[39] T.Okoshi, K.Kikuchi and A.Nakayama, "Novel method for high resolution measurement of laser output," *Electron. Lett.* vol. 16, No. 16, pp.630-631, July, 1980.

[40] T.Shen and G.P.Agrawal, "Computer simulation and noise analysis of the system performance of 1.55 μm single-frequency semiconductor lasers," *J. of Lightwave Technol.*, vol. LT-5, No. 5, pp.653-659, May, 1987.

[41] K.Ogawa, "Semiconductor laser noise: Mode partitiion noise," Chapter 8, *Semiconductors and Semimetals*, vol.22, Part C, Academic Press, Inc., 1985.

[42] K.Y.Lau and A.Yariv, "Ultra-high speed semiconductor lasers," *IEEE J. Quantum Electron.*, vol. QE-21, No. 2, pp.121-136, Feb., 1985.

[43] T.L.Koch and W.T.Tsang, "DFB lasers: set to profit from fiber optic advances," *Photonics Spectra*, pp.75-84, May, 1986.

[44] B.Zhou, J.Wang and H.Zhang, "Improvement of side-mode suppression ration of a single-mode SCC semiconductor laser," *Electron. Lett.* vol. 21, No. 19, pp.877-878, Sept., 1985.

[45] G.Wenke, R.Gross and E.Patzak, "Characteristics of a compact three cavity laser configuration," *J. of Lightwave Technol.*, vol. LT-5, No. 4, pp.608-615, April, 1987.

[46] C.Baack, *Optical Wideband Transmission Systems*, CRC Press, Inc., 1986.

[47] H.Temkin *et al.*, "Reflection noise in index-guided InGaAsP lasers," *IEEE J. Quantum Electron.*, vol. QE-22, No. 2, pp.286-293, Feb., 1986.

[48] R.Wyatt and W.J.Devlin, "10 kHz linewidth 1.5 μm InGaAsP external cavity laser with 55 nm tuning range," *Electron. Lett.* vol. 19, No. 3, pp.110-112, Feb., 1983.

[49] N.K.Dutta, N.A.Olsson and K.Y.Liou, "Effect of external optical feedback on spectral properties of external cavity semiconductor lasers," *Electron. Lett.* vol. 20, No. 14, pp.588-589, July, 1984.

[50] S.Ho, S.Ezekiel, J.R.Haavisto and J.Danko, "Optical feedback phase stabilization of a semiconductor laser," *J. of Lightwave Technol.*, vol. LT-4, No. 3, pp.312-315, Mar., 1986.

[51] E.Patzak *et al.*, "Spectral linewidth reduction in semiconductor lasers by an external cavity with weak optical feedback," *Electron. Lett.* vol. 19, No. 22, pp.938-940, Oct., 1983.

[52] M.Nakamura, "Longitudinal-mode behaviors of mode-stabilized Al$_x$Ga$_{1-x}$As injection lasers," *J. Appl. Phys.*, vol 49, No. 9, pp.4644-4648, Sept.,1978.

[53] K.Hagimoto, N.Ohta and K.Nakagawa, "4 Gbit/s direct modulation of 1.3 μm InGaAsP/InP semiconductor lasers," *Electron. Lett.*, vol., 18, No. 18, pp.796-798, Sept., 1982.

[54] J.Yamada, "Characteristics of Gbit/s optical receiver sensitivity and long span single-mode fiber transmission at 1.3 μm," *IEEE J. Quantum Electron.*, vol. QE-18, pp. 718-727, 1982

[55] W.T.Tsang, N.A.Olsson, R.A.Logan and R.A.Linke, "Demostration of multilevel multichannel optical frequency shift keying (FSK) with cleaved-coupled-cavity (C^3) semiconductor lasers," *Electron. Lett.*, vol. 19, No. 9, pp.341-343, April, 1983.

[56] H.C.Patangia, "Temporal and spectral characteristics of single-longitudinal-mode short-coupled-cavity (SCC) InGaAsP lasers under multigigahertz direct modulation," *Electron. Lett.*, vol. 20, No. 20, pp.842-844, Sept., 1984.

[57] S.Kobayashi, Y.Yamamoto, M.Ito and T.Kimura, "Direct frequency modulation in AlGaAs semiconductor lasers," *IEEE J. Quantum Electron.*, vol. QE-18, No. 4, pp.582-595, April, 1982.

[58] H.S.Sommers,Jr., "Complete experimental evaluation of the carrier dependence of the refractive index from the frequency modulation spectra of single mode injection lasers," *Appl. Phys. Lett.*, 42 (11), pp.928-930, June, 1983.

[59] G.Jacobsen, H.Olesen and F.Birkedahl, "Current/Frequency-moudlation characteristics for directly optical frequency-modulated injection lasers at 830 nm and 1.3 mm," *Electron. Lett.* vol. 18, No. 20, pp.874-876, Sept., 1982.

[60] T.Kimura and Y.Yamamoto, "Optical devices for coherent transmission systems," Optical Devices & Fibers, Jarect vol. 5., Ohmsha, Ltd. and North-Holland Publishing Co., 1983.

[61] R.S.Vodhanel *et al.*, "FSK heterodyne transmission experiments at 560 Mbit/s and 1 Gbit/s", *J. of Lightwave Technol.*, vol. LT-5, No. 4, pp.461-468, April, 1987.

[62] S.Saito, Y.Yamamoto and T.Kimura, "S/N and error rate evaluation for an optical FSK-heterodyne detection system using semiconductor lasers," *IEEE J. Quantum Electron.*, vol. QE-19, No. 2, pp.180-192, Feb., 1983.

[63] S.B.Alexander and D.Welford, "Equalisation of semiconductor diode laser frequency modulation with a passive network," *Electron. Lett.* vol. 21, No. 9, pp.361-362, April, 1985.

[64] H.Olesen and G.Jacobsen ,"A theoretical and experimental analysis of modulated laser fields and power spectra," *IEEE J. Quantum Electron.*, vol. QE-18, No. 12, pp.2069-2080, Dec., 1982.

[65] E.Emura *et al.*, "Novel optical FSK heterodyne single filter detection system using a directly modulated DFB laser diode," *Electron. Lett.*, vol. 20, pp.1022-1023, 1984.

[66] M.Ohtsu and S.Kotajima, "Linewidth reduction of a semiconductor laser by electrical feedback," *IEEE J. Quantum Electron.*, vol. QE-21, No. 12, pp. 1905-1912, Dec., 1985.

[67] H.Tsuchida and T.Tako, "High speed frequency stabilization of AlGaAs semiconductor laser," *Jpn. J. Appl. Phys.*, vol. 22, No. 10, pp.1543-1545, Oct., 1983.

[68] H.Tsuchida, M.Ohtsu and T.Tako, "Frequency stabilization of AlGaAs DH lasers," *Jpn. J. Appl. Phys.*, vol. 20, No. 6, pp.L403-L406, June, 1981.

[69] S.Saito, O.Nilsson and Y.Yamamoto, "Frequency modulation noise and linewidth reduction in a semiconductor laser by means of negative frequency feedback technique," *Appl. Phys. Lett.*, vol. 46, No. 1, pp.3-5, Jan., 1985.

[70] K.Kuboki and M.Ohtsu, "Frequency offset locking of AlGaAs semiconductor lasers," *IEEE J. Quantum Electron.*, vol. QE-23, No. 4, pp.388-393, April, 1987.

[71] K.Vahala and A.Yariv, "Semiclassical theory of noise in semiconductor lasers-Part II", *IEEE J. Quantum Electron.*, vol. QE-19, No. 6, pp.1102 - 1109, June, 1983.

[72] M.Ohtsu *et al.*, "Estimation of the ultimate frequency stability of semiconductor lasers," *Jpn. J. Appl. Phys.*, vol. 22, No. 7, pp.1157-1166, July, 1983.

[73] R.Kist and W.Sohler, "Fiber-optic spectrum analyzer," *J. of Lightwave Technol.*, vol. LT-1, No. 1, pp.105-109, March, 1983.

[74] S.J.Petuchowski, T.G.Giallorenzi and S.K.Sheem, "A sensitive fiber-optic Fabry-Perot interferometer," *IEEE J. Quantum Electron.*, vol. QE-17, No. 11, pp.2168-2170, Nov., 1981.

[75] J.Stone, "Optical-fibre Fabry-Perot interferometer with finesse of 300," *Electron. Lett.* vol. 21, No. 11, pp.504-505, May, 1985.

[76] D.L.Franzen and E.M.Kim, "Long optical-fiber Fabry-Perot interferometers," *Applied Optics*, vol. 20, No. 23, pp.3991-3992, Dec., 1981.

[77] L.J.Cimini, J.Stone and L.L.Buhl, "Optical-fibre Fabry-Perot frequency discriminator for communications applications," *Electron. Lett.* vol. 23, No. 9, pp.463-464, April, 1987.

[78] A.Yariv,*Optical Electronics*,third edition, CBS College Publishing, 1985.

[79] G.W.Kaye and T.H.Laby, *Tables of physics and chemical constants*, Longman, London, 1975.

[80] G.Cormack, J.Binder and M.Shewchuk, "The EF-FFT (Extended function fast fourier transform) applied to the analysis of time domain reflectometer waveforms," IEEE pacific Rim Conference on Communications, Computer and Signal Processing, Victoria, 1987.

[81] *Tektronix CT-1 Nanosecond Current Transformer Operating Manual*

APPENDIX I

THE MATERIAL INVOLVED HAS BEEN REMOVED BECAUSE OF THE UNAVAILABILITY OF COPYRIGHT PERMISSION

PARAMETERS FOR HITACHI HLP 5400 LASER [45]

APPENDIX II

LASER CURRENT & TEMPERATURE CONTROLLER CIRCUIT

A high speed laser driver circuit was built to provide both control of the DC laser current and to allow for the injection of the AC injection current derived from the electrical feedback system. It was also designed to provide a current source for the frequency modulation experiment which has been covered in Chapter 4.

The schematic diagram for the laser driver is shown in Fig. A1. A gallium ascenide (GaAs) power FET (NEC 900175) was incorporated in the high speed circuit to configure a voltage controlled current source by adjusting the potential difference between the gate and source of the FET. This high speed circuit was shielded carefully from the surrounding circuitry to eliminate electromagnetic interference. The input signal to the circuit was designed to have a short physical length to the laser diode because, as discussed in the previously, the electrical feedback loop should be kept as short as possible. A 16 Ω resistor was placed in series with the drain of the power FET to limit the maximum current passing through the laser diode. A lower cutoff frequency for the circuit was approximately 1.5 kHz with a 2.2 μF DC blocking capacitor. The 3 dB cutoff at high frequency was observed to be about 500 MHz using an impulse testing technique [80]. A Tektronix CT-1 nanosecond current transformer was connected to the laser diode to measure the high frequency signal currents in the laser. The current probe had a sensitivity of 5mV/mA into a 50 Ω oscilloscope input. Fig. A2 shows the frequency response of the current probe provided by the manufacturer. A 1.3 μm HLP 5400 InGaAsP semiconductor laser was used in the experiments. The threshold current and the lasing spectrum of the laser is temperature dependent. Therefore, a temperature stabilization circuit was necessary to control the ambient temperature of the laser. Such a stabilization circuit was realized with a thermistor sensor, a Peltier cooler

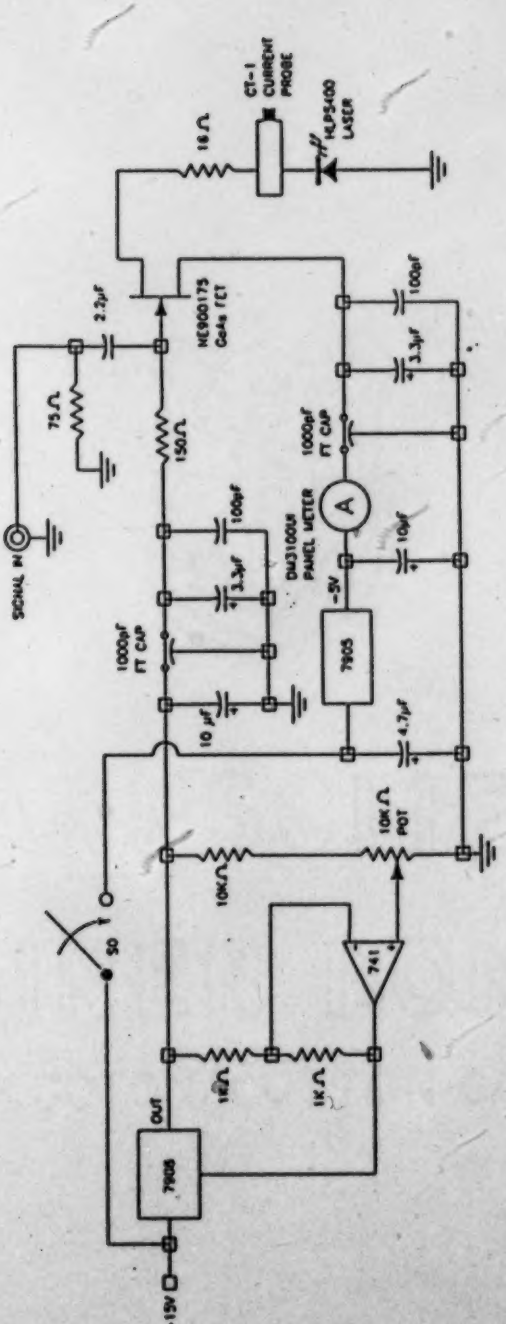

Fig. A1 Schematic diagram for the laser driver circuit

THE MATERIAL INVOLVED HAS BEEN REMOVED BECAUSE OF THE UNAVAILABILITY OF COPYRIGHT PERMISSION

Fig. A2 Frequency response for the nanosecond current probe [81]

and a control loop as shown in Fig. A3. The circuit design was adapted with minor changes from a colleague's similar unit. A similar temperature stabilization circuit was built for the fiber Fabry-Perot interferometer. The temperature of the fiber housing could be scanned by opening the switch S. The temperature gradient could be adjusted by turning the 10 kΩ pot to provide a different rate of scan. Both of the temperature controller circuits used were built to provide stabilization within the accuracy of $\pm 5 \times 10^{-3}$ degrees Celcius.

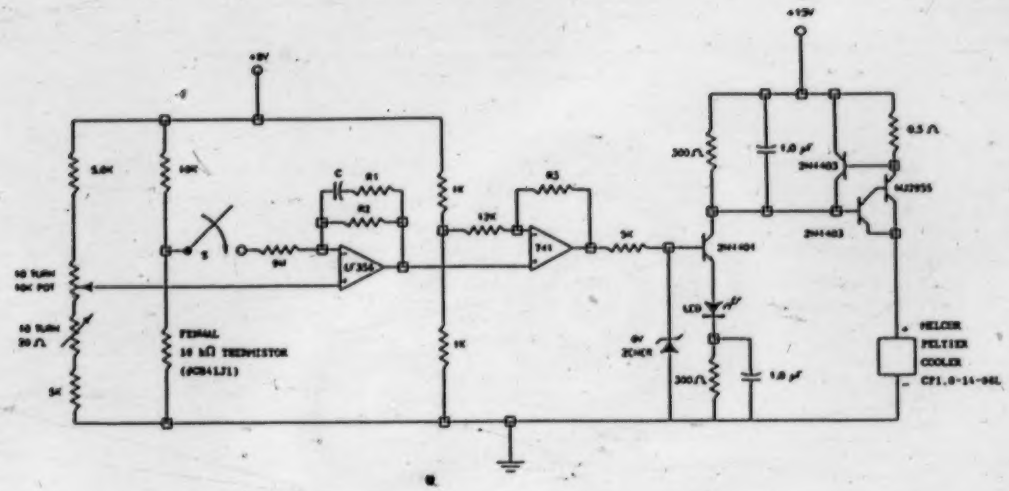

COMPONENT VALUES

	LASER	FFPI
R1	3.7MΩ	1.3MΩ
R2	2.7MΩ	3.3MΩ
R3	2.0MΩ	1.3MΩ
C	2.2μF	1.0nF
S	CLOSED	SCAN–OPEN STABILIZE–CLOSED

Fig. A3 Schematic diagram of temperature controller for the laser and the fiber-Fabry-Perot interferometer.